Universitat de Girona

THEORETICAL STUDIES OF SYSTEMS OF BIOCHEMICAL INTEREST CONTAINING Fe AND Cu TRANSITION METALS

Mireia GÜELL SERRA

Institut de Química Computacional
Departament de Química
Facultat de Ciències
Universitat de Girona

Theoretical studies of

systems of biochemical interest

containing Fe and Cu transition metals

Mireia Güell Serra

Supervised by:

Prof. Miquel Solà i Puig
Dr. Josep M. Luis Luis
Dr. Marcel Swart

Departament de Química
Àrea de Química Física

Institut de Química
Computacional

El professor Miquel Solà i Puig, catedràtic d'Universitat a l'Àrea de Química Física de la Universitat de Girona, el doctor Josep M. Luis Luis, professor agregat a l'Àrea de Química Física de la Universitat de Girona i el doctor Marcel Swart, investigador ICREA a l'Institut de Química Computacional de la Universitat de Girona, certifiquen que:

La Mireia Güell Serra, llicenciada en Química per la Universitat de Girona, ha realitzat sota la seva direcció, a l'Institut de Química Computacional i al Departament de Química de la Facultat de Ciències de la Universitat de Girona, el treball d'investigació que porta per nom:

"Theoretical studies of systems of biochemical interest containing Fe and Cu transition metals "

que es presenta en aquesta memòria per optar al Grau de Doctor en Química.

I perquè consti a efectes legals, signen aquest certificat.

Girona, 10 de juny de 2009

Prof. Miquel Solà i Puig   Dr. Josep M. Luis Luis   Dr. Marcel Swart

A la mare, al pare,
a en Marc,

a la iaia Anita i la iaia Antònia,

a l'Adrià.

Contents

1. Introduction

1. Introduction

1.1. Enzyme catalysis and copper proteins

A catalyst is a substance that increases the rate of a chemical reaction without being modified at the end of the process. Enzymes are the reaction catalysts of biological systems. They are more specific than most other catalysts and they are known to catalyze about 4.000 biochemical reactions.[1] It should be stressed that they are the most highly specialized proteins. Besides, they have a catalytic power usually greater than synthetic or inorganic catalysts. They are capable of enhancing the rate of a reaction in the range of 5 to 17 orders of magnitude.[2] All enzymes, with the exception of a small group of catalytic RNA molecules, are proteins and they are able to accelerate chemical reactions in aqueous solutions under very mild conditions of temperature and pH.

The activity of the enzymes can be decreased by certain molecules and the inhibition can be reversible or irreversible. Irreversible inhibition is frequently encountered in the action of specific toxins and poisons. However, it has to be stressed that the therapeutic action of many drugs also depends on their acting as enzyme inhibitors. Moreover, there are other factors that can affect the rate of enzymes reactions: the temperature, the pH, and the enzyme and substrate concentration.

Most enzymes catalyze the transfer of electrons, atoms or functional groups. They are classified according to the reaction where they intervene (Table 1). Furthermore, their names are assigned according to the type of transfer reaction, the donor group and the group acceptor. Many enzymes have been named by adding the suffix "-ase" to the name of their substrate or to a word or phrase describing their activity. For example, the catechol oxidase, which is an enzyme whose reaction mechanism is studied in this Thesis, is an oxidoreductase that catalyzes the oxidation of catechols to the corresponding quinones.

Class	Type of reaction catalyzed
Oxidoreductases	Transfer of electrons (hydride ions or H atoms)
Transferases	Transfer of a functional group
Hydrolases	Hydrolysis reactions
Lyases	Addition of groups to double bonds or formation of double bonds by removal of groups
Isomerases	Transfer of groups within molecules to yield isomeric forms
Ligases	Formation of C-C, C-S, C-O and C-N bonds by condensation reactions coupled to ATP cleavage

Table 1: Classification of enzymes recommended by the International Union of Biochemisty and Molecular Biology.[3]

1.1.1. Enzymatic catalysis

Like all catalysts, enzymes work by lowering the activation Gibbs energy ($\Delta G^{\ddagger}$) for a reaction, increasing the proportion of molecules that have enough energy to reach the transition state and thus dramatically increasing the rate of the reaction (Fig. 1).
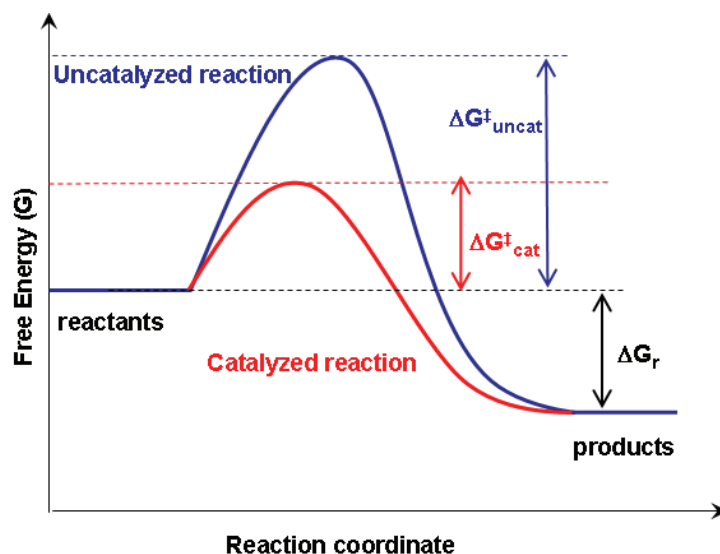
Fig. 1: Effect of a catalyst on activation energy. The catalyst lowers the free energy of activation, so more of the reactant molecules have the enough energy to reach the lowered transition state.

The understanding of the origin of the way to reduce $\Delta G^{\ddagger}$ requires finding out how the enzymes can stabilize their transition state more than the transition state of the uncatalyzed reaction. The exact strategy they adopt to accelerate reaction rates by a factor as large as 10^{17} is a very interesting issue.[4] The enormous rate enhancements could be explained by the rearrangement of covalent bonds during enzyme-catalyzed reactions. Transient covalent bonds can be formed between the functional groups of the enzyme and the substrate or some group can even be transiently transferred from the substrate to the enzyme. The noncovalent interactions, such as hydrogen bonds and hydrophobic and ionic interactions, which can be formed between the enzyme and the substrate[5] can also have a determinant role lowering the activation energy. In some cases the substrate must go through energy-demanding strained and distorted transition states to be transformed into the product. Then the enzyme binds the substrate in an intermediate conformation that resembles the transition state but has a lower energy because of the favourable energetic binding to the catalyst. Consequently, the activation energy for formation of the intermediate states and for conversion of the intermediate to product is lower than the activation energy for the uncatalyzed reaction.

Enzymes can show impressive levels of stereospecificity, regioselectivity and chemoselectivity concerning the reaction they catalyse and the substrates involved in these reactions.[6] The substrate binds to a region of the enzyme called active site. This region is often a pocket that contains amino acids chains involved in the binding of the substrate and other that participate actively in the catalysis process. The shape and the functional groups of the active site and the substrate are complementary and this fact explains the extraordinary specificity of enzyme catalysis. The selectivity of the enzymes was proposed by the first time in 1894 by the German biochemist Emil Fischer through the lock-and-key model (Fig. 2, a).[7] He suggested that the enzymes could accommodate their substrates thanks to their specific complementary geometric shapes as a key fits in its lock. In 1946, Linus Pauling proposed that the active site should not be complementary to the substrate of the reaction but to the reaction transition state.[8]
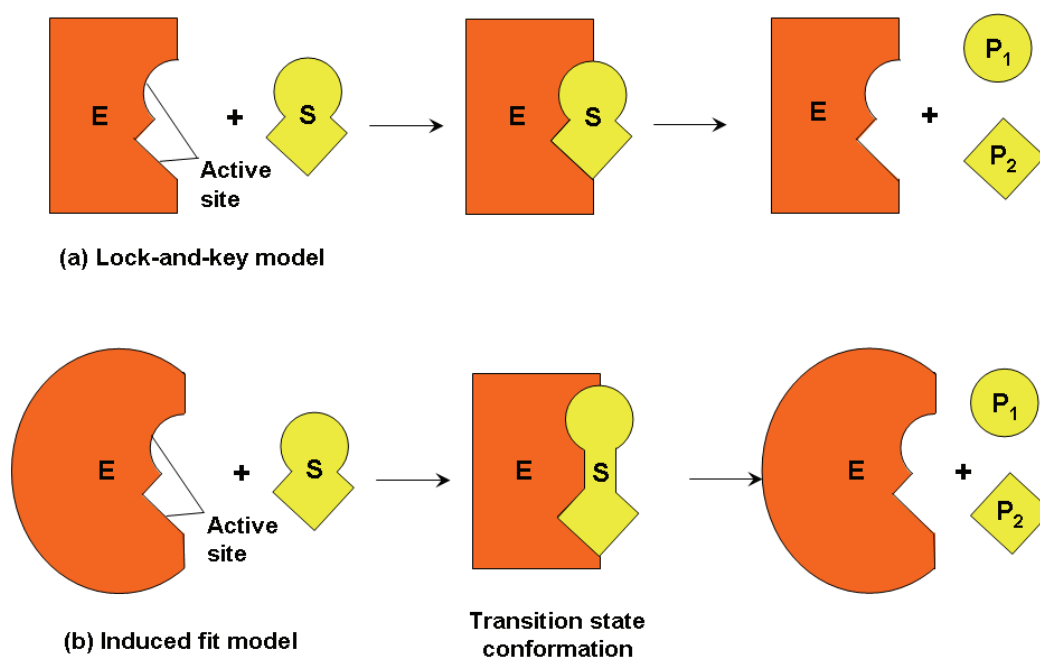
Fig. 2: Models for enzyme-substrate interaction: (a) The lock-and-key-model. (b) The induced fit model, where both enzyme and substrate are distorted on the binding.

In 1958 Daniel Koshland proposed the induced fit model, which was a modification of the lock-and-key model.[9,10] According to this model, enzymes are rather flexible structures and they do not only accommodate their corresponding substrates. Enzymes are moderately distorted to fit flexible substrates (Fig. 2, b). Then specific functional groups of the enzyme are in the proper position to catalyze the reaction.

A reaction catalyzed by an enzyme is not a simple process and there are many different factors involved in it. Theoretical chemistry can be a very useful tool to study this kind of reactions since it can analyse the elementary chemical transformations that take place in the active site of enzymes. Therefore, an enzymatic reaction can be followed step by step and the factors governing catalysis can be unravelled using theoretical chemistry.[11]

Enzymes are currently used in the chemical industry to catalyse very specific reactions. However, modern biotechnology continually needs enzymes with different specificities or capable of working under unusual conditions. Consequently, enzyme specificity can also be a drawback for industry since an active site optimal to interact with a given substrate will not be able to interact to the same degree with another molecule. For this reason, there is an increasing interest in enzyme design and engineering.[12,13] Nowadays, new or radically modified enzymes can be created using several techniques such as site-direct mutagenesis, protein hybridisation or catalytic antibody formation.

1.1.2. Metal ion catalysis

Some proteins only need their amino acid residues to act as efficient enzyme catalysts. However, others require the help of some small molecules or ions to carry out the reaction. These additional chemical components are called coenzymes. They can be either one or more inorganic ions, such as Fe^{2+}, Mg^{2+}, Cu^{2+} or Zn^{2+}, or a complex organic or organometallic molecules. Like enzymes, coenzymes are not irreversibly changed during catalysis and they are regenerated or remain unmodified. Some enzymes

require several coenzymes for activity. A coenzyme very tightly or even covalently bound to the enzyme protein is called a prosthetic group.

The enzymes that contain metal ions in their active site are called metalloenzymes. The ions can play very diverse roles and they give to the enzymes properties that these would not have in the ions absence. They can act as metal catalysts for hydrolytic reactions, where they can stabilize intermediates and/or transition states, and also as reduction/oxidation reagents. Moreover, in a lot of enzymatic reactions, certain ions do not remain permanently attached to the protein nor play a direct role in the catalytic process, but they are necessary for catalytic efficiency. It is also important to mention that transition metals can catalyse spin forbidden reactions.

1.1.3. Copper ions properties and biological ligands

Copper can have three different oxidation states, $Cu(I)$ ($3d^{10}$), $Cu(II)$ ($3d^9$) and $Cu(III)$ ($3d^8$). In biological systems, Cu works as a $1e^-$ shuttle, alternating between $Cu(I)$ and $Cu(II)$. This fact involves that enzymes active sites are designed to cope with the remarkably different coordination preferences for these two ions. Although the $Cu(III)$ oxidation state is generally considered to be unreachable due to the highly positive $Cu(III)/Cu(II)$ redox potentials that result from the coordination of amino acid residues such as imidazoles and phenolate ions, it may also be relevant in certain systems.[11]

$Cu(I)$ is a soft cation, it presents coordination numbers from two to four and it prefers sulphur ligands, N-donors (such as pyridines, imidazoles and nitriles) and π-acid ligands (such as carbon monoxide). When $Cu(I)$ is coordinated with polydentate ligands, steric factors and/or structural constraints control its coordination. Several geometries can be found in $Cu(I)$ complexes thanks to their high lability and geometric flexibility. Tetrahedral or trigonal-monopyramidal 4-coordinated complexes are the most common, but T- or Y-shaped 3-coordinated and linear 2-coordinated complexes are also frequently observed. On the other hand, five-coordinated $Cu(I)$ complexes are rare and they always have at least one Cu-ligand bond that is significantly longer than the others.[14-16] One aspect of $Cu(I)$ chemistry that should be highlighted is its capability to coordinate and activate dioxygen, O_2, turning it into a form able to intervene in a wide range of chemical reactions.

$Cu(II)$ has a smaller ionic radius and it is harder than $Cu(I)$. It generally binds anions (such as carboxylates and deprotonaded amides) and N-donor ligands (such as hard tertiary aliphatic amines, pyridines or imidazoles). It presents coordination numbers from four to six. Bridged compounds in which two or more $Cu(II)$ ions are linked by anionic ligands (such as oxide, hydroxide) are common, and either an antiferromagnetic or a ferromagnetic coupling between the $Cu(II)$ ions is observed.[17] $Cu(II)$ is a strong Lewis acid but it is not usually used as a such in metalloenzymes, probably due to fact that the strength of $Cu(II)$-ligand bonds could prevent a fast enzymatic turnover. The d^9 configuration of $Cu(II)$ in an octahedral field leads to a significant Jahn-Teller distortion that is usually manifested as an axial elongation of the octahedron (four short and two long bonds). An extreme example of Jahn-Teller effect is the complete loss of axial ligands that leads to a square-planar geometry. Generally, $Cu(II)$ compounds have square-planar geometries with ligands weakly associated in the axial position(s) at distances of 2.3-2.6 Å. In these structures, the single unpaired electron is localized in the $d_{x^2-y^2}$ orbital. Pentacoordination with trigonal-bipyramidal geometry is also common and in this case the electronic ground state frequently has the unpaired electron in the d_{z^2} orbital.

While there is a wide variety of Cu(I) and Cu(II) complexes described in the literature, it is much less usual to find those of Cu(III). This kind of compounds are usually stabilized by strongly basic anionic ligands in a square-planar geometry.[18-20] Although a d^8 Cu(III) centre can exist in a high-spin state,[21] all discrete Cu(III) complexes with oxygen ligation are low-spin and diamagnetic.

In metalloproteins, the metals ions of the active sites coordinate with nitrogen, oxygen and sulphur ligands from functional groups found in the side chains of certain amino acids (see Scheme 1).[22] The side chains of histidine, tyrosine, cysteine and methionine amino acids serve as common coordinating ligands for copper ions in proteins. The imidazole group of histidine is an usual ligand for both Cu(I) and Cu(II) and it has two different nitrogen atoms, π-N_{His} or τ-N_{His}, that can and do bind to copper. Tyrosine is only found in the active site of galactose oxidase [23,24] as a copper ligand and it is involved in organic radical formation. Cysteine, as a soft ligand, stabilizes Cu(I) ions. This amino acid is found in all known biological copper electron-transfer sites[25] and the great extent of the covalency of the Cu(I)-S and Cu(II)-S bonds is thought to provide electron-transfer pathways into or out from the copper centre in the protein. Methionine, which contains a thioether sulphur atom, is a neutral, soft, sulphur donor that can coordinate reversibly to Cu(II) and Cu(I) centres. It is found in either catalytic or electron-transfer sites and its role, especially in monooxygenases, is currently under investigation.[23]
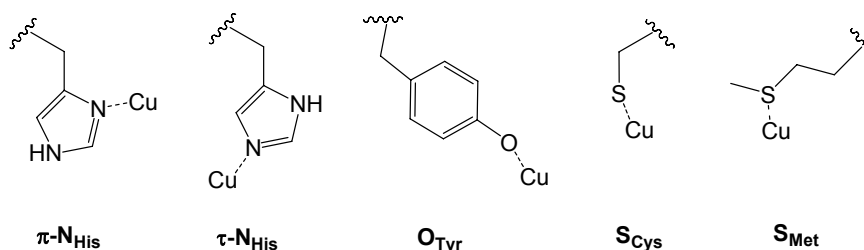
Scheme 1: The histidine (His), tyrosine (Tyr), cysteine (Cys) and methionine (Met) amino acids side chains, which serve as common coordinating ligands for copper ion in proteins.[11]

Carboxylate-containing amino acids, such as aspartic and glutamic acids, are usual for zinc, iron and manganese metalloproteins. However they are rare ligands for copper. Indeed, only two examples with glutamic acid at copper-containing active sites are known: the unusual "red" electron-transfer protein nitrocyanin,[26] and the quercetin 2,3-dioxygenase.[27] Weak interactions between carbonyl groups of the certain amino acids and copper centres have been observed in blue electron-transfer proteins, as well as the dicopper core electron-transfer sites found in cytochrome c oxidase and nitrous oxide reductase.[25] It has also been found a glutamine acting as weak ligand in the electron-transfer protein stellacyanin as well as in particulate methane monooxygenase (pMMO).[28]

1.1.4. Copper proteins

Copper is an essential trace element for living systems since it is a key cofactor in a wide range of biological oxidation-reduction reactions.[29,30] Protein active-site copper ions intervene in different processes such as electron transfer reactions and reversible O_2 binding and transport. They are also involved in oxygenation and oxidation-dehydrogenation reactions.

Proteins containing copper ions at their active site can be classified by Cu centre type, according to their biological function, by type and number of prosthetic centres and by sequence similarity. Historically, all copper proteins were divided into three different groups according to their spectroscopic features: the type-1 or blue copper, type-2 or normal copper and type-3 or coupled binuclear copper centres. However, over the last years, copper proteins whose characteristics do not fit in any of the previously mentioned groups have been discovered. For this reason the previous copper proteins groups list has been expanded and the current classification distinguishes seven different types of active sites: type-1, type-2, type-3, type-4, Cu_A, Cu_B and Cu_Z.[31]
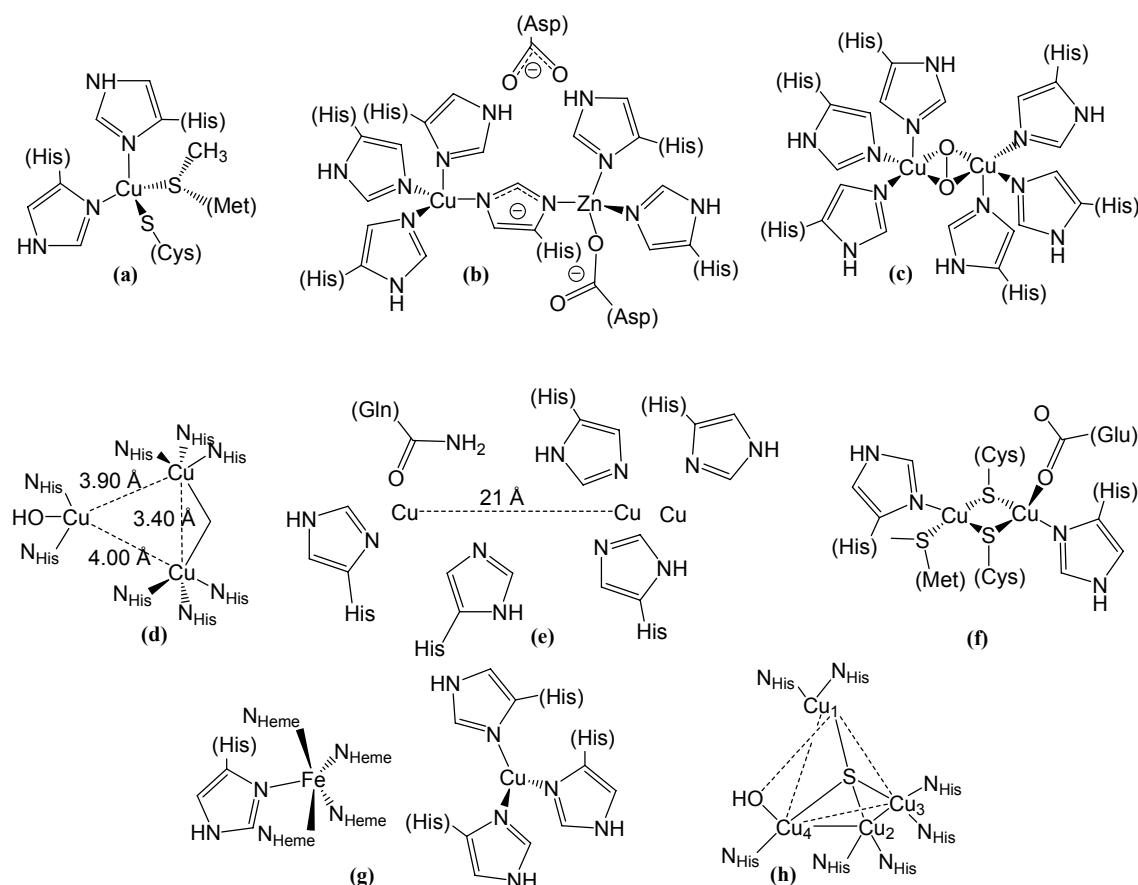
Scheme 2: Schematic representations of selected active sites of copper proteins: plastocyanin (type-1,a), Cu-Zn superoxide dismutase (type-2, b), oxyhemocyanin (type-3, c), ascorbate oxidase (type-4, or multicopper site, d), methane monooxygenase (multicopper site, e), nitrous oxide reductase (Cu_A site, f) cytochrome c oxidase (Cu_B site, g) and nitrous oxide reductase (Cu_Z, h).[31]

Type-1 active site.

Type-1 active site copper proteins are also named ''blue copper proteins'' because of their intense blue colour in the oxidized state due to a Ligand-to-Metal Charge Transfer (LMCT) transition from a cysteine sulphur to the copper(II) ions. Their active sites contain a single copper ion which is coordinated to two nitrogen donor atoms from two histidine residues and a sulphur atom from a cysteine residue in a trigonal planar rearrangement. Often the copper ions have also a weakly coordinated sulphur atom from, in most cases, a methionine residue in the axial position that distorts the geometry towards tetrahedral (Scheme 2, a).[32] Although this active site is found in

simple electron transfer proteins, such as plastocyanin,[32] azurin,[33] pseudoazurin and amicyanin,[33] it can also be found in some multicopper oxidases, such as ascorbate oxidase, and in redox enzymes, such as nitrite reductase.

Type-2 active site.

Type-2 active site copper-containing proteins are also called ''normal'' copper proteins because their EPR features are similar to common copper coordination compounds. They are almost colourless and their EPR spectra distinguish them from the type-1 active site proteins. Although this group includes Cu sites with a variety of amino acids ligands and geometries, generally the metal ion is ligated to four N and/or O donor atoms in either square-planar or distorted tetrahedral geometry.[29,30] The proteins of this class are mainly involved in catalysis, since the presence of vacant coordination sites allows the catalytic oxidation of substrate molecules. They intervene in the disproportionation of the $O_2^{\cdot-}$ superoxide anion, the selective hydroxylation of aromatic substrates or the C–H bond activation of benzylic substrates and primary alcohol oxidations. The type-2 active site is found in copper-zinc superoxide dismutase (Scheme 2, b),[34] prokariotic and eukaryotic amine oxidases, phenylalanine hydroxylase,[35] galactose oxidase[24] and lysyl oxidase.[36]

Type-3 active site

Type-3 active site contains a dicopper core, in which each one of the copper ions is coordinated to three nitrogen donor atoms from three histidine residues.[29,30] The copper(II) ions in the oxidized state of these proteins exhibit no EPR signal because they are strongly antiferromagnetically coupled. These proteins are capable of binding reversibly to dioxygen at ambient conditions and they are involved in O_2 transport and activation. This group is formed only by three proteins: hemocyanin,[37] tyrosinase[38] and catechol oxydase.[39] On one hand, hemocyanin (Scheme 2, c) is responsible for dioxygen transport in certain mollusks and arthropods. On the other hand, tyrosinase and catechol oxidase use dioxygen to oxidate phenols to catechols (tyrosinase) and then to *o*-quinones (tyrosinase and catechol oxidase), which afterwards polymerize and form the pigment melanin.

Type-4 active site

Type-4 active site proteins contain a trinuclear copper cluster formed by a type-2 and a type-3 active site. Some of them contain an additional type-1 centre which is connected to the trinuclear cluster by a cysteine-histidine electron pathway and they are referred to as multicopper oxidases, or blue oxidases.[29] This kind of proteins catalyzes oxidation reactions of organic substrates. Laccase (polyphenol oxidase),[40] ascorbate oxidase (Scheme 2, d)[41] and ceruloplasmin,[42] are some of examples of type-4 active site copper proteins.

Cu$_A$ active site

Cu$_A$ active site is formed by a dicopper core, where the two copper ions are bridged by two sulphur atoms from two cysteine residues. One of the coppers is coordinated to a methionine and the other to a carbonyl oxygen. Besides, each copper is bound to a nitrogen atom from a histidine residue and both metal ions have a tetrahedral

geometry. This kind of active site is also called mixed-valence copper site due to the fact that in the oxidized form, each of the two copper ions has a mixed-valence oxidation state, which is formally represented as Cu(1.5)Cu(1.5). This active site shows a very characteristic EPR spectrum and it has a purple colour in the oxidized state. Cu_A active sites participate in long-range electron transfer reactions and some examples of this kind of proteins are cytochrome c oxidase[43] and nitrous oxide reductase (Scheme 2, f).[44]

Cu_B active site

Cu_B active site contains a single copper ion which is coordinated to three nitrogen atoms from three histidine residues in a trigonal pyramidal geometry. The vacant coordination position of the copper ion is oriented towards the open coordination position of an heme iron. There is a strong antiferromagnetic coupling between the copper and the iron metal ions in the oxidized state, probably through an O-atom bridge. This kind of active site carries out the four-electron reduction of dioxygen to water and it has been found in *Paracoccus denitrificans* and cytochrome c oxidases (Scheme 2, g).[45]

Cu_Z active site

Cu_Z active site is a tetranuclear cluster formed by four copper atoms which are coordinated by seven histidine residues and a hydroxide anion. Three of the four copper ions are coordinated by two histidine residues, while the remaining copper ion is coordinated by one histidine residue and the hydroxide anion. Moreover, the four metal ions are bridged by a single sulphur atom.[46] The distances between some of the copper ions, Cu_2-Cu_4 and Cu_2-Cu_3 atoms (see Scheme 2, h), are very short (ca. 2.5–2.6 Å), and, consequently, they could be considered metal–metal bonds. On the other hand, the rest of copper distances are much longer (3.0–3.4 Å).[47] The oxidation states of the copper ions in the resting state remain still unclear, since the EPR spectra of this active site can be explained by either $Cu(I)_3Cu(II)$ or $Cu(I)Cu(II)_3$ oxidation schemes. The Cu_Z active site has been found in the nitrous oxide reductase (Scheme 2, h), where it intervenes in the reduction of N_2O to N_2.[46,47]

1.1.4.1. Tyrosinase and catechol oxidase

As it has been previously mentioned, tyrosinase[48] and catechol oxidase[49] are type-3 active site copper-containing proteins. Tyrosinase is found in bacteria, fungi, plants and animals and it catalyzes the *o*-hydroxylation of monophenols to the corresponding catechols (phenolase activity) and the subsequent oxidation to the resulting *o*-quinones (catecholase activity) (Scheme 3).

These reactions represent the initial steps of melanin biosynthesis in vertebrates. Besides, this chemistry is also observed as the "browning" reaction which takes place in fruits and vegetables due to long term storage or when they are cut or damaged and, consequently, exposed to dioxygen. Dioxygen binding to this enzyme occurs in the coupled binuclear active site, leading to oxy-tyrosinase, whose structure has been published quite recently.[38] In tyrosinase, active site access to a mono- and diphenolic substrates can occur. On the contrary, the hemocyanine active site is buried or protected and it is only capable of reversibly binding to oxygen.[29]
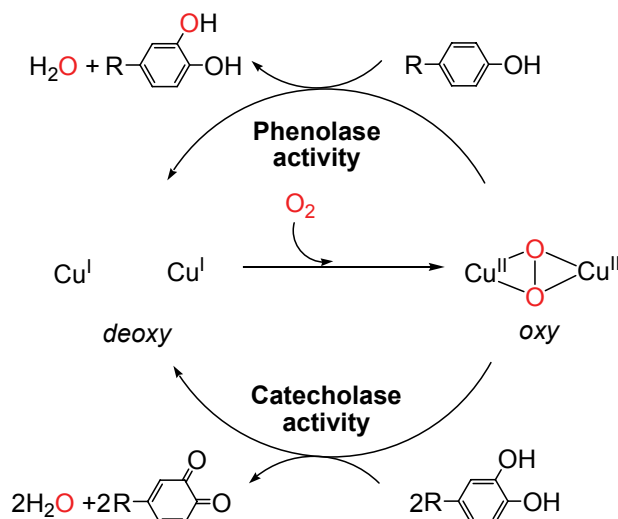
Scheme 3: Tyrosinase catalytic reactions: phenolase and catecholase[11]

In 1985, a first proposal was suggested for the molecular mechanism of the monophenolase and diphenolase activity of tyrosinase based on the geometric and electronic structure of the oxyhemocyanin active site.[50] In the monophenolase cycle, the monophenol binds to the axial position of one of the coppers of the oxy site and undergoes a rearrangement towards the equatorial plane which orients its *ortho*-position for hydroxylation by peroxide (Scheme 4). This generates a coordinated *o*-diphenolate, which is oxidized to the quinone, resulting in a deoxy site ready for further dioxygen binding. In the catecholase cycle, both the oxy and met sites react with *o*-diphenol, oxidizing it to the quinone. When comparing the kinetic constants for monophenolic versus diphenolic substrates, it is found that bulky substituents on the ring dramatically reduce the monophenolase but not diphenolase activity.[50] This suggests that while the monophenolic substrates require the axial to equatorial arrangement for *ortho*-hydroxylation, the diphenolic substrates do not need to undergo rearrangement at the copper site for simple electron transfer. The fact that *o*-diphenol but not *m*- or *p*-diphenol are oxidized by tyrosinase supports the bridged bidentate coordination mode indicated in Scheme 4, although a bidentate mode bound to one copper is also a possibility. Variations of the catalytic mechanism of tyrosinase were proposed later based on DFT calculations[51] and on the crystallographic structure of the enzyme which has been obtained quite recently.[38]

Catechol oxidase is only found in plant tissues and in crustaceans. It catalyses the oxidation of a wide range of *o*-diphenols (catechols), such as caffeic acid and its derivatives, to the corresponding *o*-quinones (catecholase activity).[49] The resulting *o*-quinones are highly reactive compounds that auto-polymerize and form melanin, a brown polyphenolic pigment, which have been suggested to protect plants from attacks of pathogens or insects.[52] Since catechol oxidase is often found tightly bound in the thylakoid membrane, a role in photosynthesis seems very likely. On the other hand, it has also been proposed that this enzyme intervenes in the biosynthesis of diphenols and in the hardening of seed coats. At this point it should be stressed that catechol oxidase lacks monophenolase activity.
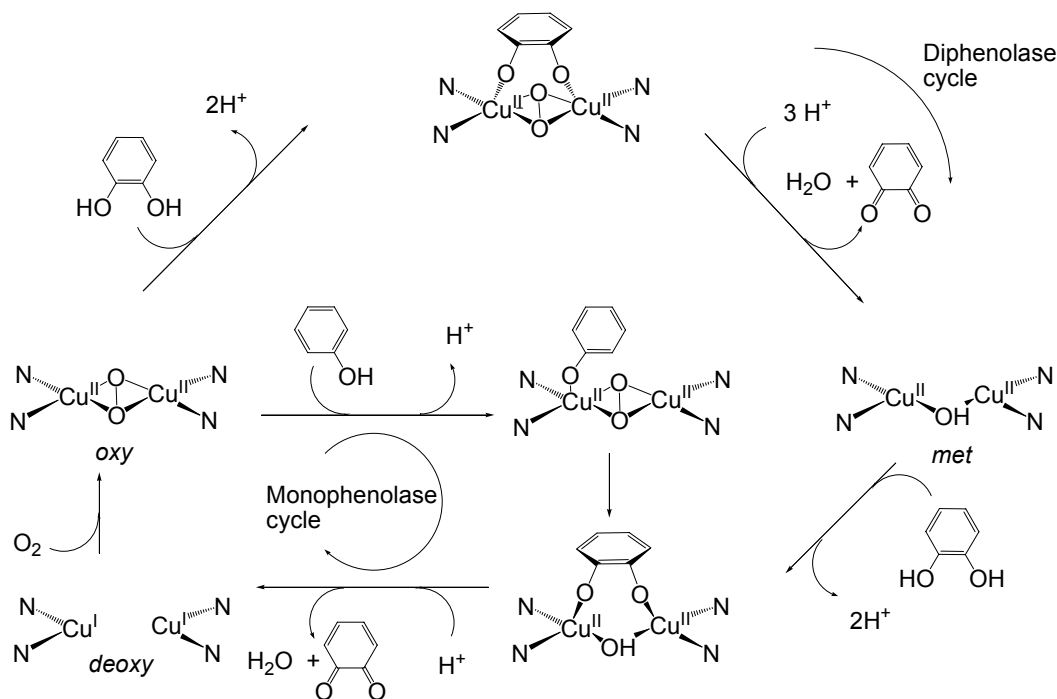
Scheme 4: Tyrosinase catalytic mechanism proposed by Solomon and coworkers.[50]

The catechol oxidase was isolated for the first time in 1937.[53] Subsequently, they were purified from a wide range of vegetables and fruits, such as potato, spinach, apple and grape berry,[53] and more recently, from litchi fruit.[49]

In 1998, Krebs and co-authors[54] reported the crystal structures of the catechol oxidase in three catalytic states: the native met (Cu(II)Cu(II)) state, the reduced deoxy (Cu(I)Cu(I)) form, and in the complex with the inhibitor phenylthiourea. They proposed a mechanism for the catalytic process, based on biochemical and spectroscopic,[29,55] as well as structural[54] data, which is almost identical to the diphenolase cycle proposed previously for tyrosinase by Solomon and coworkers[50] depicted in Scheme 4.

The origin of the differences in reactivity of tyrosinase and catechol oxidase remains unclear but it could be due to different structural requirements for the different reactions that intervene in monophenolase and diphenolase cycles.[38]

1.1.4.2. Peptidylglycine α-hydroxylating monooxygenase (PHM) and dopamine β-monooxygenase (DβM)

Peptidylglycine α-hydroxylating monooxygenase (PHM) and dopamine β-monooxygenase (DβM) belong to a small group of copper proteins that is only found in higher eukaryotes.[56] The former is the most extensively studied of the two domains of the peptidylglycine α-amidating monooxygenase (PAM), which carries out the activation of many peptide hormones and neuropeptides that need the amidation of their C terminus for biological activity. PHM transforms C-terminal glycine-extended peptides to their α-hydroxylated products, while DβM catalyzes the transformation of dopamine to norepinephrine (Scheme 5) and both enzymes transform the nonincorporated oxygen into water using equivalents of ascorbate.
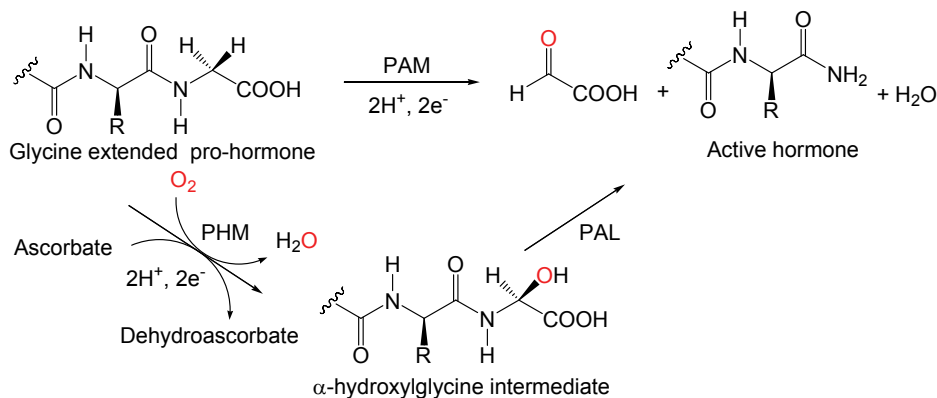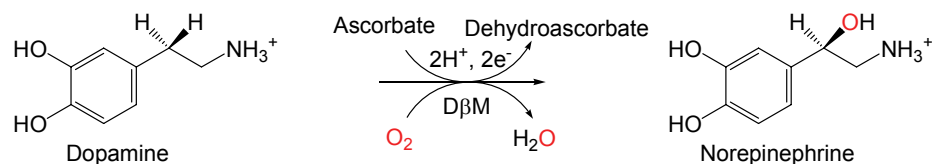
Scheme 5: Enzymatic hydroxylations of substrates by (a) dopamine-β-monooxygenase (DβM) and (b) peptidylglycine α-hydroxylating monooxygenase (PHM).

Although PHM and DβM intervene in reactions whose substrates are very different, these proteins resemble a lot in many other aspects. Both of them contain two type-2 centres widely separated in space (~11 Å away in PHM) and with no direct bridging ligands and no observable magnetic interactions. One of the centres (Cu_H) intervenes in electron transfer, whereas the other one (Cu_M) is involved in the incorporation of oxygen into the substrate. The crystallographic structure of PHM indicates that in the Cu_M site, where dioxygen coordinates and substrate hydroxylation takes place, the copper ion is ligated to two histidines and one methionine residues. On the other hand, in the Cu_H site the copper ion is coordinated to three histidine residues from the protein.

Several studies have been used to try to understand the mechanism of the reactions catalyzed by PHM and DβM, but there are still key aspects that remain unsolved.[57] Perhaps the most intriguing aspects are the electron transfer between the active-site coppers, the reduction of molecular oxygen and the hydrogen abstraction. Four different mechanisms for O_2 activation in PHM and DβM have been proposed,[56] ranging from the formation of an one-electron reduced intermediate ($Cu(II)-O_2^{\cdot-}$), to two electron reduced species ($Cu(II)-O_2^{2-}$), or metal hydroperoxo ($[Cu(II)-OOH]^+$) and finally to a highly reduced $Cu(III)$-oxo species formed via the reductive cleavage of $[Cu(II)-OOH]^+$. The mechanism that involves ($Cu(II)-O_2^{2-}$) (Scheme 6) is the one capable of rationalizing the huge amount of data available for PHM and DβM. The catalytic cycle starts with the fully reduced enzyme ($Cu(I)_H Cu(I)_M$). When the substrate is present, dioxygen molecule reacts with the Cu_M copper ion, forming a reactive Cu/O_2 intermediate, which cleaves the substrate C-H bond. The C-H bond cleavage takes place through a H-atom abstraction mechanism and generates a substrate radical. Subsequently, the $Cu(II)_M$-OOH intermediate is proposed to undergo a reductive cleavage to produce water and a $Cu(II)_M$-oxo radical, which then rapidly recombines with the substrate-derived radical to give the alcohol product.
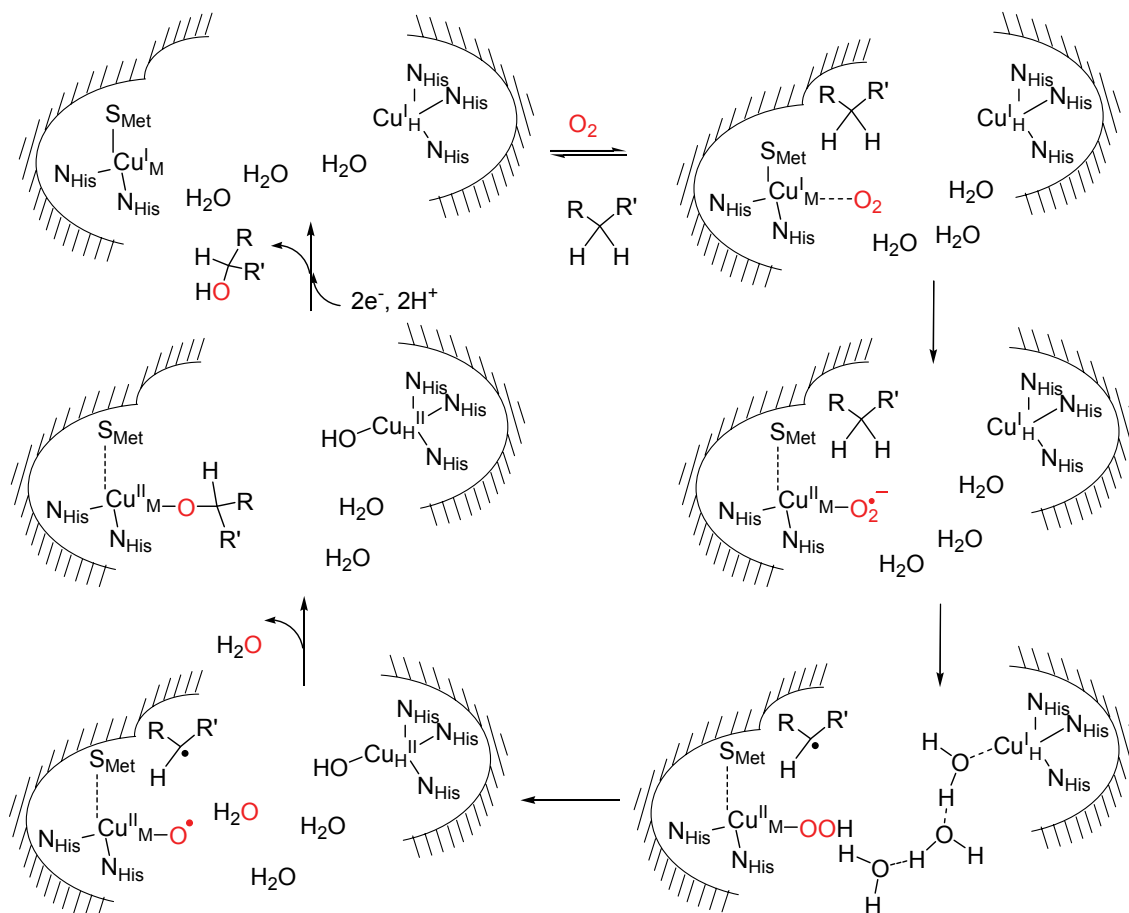
Scheme 6: Proposed mechanism of DβM and PHM.[58]

At this point it should be said that a PHM X-ray structure with a dioxygen bound in an end-on fashion compatible with the mechanism shown in Scheme 6 has been obtained quite recently.[59] Moreover several computational studies indicate than an intermediate with a Cu(II)-(O_2·⁻) would be capable of abstracting H-atoms from the substrate molecules.[60] However, more studies, either experimental or computational, are needed in order to provide more insight on the understanding of the reaction mechanism of PHM and DβM.[57]

1.1.5.Functional mimics

The enzymes that contain metals in their active sites catalyse reactions in a way that is notable for many reasons. First of all, they are very specific with substrates as well as regioselective and/or stereoselective. Furthermore, they work under mild conditions which means that they intervene in "green" processes. Consequently, the relationship between the structure and the function of metalloenzymes has been and it is extensively studied.

The recent development of crystallographic and spectroscopic techniques helped to gain a deeper understanding of the function of these enzymes through the obtained high-resolution structures of the resting states and reactive metalloenzymes intermediates. Moreover, it should be mentioned that the knowledge of enzyme structures has fuelled the design of bioinspired or biomimetic catalysts. These synthetic

catalysts do not need necessarily to duplicate the chemical or physical characteristics of the enzymes, but they serve to sharpen or focus the scientific questions asked. They have the advantage of widening the range of possible substrates, raising the production, tuning selectivity and/or specificity and providing insight into the various factors governing the reaction of interest. Therefore, mechanistic studies of bioinspired catalysts can help to unravel certain biological pathways. In fact, some recent iron and copper biomimetic catalysts have shed some light to the fundamental reaction steps and reactive intermediates relevant to metalloenzymes.[61,62] These kind of complexes can also be very helpful to develop the environmentally friendly catalytic chemistry by offering alternatives to toxic or expensive metal reagents and undesirable reaction media.

1.1.5.1. The synthetic model approach for Cu(I)/O$_2$ Chemistry

In metalloproteins, Cu can be found in mononuclear and coupled multinuclear configurations. In fact, enzymes with one, two, three, or four copper ions in their active sites are known, and the variations in ligand environment and reactivity patterns are immense. The main role of most copper enzymes is O$_2$ activation and subsequent substrate oxidation. The formation of the dioxygen adduct leads to copper-mediated reduction of O$_2$ to superoxo (O$_2^{\cdot-}$), peroxo (O$_2^{2-}$), or O-O cleaved products (copper-oxo, formally O^{2-}), which are the active species responsible for substrate oxidative transformations. Copper-containing enzymes that perform the O$_2$ activation can be divided into three different groups: monooxygenases, dioxygenases and oxidases. Monooxygenases and dioxygenases incorporate one and both atoms of O$_2$ to organic substrates, respectively, while oxidases catalyse redox reactions where O$_2$ is the electron acceptor and it is reduced to H$_2$O or H$_2$O$_2$. At this point, it has to be highlighted that the number of copper ions of the active site does not correlate with the reactivity.

The imitation of the enzymatic reactions with simple model systems and the characterization of the involved intermediates are intensively studied areas.[61,62] In fact, synthetic bioinorganic copper(I)–dioxygen chemistry has developed considerably in the last 25 years.[61-66] The interest in this kind of reactions and the Cu/O$_2$ species that intervene in them arises from their potential relevance to biochemical systems and synthetic catalysis. During the last years it has been a significant improvement in the understanding of the types of copper–dioxygen derived species or intermediates relevant to copper protein O$_2$ binding or activation thanks to several biochemical, biophysical and coordination chemistry studies. The chemistry observed for certain metal ions depends very much on the ligand environment and its coordination number.[67-69] Nowadays, several Cu$_n$-O$_2$(H) structure types with different spectroscopic properties and reactivity are known or partially characterized.[67] A summary of structural (and resulting spectroscopic) types, nearly all now well established, is shown in Scheme 7. As it can be seen by the number of entries of Scheme 7, A through N, there are, at least, fourteen Cu$_n$-O$_2$(H) structural/spectroscopic types. Some of these model systems are very important for copper enzyme chemistry since their structures are found in several relevant copper metalloenzymes. In particular, Structure B should be highlighted as it has been observed for a PHM X-ray structure. Besides, structure G is also very important due to the fact that it is present in the crystallographic structures of the three type-3 copper containing enzymes, hemocyanin,[70] tyrosinase[29] and catechol oxidase.[39]
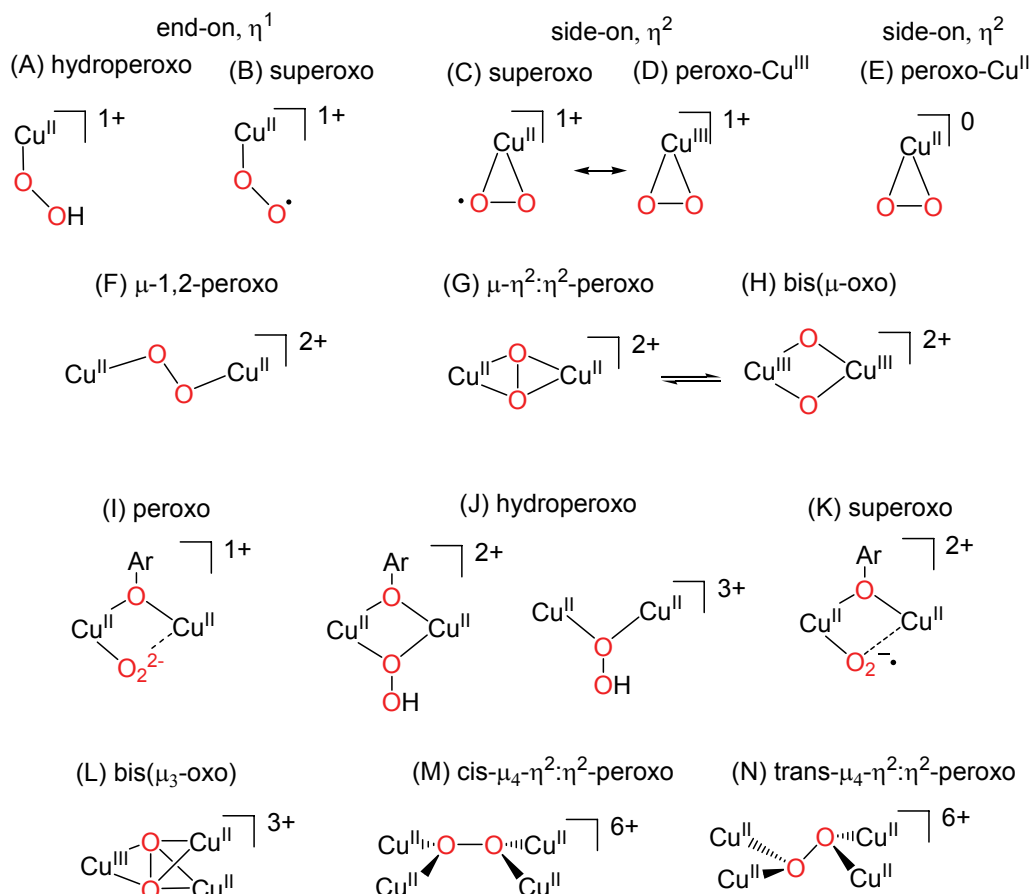
Scheme 7: Cu_n-O_2 (n=1-4) structural types: mononuclear (A-E), binuclear (F-K), trinuclear (L) and tetranuclear (M,N) dioxygen species, which are formally superoxo ($O_2^{\cdot-}$), hydroperoxo (HO_2^-), peroxo (O_2^{2-}) or bis(μ-oxo) (O^{2-}).[67]

1.1.5.1.1.   *Biomimetics of Tyrosinase*

The impressive capacity of tyrosinase to oxidize C-H bonds has elicited numerous efforts to create synthetic complexes with a μ-η^2:η^2-dicopper(II) core able to catalyse this reaction. Moreover, understanding how these biomimetic compounds work is also interesting since it can shed some light on the catalytic mechanism of this enzyme.

In 1955, it was already shown that the copper ion of bioinspired complexes of tyrosinase could intervene in phenol hydroxylation reactions.[71-75] Subsequently, Karlin and coworkers synthesized a dicopper(I) complex ($[Cu(I)_2(XYL-H)]^{2+}$) that reacted with dioxygen forming a μ-η^2:η^2-dicopper(II) (Scheme 8, a), which was capable to convert the unactivated arene ligand (XYL-H) into a phenol (XYL-OH).[76-79] Detailed experimental studies showed that the molecular dioxygen was the origin of the phenolic oxygen of the product and that the hydroxylation occurred by attack of the arene substrate (as nucleophile) on the electrophilic side-on bound peroxo group. Consequently, the ($[Cu(II)_2(XYL-H)(O_2)]^{2+}$) complex mimicked tyrosinase both in the active site structure and the arene hydroxylation chemistry. Later, Tolman and coworkers synthesized a copper complex using an amine and a pyridine ligand bound to an arene that underwent endogenous aromatic hydroxylation (Scheme 8, b).[80] Unlike the previously described complex, in this case a bis-μ-oxo-dicopper(III) core was responsible for the monoxygenase activity.

16
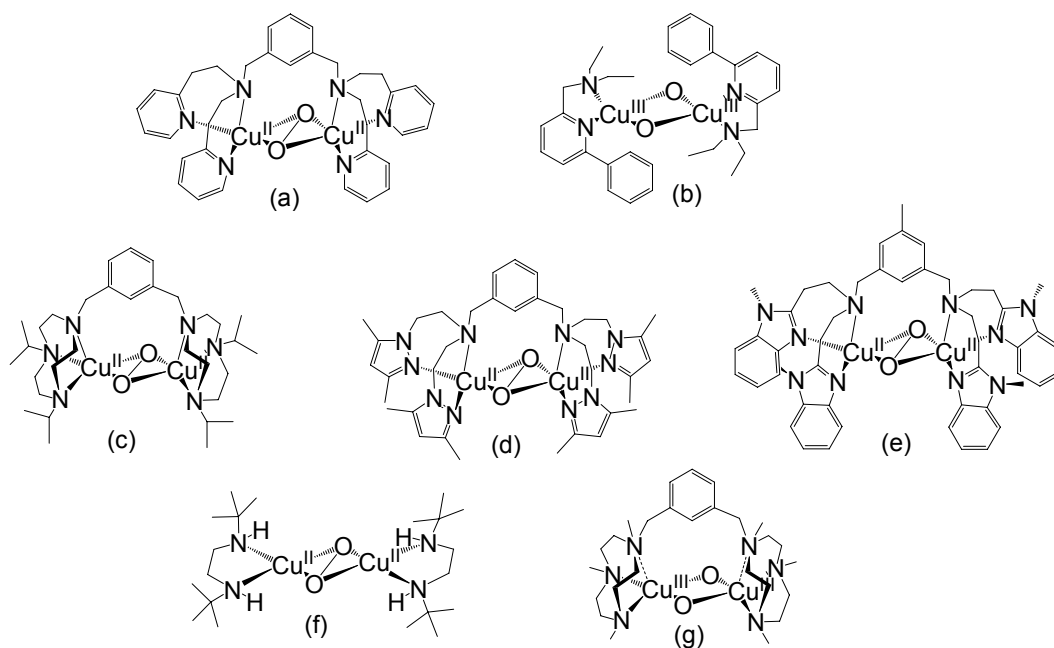
Scheme 8: Biomimetic compounds of tyrosinase: a) ([Cu(II)$_2$(XYL-H)(O$_2$)]$^{2+}$),[76-79] b) ([Cu(II)$_2$(2-(diethylaminomethyl)-6-phenylpyridine) (μ-O)$_2$]$^{2+}$),[80] c)[Cu(II)$_2$(m-XYL^{iPr4})(O$_2$)]$^{2+}$,[81] d)[Cu(II)$_2$(mxyN$_6$)(O$_2$)]$^{2+}$,[82] e)[Cu(II)$_2$(MeL66)(O$_2$)]$^{2+}$,[83] f)[Cu(II)$_2$(DBED)(O$_2$)]$^{2+}$,[84,85] and g)[Cu(III)$_2$(μ-O)$_2$(m-XYL^{MeAN})]$^{2+}$.[20]

Nowadays, a wide range of model systems with either μ-η^2:η^2-peroxo-dicopper(II) or bis(μ-oxo)dicopper(III) core, involved in complex reactions leading to catechol or quinone has been described (Scheme 8).[61,85] Due to the fact that the interconversion between the μ-η^2:η^2-peroxo and the bis(μ-oxo) structures of the dicopper core is extremely rapid, it is difficult to know which isomeric form is in charge of the *o*-phenol hydroxylation.[61,62,86] At this point it is important to mention that these biomimetic compounds use phenolates as a substrate while tyrosinase catalyses the hydroxylation of phenols.

Recently, by means of spectroscopic studies, Stack and coworkers demonstrated that the binding of a phenolate substrate in [Cu(II)$_2$(DBED)(O$_2$)]$^{2+}$ (Scheme 8, f) lead to O-O bond cleavage of side-on peroxo complex, generating a bis(μ-oxo)dicopper(III) species.[85] Further mechanistic studies showed that the subsequent *o*-hydroxylation step had the hallmarks of an electrophilic aromatic mechanism. Consequently it was suggested a mechanism where the O-O bond cleavage is prior to the C-O bond formation as an alternative to tyrosinase generally accepted mechanism where the O-O cleavage is concerted or posterior to the C-O bond formation. In addition, Company and coworkers synthesised a bis(μ-oxo) complex (Scheme 8, g) capable of binding and hydroxylating phenols.[20] Therefore, the bis(μ-oxo) structure could be the active oxygenating agent in tyrosinase.

1.1.5.1.2. *Biomimetics of peptidylglycine α-hydroxylating monooxygenase (PHM) and dopamine β-monooxygenase (DβM)*

The investigation of the oxidative reactions induced by mononuclear copper-dioxygen complexes is not trivial since these intermediates are difficult to prepare and characterise. This is due to their tendency to dimerise to relatively stable binuclear

complexes, which are models for type-3 copper proteins, and their low reactivity because of the sterical crowding around the Cu metal ion. Recently, several examples of this kind of complexes have been obtained by the use of sterically demanding ligands. One of the first mononuclear copper-dioxygen complexes is a side-on superoxo compound synthesised by Kitijima and coworkers using a *tris*-pyrazolylborato ligand (Scheme 9, a).[87] Further examples for these systems are the compounds with β-diketiminato, anilido-imine or 2-pyridinecarbaldehyde imine ligands (Scheme 9, b) prepared and studied by Tolman and coworkers.[88-90] Itoh and co-workers synthesized a series of mononuclear copper(II) complexes with tridentate ligands[91,92] that react with H_2O_2 to form alkylperoxo complexes (Scheme 9, c) that undergo an efficient aromatic ligand hydroxylation reaction.[91] Karlin and coworkers were also able to notice an aromatic ligand hydroxylation of a mononuclear copper complex with the ligand 6tBP, which is a derivative of the TMPA ligand (TMPA = tris(2-pyridylmethyl)-amine) (Scheme 9, d).[93] In this case, a hydroperoxo complex was formulated as the intermediate for this reaction. Besides, Karlin and coworkers also synthesized another copper(II) superoxo complex with a NMe_2-TMPA ligand that is capable to induce hydroxylation and hydroperoxylation of phenols (Scheme 9, e).[93,94] Moreover, they also observed the *N*-dealkylation of a ligand by a hydroperoxo complex very similar to the previous one (Scheme 9, f).[95]
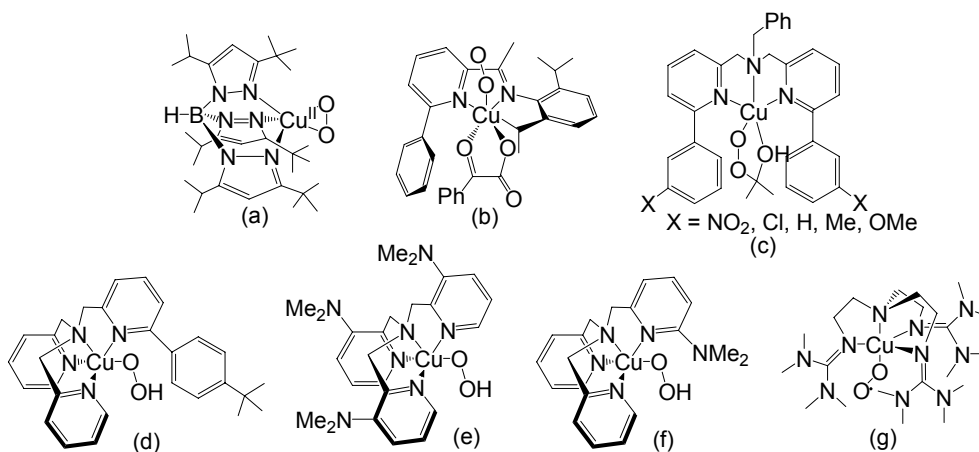
Scheme 9: Copper-dioxygen model systems for DβM and PHM: a) side-on copper(II) superoxocomplex,[87] b) end-on copper–dioxygen complex,[90] c) copper(II) alkylperoxo complex,[91,92] d) [93], e) [94] and f) copper(II) hydroperoxo complex,[95] and g) copper(II) superoxo complex[96]

It has to be highlighted that for all the previously mentioned monocopper complexes the hydroxylation reactions were observed only for aromatic ligands, while the reaction that takes place in DβM and PHM enzymes is the hydroxylation of aliphatic ligands. However, very recently Karlin and coworkers detected the hydroxylation of a methyl group of the ligand of the $[Cu(II)(TMG_3tren)-(O_2^{\cdot-})]^+$ (TMG_3-tren = 1,1,1-tris(2-$[N^2$-(1,1,3,3-tetramethylguanidino)]ethylamine) complex (Scheme 9, g).[96] This system is also capable of oxidizing and oxygenating several monophenols and diphenols, like the earlier described $[Cu(II)(NMe_2$-TMPA$)-(O_2^{\cdot-})]^+$ complex (Scheme 9, e).[93,94] Several experimental details for this system lead to the conclusion that the initial step of all the hydroxylation reactions is the abstraction of a hydrogen atom from a phenol. However, it is not known whether the hydroperoxo intermediate is responsible for the hydroxylation reaction or whether the O-O bond cleavage is necessary for the reaction to take place.[57]

Studies on the previously mentioned monocopper(II) complexes has shed some light on the nature of the biological promoted oxidative processes in DβM and PHM enzymes. Nevertheless, there are important differences between the coordination spheres of the Cu ions in the biological systems and in their corresponding biomimetic compounds. Moreover, a lot of aspects of the catalytic mechanism of the enzymes remain unknown. Consequently, the increasing interest on this oxygen activating systems will probably lead to the synthesis of more bioinspired systems that could help to gain understanding of the DβM and PHM catalytic cycles.

1.2. Spin crossover compounds

In Nature it is usual to find organometallic compounds which can easily change their spin state. For instance in the catalytic cycles of some enzymes containing transition metals, the ground state does not correspond always to the same spin state.[11] This means that different spin states can intervene in different steps of the mechanism.

Iron is one of the most widely and diversely used metals in all of biology,[97-100] since it can exist in a number of oxidation states, which makes it ideal for participation in electron-transfer and oxidation/reduction reactions. Iron-containing proteins are very numerous and diverse and they are classified on the basis of the local coordination environment about the iron ion into three different categories: heme, iron-sulfur and non-heme. Heme proteins coordinate iron using a porphyrin macrocycle and are involved in processes such as reversible O_2 binding and substrate oxidation via O_2 activation. Iron-sulfur proteins use inorganic sulphur and amino acid residues to generate iron clusters employed to shuttle electrons and reduce N_2. Finally, non-heme iron proteins typically bind iron using only amino acid residues and they are functionally diverse, performing reactions such as reversible O_2 binding, the oxidation of unactivated C-H bonds and the detoxification of biologically harmful radicals.

Cytochrome P450, an heme iron-containing enzyme that is one of the most versatile enzymes in nature,[101] is a very good example to illustrate the changes in the spin state that can take place in the active site of enzymes (see Scheme 10). The catalytic cycle of this enzyme starts from the resting state (**1**), where the five electrons of the Fe(III) ion are mainly in the low-spin doublet configuration (LS). In the first step, the entrance of the substrate displaces the water molecule, leaving a pentacoordinated Fe(III)-porphyrin (**2**). With a coordination number of five, the iron changes the spin state (often partially) to a sextet high-spin (HS). In the next step, the HS Fe(III) takes up an electron from a reductase protein and structure **2** is reduced to a HS Fe(II) complex (**3**).[102] Subsequently, molecular oxygen binds to structure **3** and it leads an oxy-P450 complex (**4**), which has a singlet spin state. Structure **4** is a good electron acceptor and it is the last relatively stable intermediate in this cycle. Then a second reduction of the system takes place and it generates a peroxo-Fe(III) intermediate (**5**). Generally, this step is thought to be the rate-determing step of the catalytic cycle.[103] Due to the fact that structure **5** is a good Lewis base, it is quickly protonated to form hydroperoxo-Fe(III) intermediate (**6**) that is also called Cpd 0. Structure **6** is still a good Lewis base and it abstracts an additional proton. Subsequently, the heterolysis of O-O bond and the formation of Cpd I (**7**) and a water molecule occur. Finally Cpd I transfers an oxygen atom to the substrate. The details of the cycle going from **5** to **1** remain unclear and the mechanism of the substrate oxidation is still highly debated. In fact the oxygenation of the substrate to form a product complex has been investigated by many experimental

methods. However, very few direct measurements have been possible due to the high reactivity and lack of significant accumulation of these intermediates in kinetic studies.[104]
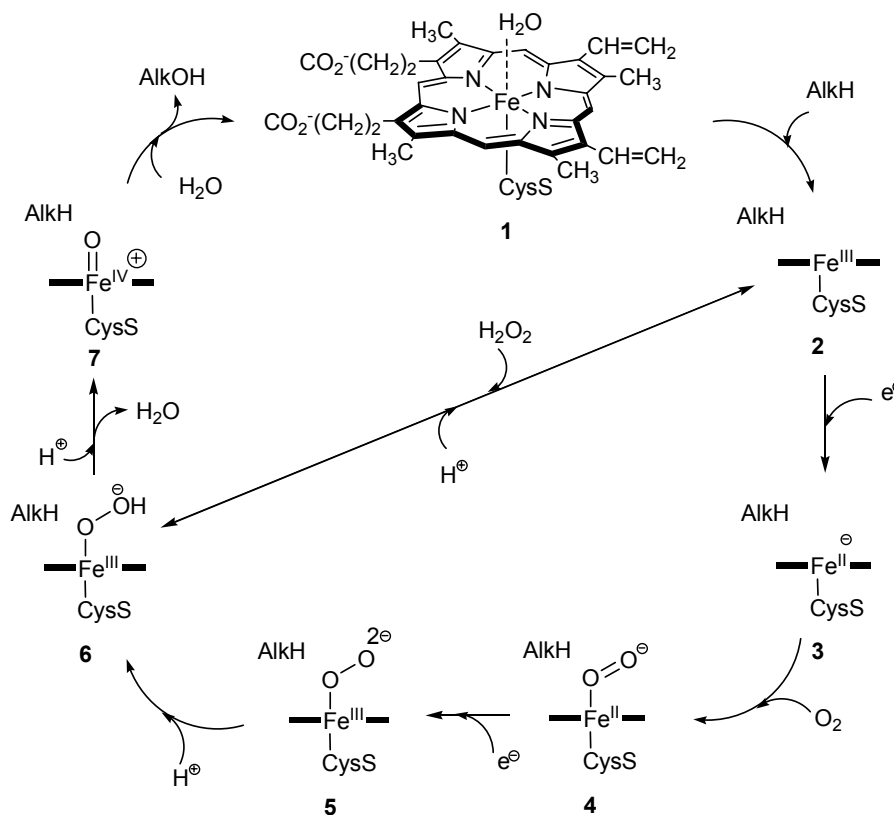
Scheme 10: Schematic representation of the catalytic cycle of P450.[105]

A very important type of systems that are easily capable of changing their spin state is the one formed by the spin-crossover (SCO) compounds. They are capable to switch between HS and LS states in response to external stimuli such as temperature, pressure, or light.[106,107] The first thermal spin-crossover compounds were reported in the 1930,[108] but it was in the early 1960s, when the phenomenology of thermal spin-crossover was first precisely described.[109] The field started to raise an increasing interest in 1993, when the first molecule-based material to undergo a thermal spin-transition that exhibits a thermal hysteresis at room temperature was discovered.[110]

The HS and LS states of SCO complexes have different magnetism, optical properties, dielectric constant, colour and structure.[111,112] These properties can change due to the effect of several factors such as temperature, pressure, irradiation at different wavelengths, which made the SCO phenomenon one of the most interesting examples of bistability in molecular materials. In fact, nowadays the synthesis and characterisation of molecular materials with switching properties is receiving an increasing attention due to their potential technological applications, such as sensors or memory devices.[113-116]

1.2.1. Perturbation of spin crossover compounds

As it has been mentioned before the spin crossover phenomenon is driven by several physical stimuli. The thermal spin transition takes place at a temperature where the zero-point energy difference between the HS and the LS states ($\Delta E^o_{HL}=E^o_{HS}-E^o_{LS}$) is

of the same order of thermally accessible energies (k_BT).[107] In solution this process occurs gradually as the temperature is changed and a range of approximately 150 K is usually needed to be completed. In the solid state, the thermal spin-transitions are much more diverse and they can be either gradual, as in solution, or abrupt, which means that they are complete in a temperature range of 1 or 2 K.[117] The spin transition temperature ($T_{1/2}$) corresponds to the temperature at which the two states of different spin multiplicity are present in the ratio 1:1 ($\gamma_{HS} = \gamma_{LS} = 0.5$).

Spin crossover in transition metal compounds can also be caused by the application of pressure.[109] Since the volume of the LS state of a molecule is always smaller than its HS form, increasing pressure shifts the $T_{1/2}$ to higher temperature as the LS state is stabilised.[118] On the other hand, the application of a very strong magnetic field to a sample has the reverse effect of stabilising its HS state.[119] This is due to the fact that the magnetic field can interact more strongly with the HS form of the compound, which is always more paramagnetic. Consequently, the $T_{1/2}$ is shifted to lower temperature as the field strength is increased.[120]

Spin-state conversions can also be induced in the solids by laser irradiation.[121] By means of a green laser, a spin-transition compound can be switched from the LS to the HS state, which is metastable at the temperature of the experiment. Some systems can remain in their excited spin-state for weeks at low temperatures, which is an effect known as ''light-induced excited spin-state trapping (LIESST)''.[111,122] This situation can only occur when the temperature is lower than the barrier for the thermal relaxation of the complex. In this scenario, the compound can only relax by quantum-mechanical tunnelling, which is a slow process when the structures of ground and excited states are very different.

1.2.2. Different types of spin crossover compounds

Spin crossover phenomenology is observed for compounds with octahedral coordination and metal ions with d^4, d^5, d^6 and d^7 configurations. This is due to the fact that in these systems there are two different ways of accommodating the valence d electrons on the t_{2g} and e_g orbitals.

The majority of the reported SCO compounds contain Fe(II), d^6, and Fe(III), d^5, metal ions. The Co(II), d^7, is present in some of these systems, whereas Cr(II), d^4, Mn(III), d^4, Mn(II), d^5, and Co(III), d^6, are much more rare.[123] Only a single SCO compound has been proposed for Ni(III), d^7.[124] There are also a few examples for the second transition series.[106]

Octahedral Fe(II) coordination complexes accounts for the majority of SCO compounds. Most of them have the general formula $[FeL_6]^{n+}$ or $[Fe(NCX)_2L_4]$. The 'L' ligand corresponds to a nitrogen donor, usually from a heterocyclic group of a monodentate or polydentate ligand (see Scheme 11), while NCX$^-$ is isothiocyanate (X = S), isoselenocyanate (X = Se) or a related pseudohalide. At this point it is important to note that the combination of Fe(II) and N–ligands leads to the greatest change in metal–ligand bond lengths between the high- and low-spin states among all the SCO complexes.[123,125-127] Abrupt spin-transitions in a temperature range smaller than 5 K are quite common for solid Fe(II)/N–ligand complexes, which is caused by the big structural changes that induce large cooperativity between spin centres during spin-crossover.

The SCO complexes that have the most diverse coordination environment and the widest range of donor atom sets are the Fe(II) ones. Despite the amount of similarities between Fe(II) and Fe(III) SCO complexes, there are also some differences

that are worth to mention. Fe(III) complexes suffer a smaller change in the Fe-ligand distances for the spin transition, the degree of cooperativity associated with the transition in the solid state is lower, and the rate of inter-conversion of the spin states is larger. Moreover, it should be mentioned that Fe(III) spin crossover systems are less common that the ones with Fe(II) due to the tendency of the high spin of the formers to hydrolyse.
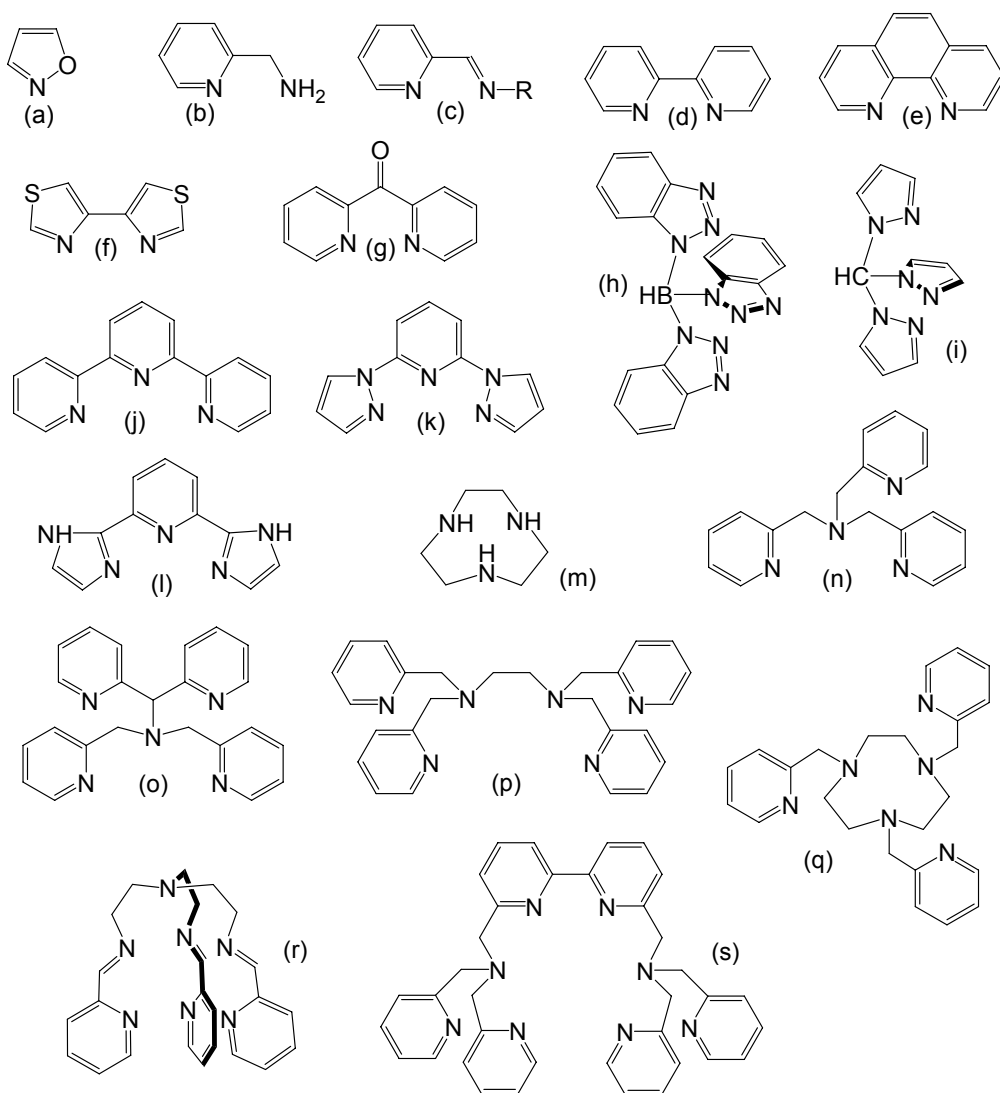
Scheme 11: N-donor ligands that form spin-crossover mononuclear iron(II) complexes organized by ligand type and in order of increasing ligand donacity: monodentate (a), bidentate ligands (b-g), tridentate (h-m), tetradentate (n), pentadentate (o), hexadentate (p-q) and higher denticity (r-s) ligands.[128]

The SCO Co(II) compounds are very diverse but they are much less common than the Fe(II) ones. This is possibly due to for the Co(II) complexes spin pairing energy is higher and the single e_g electron in low spin six-coordinate complexes have a destabilising effect.[126] Most of the features of the Fe(II) systems appear also in Co(II) with some exceptions, such as the hysteresis associated to thermal transitions and the LIESST effect. This fact can be due to the smaller changes in metal-ligand distances associated with the spin change.

There is a reduced number of examples of Co(III) SCO.[123] The d^6 configuration ions has a quite low spin pairing energy and the LS d^6 configuration has maximum ligand field stabilisation energy.[129] Consequently Co(III) coordination compounds almost always adopts a LS configuration and it is quite difficult to find SCO compounds of HS systems for this ion.

1.2.3. Detection of spin crossover

As it has been mentioned previously, the high and low spin states of SCO complexes show differences in magnetism, optical properties, dielectric constant, colour and structure. There is a wide range of experimental techniques that can be used to measure the changes that occur in the spin state transition (magnetic susceptibility measurements, ^{57}Fe Mössbauer spectroscopy, measurement of electronic and vibrational spectra, heat capacity measurements, X-ray structural studies, synchrotron radiation studies, magnetic resonance studies…).[106] The measurement of the variation of the paramagnetism was used for the detection of thermal SCO and it is still the most common technique for monitoring a spin transition. However, ^{57}Fe Mössbauer spectroscopy can give separate and well defined contributions to the overall spectrum of each one of the spin states if their lifetimes are greater than the time scale of the Mössbauer effect (10^{-7} s). This technique can be applied to Fe compounds and, consequently, it can be used to monitor the majority of the SCO systems since most of them contain a Fe metal ion.

1.2.3.1. ^{57}Fe Mössbauer Spectroscopy

Mössbauer spectroscopy is used both in chemistry and solid state physics to provide information on the electronic structure of chemical compounds.[130-133] This technique is based on the phenomenon of recoilless resonance absorption of γ rays by the atomic nuclei. It is used for more than 40 elements in the Periodic table, but only 15 of them are suitable for practical applications.[134,135] The limiting factors for Mössbauer spectroscopy are the lifetime and the energy of the nuclear excited states.[135]

The isomer shift, δ, and the quadrupole splitting, ΔE_Q, are two of the most important parameters derived from a Mössbauer spectrum.[135] The isomer shift gives information on the oxidation number and the spin state and the bonding properties,[134,135] while quadrupole splitting data yield information on molecular structure and oxidation number and spin state.

^{57}Fe is the most suited and generally used Mössbauer-active nuclide, and ^{57}Fe Mössbauer spectroscopy is usually employed for the characterisation of iron SCO systems. The isomer shift and the quadrupole splitting are significantly different for the high and low spin states of both Fe(II) and Fe(III). In the case of Fe(II) whereas the HS state has a relatively high quadrupole splitting (ΔE_Q = 2-3 mm^{-1}) and isomer shift ($\delta = 1$ mm^{-1}), these parameters are generally smaller, $\Delta E_Q \leq 1$ mm^{-1} and $\delta \leq 0.5$ mm^{-1} for the Fe(II) LS state. Consequently, if both low and high spin states of an iron compound are present in a sample to an appreciable extent and if the relaxation time for LS↔HS oscillation is longer than the Mössbauer time window, the two spin states are distinguishable by their characteristic subspectra.

1.3. Theoretical background and methods

Although the foundations of quantum chemistry were laid only about a hundred years ago, nowadays it is already used to study a wide range of phenomena both in chemistry and molecular physics. In fact, it is used to make very diverse predictions such as equilibrium structures of molecules, molecular properties, intermolecular interactions or reaction mechanisms either in chemistry or biochemistry. It should be highlighted that today quantum chemistry is a mature science that has a very important role in almost all the other branches of chemistry. This is due to the fact that theory can give a deeper understanding of chemical processes that cannot be obtained only from experiments. One of the newest applications of quantum chemistry is found in biochemistry, where it is extremely helpful to provide insight into the mechanisms for enzymatic reactions and the relation between structure and spectroscopic properties in transition metal containing proteins.

1.3.1. Elementary quantum chemistry

An atom is formed by a nucleus and electrons moving around it. The motion of the nucleus and electrons is described by the laws of quantum mechanics. After the formulation of these laws, scientists realized that the quantum mechanics could explain the structure, the properties and the reactivity of molecules. In fact, the energy of a system can be obtained solving the Schrödinger equation ($\hat{H}\Psi = E\Psi$), the basic equation of quantum mechanics. Unfortunately, this equation is really complicated and can be only solved analytically for a few very simple cases. However, analytical and numerical solutions are possible if certain approximations are applied. In fact, quantum chemistry received a boost in the 60s when scientists started using computers. Nowadays, thanks to the development of efficient computational formalisms and high-performance computers, it is possible to calculate the energy of very large chemical systems through a quantum mechanical approach.

The energy of a system, which is very useful from a chemical point of view, can be used to compute the activation energy or study in detail the different steps of a reaction mechanism. There are two different approaches to solve the Schrödinger equation: the wave-function methods and the density functional theory (DFT). A very brief overview of these two methods is going to be given in the following sections.

1.3.1.1. Wave-function methods

As it has been previously said, the solution of the Schrödinger equation for a system would give us all the information about this system. However this equation can only be solved exactly for the simplest atomic system (H) and several approximations are required to solve the Schrödinger equation of many-particle systems.[*] The most fundamental approximation is the Born-Oppenheimer approximation, which is justified by the difference of mass between the electrons and the nuclei that allows the separation of the nuclear motion from the electron motion. This fact means that the electrons adjust almost instantaneously to slower nuclear motions. Consequently, the Schrödinger equation can be separated into a nuclear and an electronic part. Then, if we are only interested in the electronic structure it is only needed to solve the electronic Schrödinger

---

[*] For overviews of wave-function methods see refs.: (136) and (137).

equation which depends parametrically on the nuclear positions. However, other approximations are necessary to build the electronic wave-function, Ψ.

The Hartree-Fock (HF) method is the reference wave-function method. The molecular orbitals for many-electron molecules are usually constructed as a linear combination of the atomic orbitals of the corresponding atoms, a procedure which is known as the linear combination of atomic orbitals (LCAO) method. Furthermore, the wave-function has to be consistent with basic quantum mechanics and with the Pauli principle. Consequently, it is written as a determinant of one-electron molecular orbitals (Slater determinant) which by construction fulfills the antisymmetry principle for electrons. Subsequently, the shapes of the orbitals in the single Slater determinant are optimized with respect to the energy applying the variational principle which leads to the Roothaan equations. Then these equations can be solved iteratively starting off by a guess of the molecular orbital coefficients leading to solutions called self-consistent field (SCF) orbitals.

The exchange energy is well described in the HF method due to the use of an antisymmetric determinant to build the wave-function. On the other hand, this method is a mean field approximation, which implies that each electron moves in the average field of the other electrons. This is the major problem of this method because in real systems the motions of all electrons are correlated. Consequently, in the model system the average distance between electrons is smaller and the total repulsion is higher compared to the real system, because the electron correlation is neglected.

The lack of electron correlation in the HF method includes a certain degree of inaccuracy in the relative energies of molecules, which makes it not suitable for investigating chemical reactions. In order to improve the accuracy of the results obtained with HF, methods which take into account the electron correlation have been developed. Some of the "post-HF" methods are the Møller-Plesset (MP) perturbation theory, the Configuration Interaction (CI) theory and the Coupled Cluster (CC) theory. However, it has to be highlighted that adding electron correlation corrections increases both the accuracy of the results and the time needed to carry out the calculations. Consequently these methods can only be applied to relatively small systems.

1.3.1.2. Density functional theory

In the wave-function methods the determination of the wave-function is needed to describe the properties of a system. The Density Functional Theory (DFT)[†] has a completely different approach: the electronic density can provide all the properties of the system and there is no need to know the explicit form of the wave-function. The use of DFT has received a boost in the 1990s and nowadays for large systems DFT is much more used than wave-function methods due to its relatively high accuracy at rather low computational cost.

The DFT method is based on the Hohenberg-Kohn theorems formulated in 1964.[140] The first one states that for non-degenerate ground states, the energy is an unique functional of the electron density, $E[\rho]$. The second one shows that $E[\rho]$ obeys the variational principle. Consequently, it is possible to calculate the energy by minimization procedures, similar to the ones used in wave-function methods. However, a fundamental problem in DFT is that the exact form of the $E[\rho]$ is not known.

As a starting point, the energy functional can be expressed as:

[†] For overviews of density functional theory, see refs. :(138) and (139).

$$E[\rho] = T[\rho] + V_{ee}[\rho] + V_{ne}[\rho] \tag{1}$$

where T is the kinetic energy, V_{ee} electron-electron repulsion and V_{ne} is the electron-nuclei attraction (the nuclear-nuclear repulsion is not included because it is a constant within the Born-Oppenheimer approximation). Since the first two terms of Eq. 1 have no relation with the nuclear positions, they can be expressed as a single functional $F[\rho]$:

$$E[\rho] = F[\rho] + V_{ne}[\rho] \tag{2}$$

In 1965, Kohn and Sham designed a new approach based on the one-electron picture in order to compute $F[\rho]$ in a simple and accurate way.[141] In the Kohn-Sham method, a fictitious system of non-interacting particles affected by an external potential is defined. In this new scheme, the total kinetic energy of the real system, $T[\rho]$, can be written as the sum of the kinetic energy of the non-interacting system, $T_S[\rho]$, and the additional kinetic energy needed to accurately describe the real interacting system $T_A[\rho]$. Moreover the electron-electron repulsion, $V_{ee}[\rho]$, could be written as the sum of the classical Coulomb interaction, $J[\rho]$, and a non-classical part containing correlation and exchange, $E_{NC}[\rho]$. Consequently Eq. 1 and Eq. 2 can be written as:

$$E[\rho] = T_S[\rho] + T_A[\rho] + J[\rho] + E_{NC}[\rho] + V_{ne}[\rho] \tag{3}$$

If we group the $T_A[\rho]$ and $E_{NC}[\rho]$ functionals in a new term called $E_{XC}[\rho]$ we obtained the following expression:

$$E[\rho] = T_S[\rho] + J[\rho] + V_{ne}[\rho] + E_{XC}[\rho] \tag{4}$$

where the kinetic energy of the non-interacting system ($T_S[\rho]$), the classical Coulomb repulsion ($J[\rho]$) and the nuclear-electron attraction ($V_{ne}[\rho]$) can be computed explicitly and the exchange-correlation term ($E_{XC}[\rho]$) includes the corrections due to exchange, correlation, and the difference between the kinetic energies of the interacting and non-interacting systems.Subsequently, a determinant of the Kohn-Sham orbitals $\phi_i(r)$ is constructed, which leads to the Kohn-Sham equation, and the total energy is minimized respect to the shape of the orbitals iteratively:

$$\left[-\frac{1}{2}\nabla^2 + \int \frac{\rho(r')}{|r-r'|}dr' + V_{ne} + \frac{\delta E_{xc}[\rho]}{\delta\rho(r)} \right]\phi_i(r) = \varepsilon_i\phi_i(r) \tag{5}$$

In the Kohn-Sham equation no approximations are introduced and if the exact exchange-correlation functional ($E_{XC}[\rho]$) could be used, the exact energies and electron density would be obtained. Consequently, the accuracy of a DFT method depends on the quality of the exchange-correlation functional.

1.3.1.2.1.   *Exchange-correlation functionals*

The exchange correlation functionals are generally split into two different terms: the exchange part and the correlation part. The exchange part is associated with the interaction of the same spin, while the correlation part represents the interaction between electrons with opposite spin.

$$E_{XC}[\rho] = E_X[\rho] + E_C[\rho] \qquad (6)$$

The Local Density Approximation

The Local Density Approximation (LDA) is the simplest approach to represent the exchange-correlation functional and it assumes that the density behaves like a homogeneous electron gas. The simplest way to describe the exchange part was proposed to Slater.[142] There are numerous formulations for the correlation energy in LDA. One of the most common formulas was developed by Vosko, Wilk and Nusair (VWN),[143] and it was parameterized to reproduce the highly accurate Monte Carlo results from Ceperley and Alder.[144,145] Another popular correlation functional is the one developed by Perdew (PL).[146]

Despite its simplicity, the LDA methods usually provide surprisingly good results.[139] They underestimate bond distances, but they yield good geometries, good vibrational frequencies and reasonable charge densities, except in the regions close to nuclei.[147] However, LDA methods are not suitable for systems with weak bonds or for making reliable thermochemical predictions and they generally overestimate the bond energy by approximately 30%.

Generalized Gradient Approximation methods

The Generalized Gradient Approximation methods (GGA) take into account the non-homogeneity of the true electron density. In their expressions, the exchange and correlation energy depend both on the density and the gradient of the density ($\nabla \rho(r)$).[139]

The development of GGA methods has followed two different approaches. The first strategy is based on numerical fitting procedures, whereas the second one was founded on basic principles derived from quantum mechanics. Exchange functionals that follow the first approach include Becke88 (B),[148] and Optx (O).[149] Examples for the second philosophy include Becke86 (B86)[150] and Perdew-Burke-Ernzerhof (PBE).[151] Exemples of GGA correlation functionals are Perdew 86 (P86),[152] Perdew-Wang 91 (PW91)[153] and Lee-Yang-Parr (LYP).[154] Although each exchange functional could, in principle, be combined with any of the correlation functionals, only a few combinations are currently in use.[139] The most used exchange functional is the Becke88 and it is combined either with P86 or LYP correlation functionals.

In general, GGA methods represent a significant increase in accuracy over LDA methods. They tend to give better total and atomization energies, structural energy differences and energy barriers. However, GGA methods are not accurate enough to predict correctly certain chemical aspects of molecules, such as the van der Waals interactions.

Quite recently a new group of DFT functionals based on the GGA has been developed.[155] These methods, which are called meta-GGA (m-GGA), depend on higher order density gradients and/or on the kinetic energy density. They represent an improvement in the determination of certain properties but they are also more

challenging from the technical point of view. Some examples for m-GGA functionals include B95,[156] TPSS[157] and VSXC.[158]

Hybrid Density Functionals Methods

Hybrid density functionals combine the exchange-correlation functional of a conventional GGA method with a percentage of HF exchange. The optimal proportion of each functional cannot be obtained from first-principles and it is found semiempirically. A way to do so is using experimental data for a representative set of small molecules. Some examples of hybrids density functionals are B3LYP,[148,154,156] BH&HLYP[148,154] and MPWIK.[153,159-161] They have allowed a significant improvement over GGAs for many properties. Consequently, they have become very popular in quantum chemistry and nowadays they are widely used. It should be noted that B3LYP is by far the most popular and most widely used functional[155] and this is the functional used to carry out an important part of the theoretical calculations of the present Thesis.

1.3.1.3.   Density functional theory for transition metal compounds

DFT can be used to describe the structure, properties and reactivity of metal-containing systems and, consequently, this methodology is used in several fields of chemistry, such as inorganic, bioinorganic and organometallic chemistry.[162] This methodology can provide reasonable good results for geometries, vibrational frequencies, energies, certain spectroscopic properties and Mössbauer parameters.[163] Although non-experts can easily make predictions thanks to the wide range of programs having this methodology implemented, one has to be aware of the limitations of DFT.[164]

It should be highlighted that significant variations, around 20 kcal/mol, in the spin-state splitting in transition metal compounds have been found when using different DFT methods.[165,166] In fact, this effect is usually observed for first-row transition metal systems, which are the ones that display HS states more often.

Generally, GGA functionals tend to overstabilize LS forms and hybrid functionals, that contain a certain proportion of HF exact exchange, lead to better results in numerous cases. Actually, 15% HF exact exchange seems to provide the better description of the spin-state energetics for some compounds.[167,168] However, the optimal degree of exact exchange varies depending on the compounds and there is little agreement on which method has to be used to obtain the most accurate results.

Moreover, since it is hard to carry out benchmark studies for transition compounds, it also complicated to know what the correct value is and the functional that reproduces it.[165,166] On the other hand, according to recent studies,[165,166] it seems that the spin-state energetics dependence on the degree of exact exchange included in the functional comes from significant self-interaction errors that arise when using GGA functionals. However, it is quite improbable to find a degree of exact exchange that leads to the correct spin-state splitting for the majority of metallic compounds. At this point it should be stressed that there are a few GGA and meta-GGA functionals that give better results for the spin-state splitting for certain systems.[149,151,169]

As it has been mentioned previously, two different strategies have been used to develop the DFT functionals currently used: (i) the explicit parameterization to reproduce as well as possible experimental properties of compounds mostly including main-group elements and (ii) the development including as many physical constraints as possible in the construction of the new functional. Although the functionals using the second approach are only tested with respect to experimental data after their

construction, the results from previous benchmark studies have had some influence in their conception. It seems that the inclusion of transition metal compounds into the groups of compounds used to parameterize or test the new functionals could lead to an improvement of the description of this kind of compounds, but perhaps also for main-group systems. Taking into account spin-state splitting in the parametrization of functionals could be extremely useful because this property is very sensitive to the functional used to carry out the theoretical calculations.

DFT can be very useful to predict spin-state splitting of compounds containing transition metals, but the functional used to carry out the calculation has to be chosen with care. However, today it does not exist a functional capable of giving the correct spin-state energetic for any metallic system. Consequently, all computational projects should test the chosen functional comparing the obtained results with available experimental data if possible. In case it is not possible to carry out any benchmark study, it is suggested to use several functionals, GGA and hybrid functionals, and interpret the results very carefully if large differences are found.

1.3.1.4.   Basis Sets

Basis sets are groups of functions used in wave-function and DFT calculations to describe the electron distribution.[138] A wide range of basis sets is available and some of them are described in the following sections.

1.3.1.4.1.   Slater and Gaussian Type Orbitals

The most accurate basis sets for quantum-chemistry programs are formed by Slater-type orbitals (STO's, see Eq. 8), because they have a cusp at the nucleus and an exponentially decaying long tail.

$$\phi^{STO} = N Y_{l,m}(\theta,\varphi) r^{n-1} e^{-\zeta r} \tag{8}$$

However, three- and four-center two-electron integrals with these orbitals are not analytically available, and therefore they are often replaced with Gaussian type-orbitals (GTO's, see Eq. 9), for which these integrals are much simpler.

$$\phi^{GTO} = N Y_{l,m}(\theta,\varphi) r^{(2n-2-l)} e^{-\zeta r^2} \tag{9}$$

At this point it has to be stressed that GTO's do not have a cusp at the nucleus and they fall off to zero rapidly. Consequently, a number of primitive GTO's is combined to form a contracted one that resembles better the STO shape.

1.3.1.4.2.   Classification of Basis Sets

The *minimum basis set* is a basis set where only enough functions to contain all the electrons of the neutral atoms are employed. Doubling of all basis functions leads to a Double Zeta (DZ) basis set, which allows a much better description of the electron distribution. If only the valence orbitals are doubled, a split valence basis is obtained

which is called Valence Double Zeta (VDZ). The number of basis function can be multiplied by three, four and five obtaining Triple Zeta (TZ), Quadruple Zeta (QZ) and Quintuple Zeta (5Z), respectively.

Polarization functions are added to basis sets to describe better the distortion of the molecular orbitals. On the other hand, diffuse functions are needed when loosely bound electrons are present, for example in anions or excited states, or when the property of interest is dependent on the wave-function tail, for exemple polarizability.

1.3.1.4.3.   Contracted Basis Sets

The most common approach to construct GTO basis sets is combining a full set of individual GTOs, the so-called primitives (PGTOs), into a smaller set of functions by forming fixed linear combinations (contractions). Contraction is particularly useful for the inner electrons orbitals, because a relative large number of functions is required to represent the wave-function cusp near the nucleus. Contracting a basis set reduces the flexibility of the basis set, but it also reduces significantly the computational cost of the calculations.

Pople Style Basis Sets

STO-nG basis set[170]

The exponents of the PGTO are determined by fitting to the STO minimum basis. Using more than three PGTOs to represent the STO gives little improvement and the STO-3G basis is a commonly used minimum basis.

k-nlG and k-nlmG basis set[171-173]

In these basis sets the *k* indicates the number of PGTOs used to represent the core orbitals and the *nlm* indicate both the number of functions assigned to each valence orbitals and the number of PGTOs used for their representation. Two values indicate a split valence, while three values indicate a triple split valence. This type of basis sets has the further restriction that the same exponent is used for both the s- and the p-functions in the valence, which increases the computational efficiency, but decreases the flexibility of the basis set.

Dunning-Huzinaga Basis Sets

The Dunning-Huzinaga type basis sets do not need equal exponents for the s- and p- functions like in the Pople style basis sets. Consequently they are more flexible, but computationally also more expensive.[174]

Correlated Basis Sets: Atomic Natural Orbitals Basis Sets and Correlation Consistent Basis Sets

The Atomic Natural Orbitals basis sets (ANO) are obtained applying the general contraction scheme to Natural Orbitals, which are obtained from a correlated calculation on the free atom, typically at the CISD level.[175]

The Correlation Consistent basis sets are constructed with the aim of recovering the correlation energy of the valence electrons. Their name refer to the fact that the basis sets are designed so that functions which contribute similar amounts of correlation

energy are included at the same stage, independently of the function type.[176] Several Correlation Consistent basis sets with different final number of contracted functions are available: cc-pVDZ, cc-pVTZ, cc-pVQZ, cc-pV5Z and cc-pV6Z (correlation consistent polarized Valence Double/Triple/Quadruple /Quintuple/Sextuple Zeta).

The main improvement of the ANO and Correlation Consistent Basis Sets is their capacity of converging toward the basis set limit.

1.3.1.4.4.   *Effective Core Potential Basis Sets*

Heavy atoms need a relatively large number of basis functions to expand the corresponding orbitals; otherwise the valence orbitals will not be properly described. However, it is known that the most inner electrons in this kind of atoms are usually unimportant in a chemical sense since they do not contribute either to the chemical properties or reactivity of molecules. In order to save computational effort without losing much accuracy, the core electrons of these elements can be described effectively using an *Effective Core Potential* (ECP), which is also called *Pseudopotential* (Eq. 10).

$$U^{ECP} = \sum_i a_i r^{n_i} e^{-\alpha_i r^2}$$

(10)

In the ECPs the core electrons are modelled by a suitable function and only the valence electrons are treated explicitly. Consequently the use of ECPs reduces the computational cost of theoretical calculations and quite good results are obtained at a fraction of the cost of a calculation involving all electrons. Moreover, thanks to ECPs all the atoms of the periodic table are accessible to certain wave-function and DFT calculations. Furthermore, it should be stressed that relativistic effects can be taken into account in the construction of ECPs.

1.3.2. Theoretical study of reaction mechanisms

1.3.2.1.   Transition state theory

The Transition State Theory (TST)[177,178] was developed simultaneously by Eyring and by Evans and Polanyi during 1930s.[179] Its main goal was to calculate chemical reactions rate constants, which can often be measured experimentally. However, unfortunately, TST was not very successful doing so.[180] This fact was due to the high accuracy needed in the evaluation of the potential energy surface (PES) in order to compute reaction rates. Nevertheless, this theory has provided a very useful tool to unravel how chemical reactions occur and it is very valuable to compute the enthalpy, the entropy and the free energy activation for reactions whose rate constants are known experimentally.[138]

According to TST, a chemical transformation proceeds from one energy minimum, reactants, to another energy minimum, the products, through an intermediate maximum, the transition state (TS). The reaction coordinate (RC) is the lowest energy path that leads from reactants to products on a multidimensional PES and it has maximum of energy called TS (Scheme 12). In a PES, the TS corresponds to a first-order saddle point, that has a maximum in the reaction coordinate direction and minima in all the other coordinates.
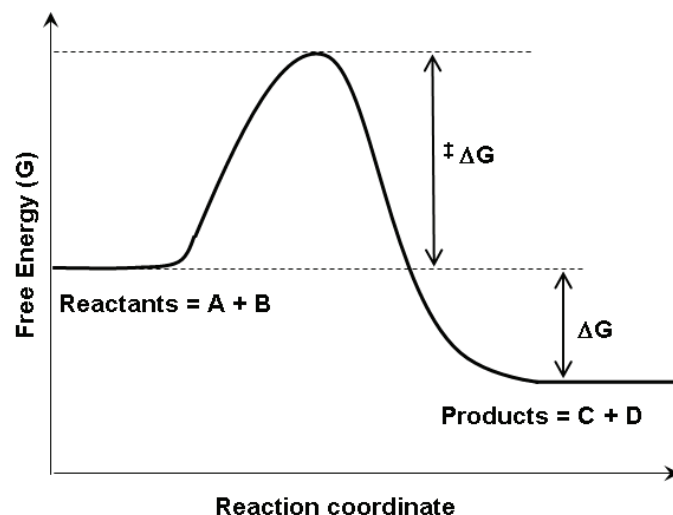
Scheme 12: Reaction path an elementary single-step bimolecular reaction

The TST assumes an equilibrium energy distribution in all possible quantum states at all the points of the reaction coordinate. Supposing that the molecules at the TS are in equilibrium with the reactant molecules and taking into account that the probability of finding a molecule in a certain quantum state is proportional to a Boltzmann distribution, the following expression can be written:

$$k = \frac{k_B T}{h} e^{-\Delta G^{\ddagger} / RT} \tag{11}$$

where k is the rate constant, k_B is Boltzmann's constant, h is Planck's constant and $\Delta G^{\ddagger}$ is the Gibbs free energy difference between the TS and reactant. The $\Delta G^{\ddagger}$ is calculated at the saddle point of the Born-Oppenheimer PES, which is characterized by having a single imaginary frequency that corresponds to the normal mode that occurs along the reaction path.

Examination of Eq. 11 shows that an increase of $\Delta G^{\ddagger}$ by 1.36 kcal/mol results in a reaction ten times slower (k/10) at a temperature of 298.15K. Consequently the rate constant k can only be predicted to an order of magnitude when using TST, since an accuracy of 3 kcal/mol for the relative energies is considered a good value for the majority of computational methods.[166]

The TST expression only takes into account those molecules that pass from the reactant to products through the TS. In order to include the quantum mechanical effect known as tunnelling, which refers to molecules that tunnel through the barrier to form the product, a transmission effect, κ, can be introduced. This factor can also take into consideration the "recrossings", which refer to reactant molecules that pass through the TS but go back to the reactants side.

Computational chemistry can be very useful to study chemical and biochemical reactions. In fact, the free energy of reactants, products, intermediates and transition states can be found using theoretical calculations. Therefore the shape of the potential energy surface along a certain reaction coordinate, which supplies thermodynamic and kinetic information about a given reaction mechanism, can be obtained. At this point, it

should be highlighted that in the case of a multistep mechanism, the rate-limiting step corresponds to the one whose transition state has the highest activation barrier.

1.3.2.2.   Chemical models

In order to carry out an accurate theoretical study of a certain reaction mechanism both the computational method and the chemical model chosen are important to obtain reliable results. Constructing a good model implies collecting all the available experimental data about the system one has the intention to study. Once the model is set up, the PES can be explored and information about the reaction mechanism can be obtained.

Nowadays there is a growing interest in the study of enzymatic reactions involving transition metals. However, enzymes are formed by several thousands of atoms and it is impossible to study the whole system using a quantum chemical method. There are two different strategies to tackle this problem.[181] In the first approach a combination of quantum mechanics and molecular mechanics (QM/MM) methods is used to take into account the entire enzyme. The active site is studied by an accurate quantum method, while the rest of system is treated with molecular mechanics. The QM/MM methods were pioneered by Warshel, Levit, Singh and Kollman[182,183] and today there is an increasing number of variations.[184] The second approach, which is the one used in this Thesis, is based on studying a model of the active site of the enzyme. The model is based on the X-ray structure of the protein, if it is available, and includes the metal ions and the amino acids residues essential for the investigated mechanism. It has to be highlighted that the amino acids are usually reduced to smaller molecules with similar functionality.[11] For example, histidine can be replaced by imidazole, methionine by dimethylsulfide and glutamate or aspartate by acetate or formate.[185] In order to reproduce the protein strain and keep the model close to the X-ray structure, specific restrictions on some nuclear coordinates are usually applied.[186]

Quantum chemistry calculations in gas-phase manner neglect the interaction between the model complex and surrounding medium. However, the solute properties usually depend on the solvent, particularly a polar one, and the surrounding medium. Consequently, in order to reproduce the effect of the rest of the protein, the model is embedded in a dielectric continuum with a low dielectric constant ($\varepsilon = 4$). The used value for the dielectric constant corresponds roughly to a mixture of the value for the interior of a protein ($\varepsilon = 2\text{-}3$) and for water ($\varepsilon = 80$).[187] It should be noted that modelling the protein surrounding as a dielectric continuum is only valid if the hydrogen bonding interactions between the active site and the solvent are explicitly included in the quantum mechanical model.

Biomimetic compounds are much smaller than proteins and, generally, they are computationally affordable to use as a whole. However, if they are too big to be studied with a quantum mechanics method, one of the two previously mentioned approaches has to be used. It should be highlighted that if the solvent in which the reaction occurs is modelled as a dielectric continuum, the corresponding dielectric constant has to be used.

2. Objectives

2. Objectives

The presence of computational and theoretical chemistry is increasing in chemical research in nearly all fields. Theoretical calculations can help to better explain structure, properties, and reactivity in metallic compounds, in such diverse areas as inorganic, organometallic and bioinorganic chemistry. They can even give some insight into the catalytic cycles of systems as complicated as enzymes. However, it is essential to use the suitable methodology for the systems that have to be studied in order to obtain reliable theoretical results.

The goals of this Thesis can be divided into two different groups. The first group includes the theoretical study of the reaction mechanism of several copper-containing systems with different Cu_n-O_2 structures. First of all, we will study the catalytic cycle of the catechol oxidase enzyme which has a μ-η^2:η^2-peroxodicopper(II) active site. Then we will investigate the reaction mechanism of a μ-η^2:η^2-peroxodicopper(II) complex capable of hydroxylating phenolates. We have selected this particular complex because an intermediate of the reaction with a bis-μ-oxo-dicopper(III) core have been observed experimentally. Finally, we will study a copper(II)-superoxo complex capable of hydroxylating phenols with incorporated oxygen atoms derived from the $Cu(II)$-$O_2\cdot^-$ moiety. These three different studies will be carried out with the aim of providing some insight into the nature of the chemical and biological copper-promoted oxidative processes with 1:1 and 2:1 $Cu(I)/O_2$-derived species.

The goal of the second part of this Thesis is to evaluate the reliability of different theoretical approaches used to study the electronic structure and reactivity of systems containing copper, iron or other transition metals. First, we will study the ground and low-lying electronic states of CuO_2 doublet. This structure intervenes in biochemical mechanisms, such as the catalytic cycle of Cu-Zn-superoxide dismutase, whose theoretical study requires to describe correctly the interaction of $Cu(I)$ with the superoxide radical. Subsequently, we will examine the dependence on the type and the size of the basis set of the relative spin-state energies for different Fe(III) compounds computed with the OPBE functional. The correct description of the relative spin-state energies is essential to properly describe the reactivity of these compounds. Following this, we will carry out two additional studies using OPBE to test its reliability describing spin-state splittings. We will study a wide range of Fe(II) complexes with *tris*-pyrazolylborate and *tris*-pyrazolylmethane ligands, whose spin states depend very much on the substituents in the pyrazolyl rings, and in many cases even on the counterion. At last we will study complexes with triazacyclononane and tris-pyrazolylborate ligands for which experimental data are available for a series of different transition metals.

3. Publications

3.1. Theoretical study of the catalytic mechanism of catechol oxidase

Güell, M.; Siegbahn, P.E.M
J. Biol. Inorg. Chem. 12 (2007) 1251–1264

Institut de Química Computacional, Universitat de Girona, Campus de Montilivi, 17071 Girona, Spain
Department of Biochemistry and Biophysics, Stockholm University, 106 91 Stockholm, Sweden

Abstract

The mechanism for the oxidation of catechol by catechol oxidase has been studied using B3LYP hybrid density functional theory. On the basis of the X-ray structure of the enzyme, the molecular system investigated includes the first-shell protein ligands of the two metal centers as well as the second-shell ligand Cys92. The cycle starts out with the oxidized, open-shell singlet complex with oxidation states $Cu_2(II,II)$ with a μ-η^2:η^2 bridging peroxide, as suggested experimentally, which is obtained from the oxidation of $Cu_2(I,I)$ by dioxygen. The substrate of each half-reaction is a catechol molecule approaching the dicopper complex: the first half-reaction involves Cu(I) oxidation by peroxide and the second one Cu(II) reduction. The quantitative potential energy profile of the reaction is discussed in connection with experimental data. Since no protons leave or enter the active site during the catalytic cycle, no external base is required. Unlike the previous density functional theory study, the dicopper complex has a charge of +2.

Keywords: Catechol oxidase - Copper enzymes - O_2 cleavage - Hybrid density functional theory

3.2. Theoretical study of the hydroxylation of phenolates by the Cu$_2$O$_2$(N,N'-dimethylethylendiamine)$_2$$^{2+}$ complex

Güell, M.; Luis, J.M.; Solà, M.; Siegbahn, P.E.M

Departament de Química, Institut de Química Computacional, Universitat de Girona, Campus de Montilivi, 17071 Girona, Spain
Department of Biochemistry and Biophysics, Stockholm University, 106 91 Stockholm, Sweden

Abstract

Tyrosinase catalyzes the *ortho* hydroxylation of monophenols and the subsequent oxidation of the diphenolic products to the resulting quinones. In efforts to create biomimetic copper complexes that can oxidize C–H bonds, Stack and coworkers recently reported a synthetic μ-η^2:η^2-peroxodicopper(II)(DBED)$_2$ complex (DBED is *N,N'*-di-*tert*-butylethylenediamine), which rapidly hydroxylates phenolates. A reactive intermediate consistent with a bis-μ-oxo-dicopper(III)-phenolate complex, with the O–O bond fully cleaved, is observed experimentally. Overall, the evidence for sequential O–O bond cleavage and C–O bond formation in this synthetic complex suggests an alternative mechanism to the concerted or late-stage O–O bond scission generally accepted for the phenol hydroxylation reaction performed by tyrosinase. In this work, the reaction mechanism of this peroxodicopper(II) complex was studied with hybrid density functional methods by replacing DBED in the μ-η^2:η^2-peroxodicopper(II)(DBED)$_2$ complex by *N,N'*-dimethylethylenediamine ligands to reduce the computational costs. The reaction mechanism obtained is compared with the existing proposals for the catalytic *ortho* hydroxylation of monophenol and the subsequent oxidation of the diphenolic product to the resulting quinone with the aim of gaining some understanding about the copper-promoted oxidation processes mediated by 2:1 Cu(I)O$_2$-derived species.
Electronic supplementary material The online version of this article (doi:10.1007/s00775-008-0443-y) contains supplementary material, which is available to authorized users.

3.3. Theoretical study of the hydroxylation of phenols mediated by an end-on bound superoxo copper(II) complex

Güell, M.; Luis, J.M.; Siegbahn, P.E.M.; Solà, M

Institut de Química Computacional and Departament de Química, Universitat de Girona, Campus de Montilivi, 17071 Gerona, Spain
Department of Biochemistry and Biophysics, Stockholm University, 106 91 Stockholm, Sweden

Abstract

Peptidylglycine α-amidating monooxygenase and dopamine β-monooxygenase are copper-containing proteins which catalyze essential hydroxylation reactions in biological systems. There are several possible mechanisms for the reductive O_2-activation at their mononuclear copper active site. Recently, Karlin and coworkers reported on the reactivity of a copper(II)–superoxo complex which is capable of inducing the hydroxylation of phenols with incorporated oxygen atoms derived from the $Cu(II)-O_2{}^-$ moiety. In the present work the reaction mechanism for the abovementioned superoxo complex with phenols is studied. The pathways found are analyzed with the aim of providing some insight into the nature of the chemical and biological copper-promoted oxidative processes with 1:1 $Cu(I)/O_2$-derived species. Electronic supplementary material The online version of this article (doi:10.1007/s00775-008-0447-7) contains supplementary material, which is available to authorized users.

SUPPORTING INFORMATION

Theoretical study of the hydroxylation of phenols mediated by an end-on bound superoxo copper(II) complex

Mireia Güell,[a,b] Josep M. Luis,[a] Miquel Solà[a] * and Per E. M. Siegbahn[b] *

[a] *Institut de Química Computacional, Universitat de Girona, Campus de Montilivi, E-17071 Girona, Spain.*
[b] *Department of Biochemistry and Biophysics, Stockholm University, SE 106 91, Stockholm, Sweden.*

Table S1. Molecular orbitals of the uB3LYP/lacvp optimized triplet electronic state for the studied complex.

Table S2. Spin density populations for the atoms of the substrate of all stationary points located on the PES for the reaction mechanism studied at the B3LYP/lacvp level of theory.

Table S1. Molecular orbitals of the uB3LYP/lacvp optimized triplet electronic state for the studied complex.

alpha	beta
134 (-)	134 (-)
133 (-)	133 (-)
132 (-)	132 (-)
131 (↑)	131 (-)
130(↑)	130 (-)
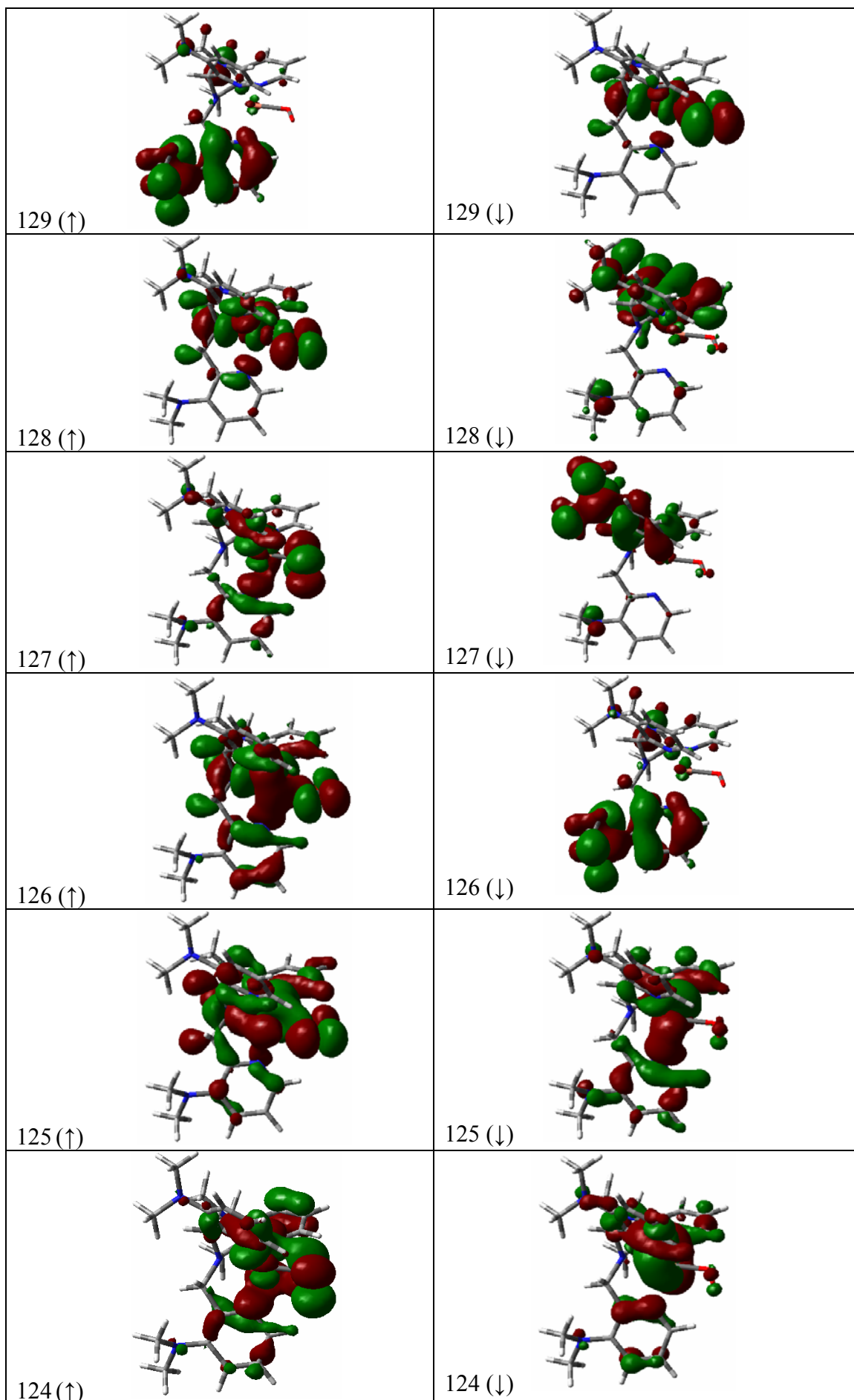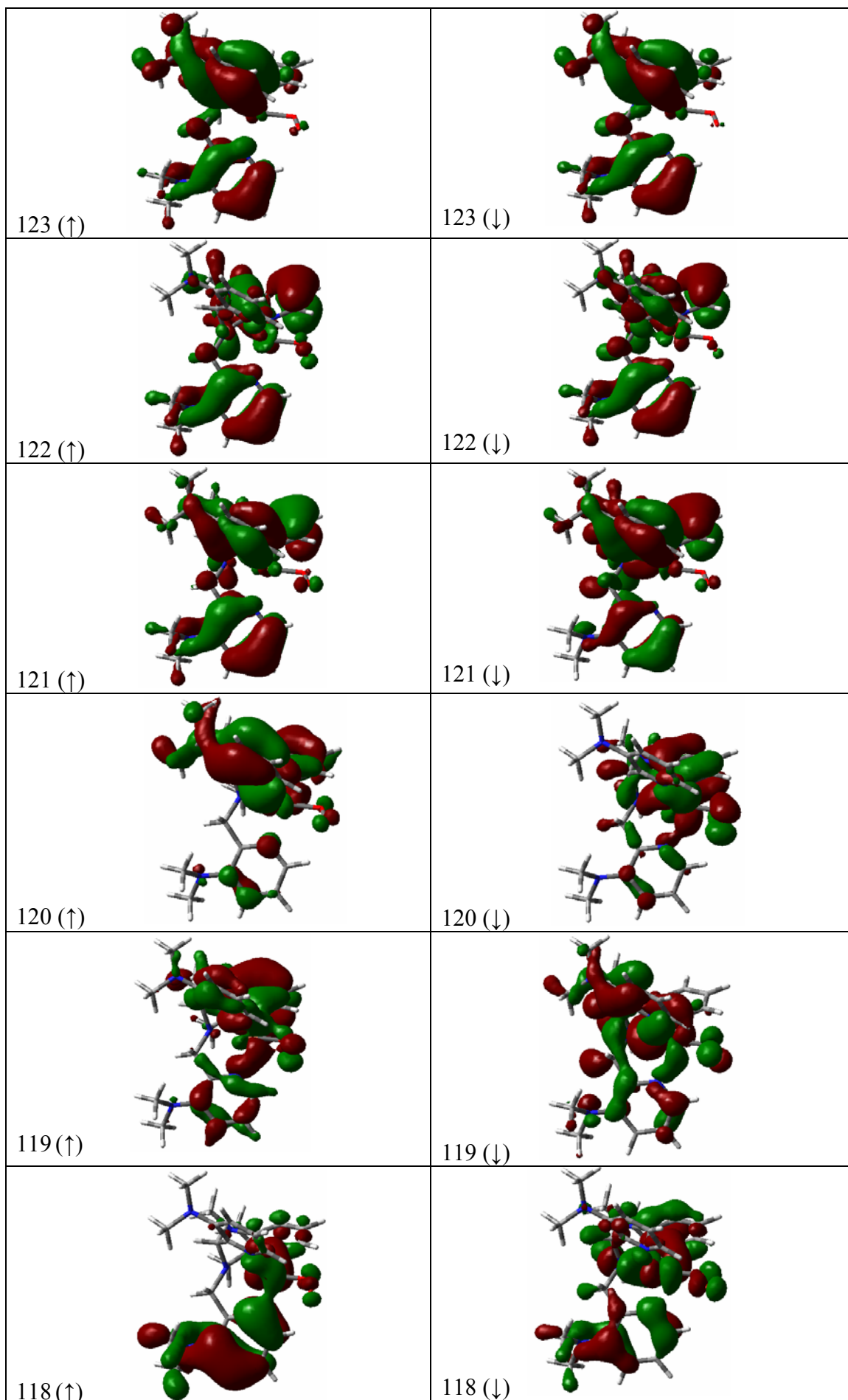
129 (↑)	129 (↓)
128 (↑)	128 (↓)
127 (↑)	127 (↓)
126 (↑)	126 (↓)
125 (↑)	125 (↓)
124 (↑)	124 (↓)

123 (↑)   123 (↓)

122 (↑)   122 (↓)

121 (↑)   121 (↓)

120 (↑)   120 (↓)

119 (↑)   119 (↓)

118 (↑)   118 (↓)

Table S2. Spin density populations for the atoms of the substrate of all stationary points located on the PES for the reaction mechanism studied at the B3LYP/lacvp level of theory.

Structures	multiplicity	Spin density				
		O_C	C_A	C_B	C_C	C_D
1	s	0.00	0.00	0.00	0.00	0.00
TS12		-0.21	0.02	-0.14	0.09	-0.21
2		-0.39	0.02	-0.29	0.17	-0.40
3		-0.44	0.09	-0.32	0.18	-0.39
TS34		-0.20	0.04	-0.15	0.10	-0.24
4		0.00	0.00	0.00	0.00	0.00
TS45		0.01	0.00	0.02	-0.01	0.01
5		0.00	0.00	0.00	0.00	0.01
TS56		0.00	0.00	-0.01	0.00	0.02
6		-0.19	0.05	-0.14	0.09	-0.19
1	t	0.01	0.00	0.00	0.00	0.00
TS12		0.22	0.02	0.15	-0.09	0.22
2		0.39	-0.02	0.29	-0.17	0.40
3		0.46	-0.11	0.32	-0.18	0.38
TS35		0.26	-0.06	0.23	-0.14	0.27
5		0.00	0.00	0.01	0.00	-0.02
TS56		0.00	0.00	0.01	0.01	0.01
6		0.40	-0.05	0.21	-0.07	0.25

3.4. The ground and low-lying electronic states of CuO$_2$. Yet another problematical species for DFT methods

Güell, M.; Luis, J.M.; Rodríguez-Santiago, L.; Sodupe, M.; Solà, M.

Institut de Química Computacional and Departament de Química, Universitat de Girona, Campus de Montilivi E-17071, Girona, Catalonia, Spain, and Departament de Química, Universitat Autònoma de Barcelona, Bellaterra, E-08193 Barcelona, Spain

Abstract

The C_{2v} and C_s ground and low-lying states of doublet CuO$_2$ are examined for a series of different density functionals (pure, hybrid, and meta-hybrid) and CCSD(T) methods. The effect of changing the B3LYP functional a_0 parameter is also explored. CCSD(T) results at the complete basis set limit show that the relative stability of the different electronic states is $^2\mathrm{A}_2(C_{2v}) < {}^2\mathrm{A}''(C_s) < {}^2\mathrm{B}_2(C_{2v}) < {}^2\mathrm{A}'(C_s) \ll {}^2\mathrm{A}_1(C_{2v}) < {}^2\mathrm{B}_1(C_{2v})$. Unlike CCSD(T), all DFT methods analyzed in this work erroneously predict the end-on $^2\mathrm{A}''$ state as the ground state for CuO$_2$ irrespective of the type of functional and percentage of Hartree−Fock (exact) exchange included in the B3LYP-like functional. Among the different functionals tested, B3LYP gives the best geometries and relative energies for the different electronic states when compared to CCSD(T) results. As for the effect of the a_0 parameter, it is found that the B3LYP-like functional yielding better geometries contains 20% of exact exchange, although somewhat unexpectedly, the B3LYP-like functional with a larger contribution of exact exchange (90%) is the one that gives the smaller standard deviation for relative energies.

SUPPORTING INFORMATION

The Ground and Low-Lying Electronic States of CuO$_2$.

Yet another problematical species for DFT methods

Mireia Güell,[1] Josep M. Luis,[1]
Luís Rodríguez-Santiago,[2] Mariona Sodupe[2] and Miquel Solà[1*]

[1] *Institut de Química Computacional and Departament de Química, Universitat de Girona, Campus de Montilivi E-17071, Girona, Catalonia, Spain.*
[2] *Departament de Química, Universitat Autònoma de Barcelona, Bellaterra, E-08193 Barcelona, Spain.*

Figure S1. Schematic and qualitative MO diagram for the interaction between the Cu (^{2}S) and O$_2$ ($^3\Sigma_g^-$) fragments in the ^{2}B$_2$ electronic state of the C$_{2v}$ CuO$_2$ species.

Table S1. Parameter Sets Employed for B3LYP Calculations.

Table S2. The S^2 expectation value for the different electronic states analyzed and methods of calculation used.

Tables S3-S8. Molecular orbitals of the UB3LYP/6-311+G(d) optimized ^{2}A"(C$_s$), ^{2}A'(C$_s$), ^{2}A$_2$(C$_{2v}$), ^{2}B$_2$(C$_{2v}$), ^{2}A$_1$(C$_{2v}$) and ^{2}B$_1$(C$_{2v}$) electronic states for the doublet CuO$_2$ species.

Table S9. Mulliken Charges for the copper atom of the Ground and Low-Lying Electronic States of CuO$_2$ at Different Levels of Theory with Basis 6-311+G(d).

Table S10. O–O bond distances (Å) in O$_2$ and O$_2^-$ species at Different Levels of Theory with Basis 6-311+G(d).

Tables S11-S17. Calculated harmonic vibrational frequencies (cm^{-1}) for the ground and low-lying electronic states of CuO, free O$_2$ and free O$_2^-$ at different levels of theory with the 6-311+G(d) basis set.

Table S18. First ionization potential (eV) of Cu computed at different levels of theory.

Table S19. Binding dissociation energies (kcal·mol^{-1}) of CuO$_2$ in its the electronic ground state with the 6-311+G(d) basis set for different parameter sets used in B3LYP-like functionals.

Figure S1. Schematic and qualitative MO diagram for the interaction between the Cu (^{2}S) and O$_2$ ($^3\Sigma_g^-$) fragments in the ^{2}B$_2$ electronic state of the C$_{2v}$ CuO$_2$ species.
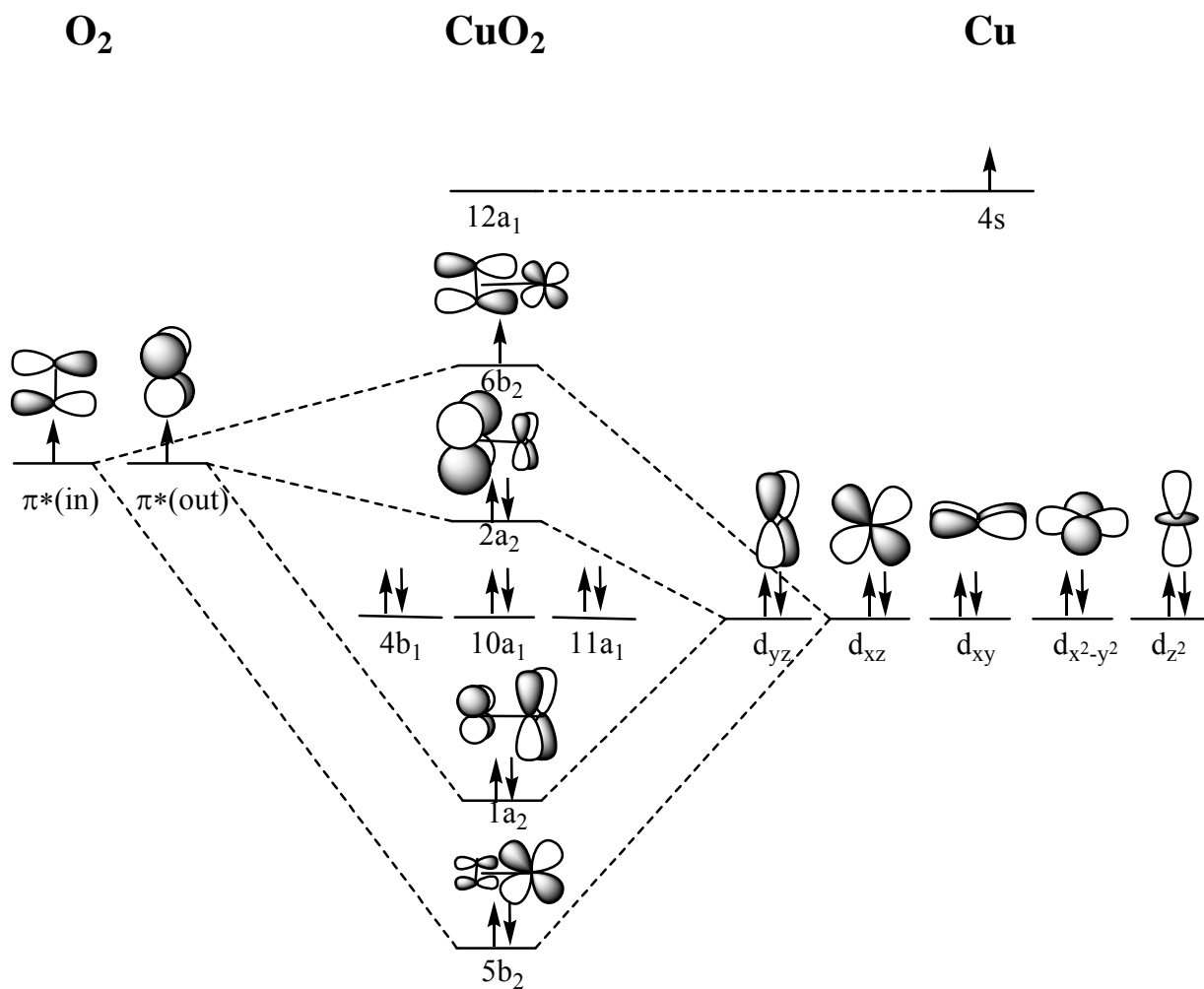
Table S1. Parameter Sets Employed for B3LYP Calculations.

Paramater set	a_0	a_x	a_c
Set 0[a]	0.000	1.000	1.000
Set 1	0.100	0.900	0.900
Set 2	0.200	0.800	0.800
Set 3	0.300	0.700	0.700
Set 4	0.400	0.600	0.600
Set 5	0.500	0.500	0.500
Set 6	0.600	0.400	0.400
Set 7	0.700	0.300	0.300
Set 8	0.800	0.200	0.200
Set 9	0.900	0.100	0.100

[a] This parameter set corresponds to BLYP functional.

Table S2. The S^2 expectation value for the different electronic states analyzed and methods of calculation used.

symmetry	state	HF	OLYP	OPBE	B3LYP	B3LYP*	BHandH	VSXC	HCTH	TPSS	CCSD(T)
C_s	$^2A''$	0.772	0.952	1.021	0.928	0.924	0.811	0.864	0.909	0.875	0.762
	$^2A'$	0.770	0.762	0.765	0.764	0.764	0.761	0.932	0.889	0.884	0.760
C_{2v}	$^2A_2$	0.784	0.757	0.757	0.758	0.757	0.763	0.758	0.757	0.755	0.753
	$^2B_2$	0.801	0.759	0.757	0.765	0.763	0.770	0.762	0.760	0.759	0.758
	$^2A_1$	1.734	0.752	0.754	0.754	0.782	1.340	0.752	0.752	0.754	0.753
	$^2B_1$	0.752	0.753	0.752	0.813	0.753	0.755	0.754	0.753	0.752	0.756

symmetry	state	B3LYP									
		0	1	2	3	4	5	6	7	8	9
C_s	$^2A''$	0.862	0.912	0.927	0.895	0.821	0.779	0.767	0.765	0.765	0.765
	$^2A'$	0.761	0.763	0.765	0.761	0.760	0.760	0.761	0.762	0.763	0.764
C_{2v}	$^2A_2$	0.755	0.756	0.758	0.760	0.761	0.763	0.765	0.767	0.769	0.771
	$^2B_2$	0.758	0.762	0.766	0.769	0.772	0.774	0.776	0.778	0.781	0.782
	$^2A_1$	0.789	0.757	0.875	1.047	1.249	1.440	1.560	1.628	1.667	1.692
	$^2B_1$	0.776	0.753	0.754	0.756	0.757	0.756	0.754	0.753	0.752	0.752

Table S3. Molecular orbitals of the uB3LYP/6-311++G(d,p) optimized $^2A_2(C_{2v})$ open-shell electronic state for the CuO_2 doublet.

alpha	beta
 12a$_1$ (-)	 2a$_2$ (-)
 6b$_2$ (↑)	 12a$_1$ (-)
 2a$_2$ (↑)	 6(b$_2$) (↓)
 11a$_1$ (↑)	 11a$_1$ (↓)
 4b$_1$ (↑)	 4b$_1$ (↓)
 10a$_1$ (↑)	 10a$_1$ (↓)
 1a$_2$ (↑)	 1a$_2$ (↓)
 5b$_2$ (↑)	 5b$_2$ (↓)

Table S4. Molecular orbitals of the uB3LYP/6-311++G(d,p) optimized $^2B_2$ (C_{2v}) open-shell electronic state for the CuO_2 doublet.
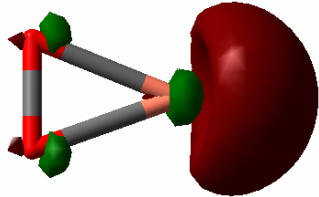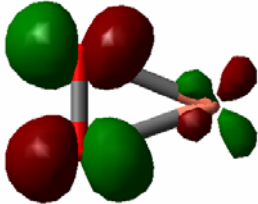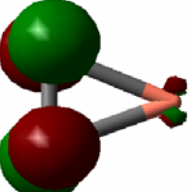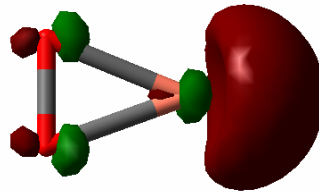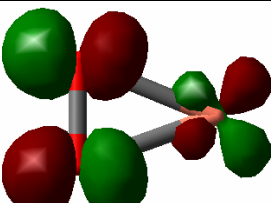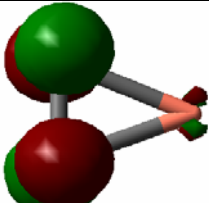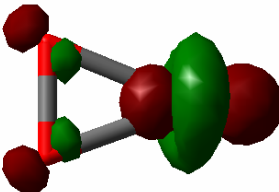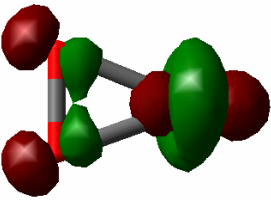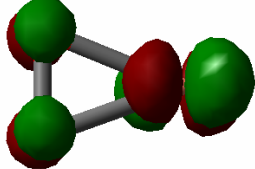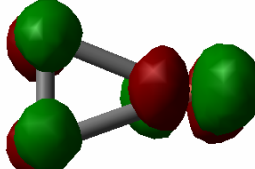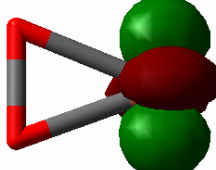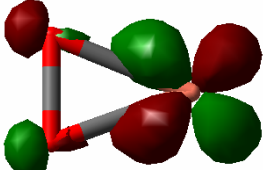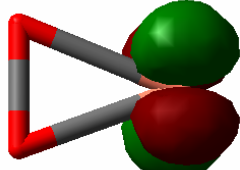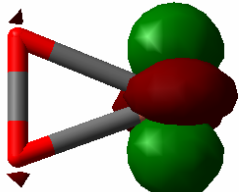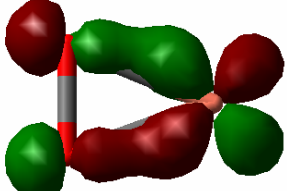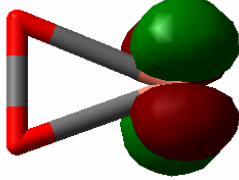
alpha	beta
12a₁ (-)	6b₂ (-)
2a₂ (↑)	12a₁ (-)
6b₂ (↑)	2a₂ (↓)
11a₁ (↑)	11a₁ (↓)
4b₁ (↑)	4b₁ (↓)
10a₁ (↑)	5b₂ (↓)
1a₂ (↑)	10a₁ (↓)
5b₂ (↑)	1a₂ (↓)

Table S5. Molecular orbitals of the uB3LYP/6-311++G(d,p) optimized $^2A_1$ (C_{2v}) open-shell electronic state for the CuO_2 doublet.

alpha	beta
6b$_2$ (-)	12a$_1$ (-)
12a$_1$ (↑)	6b$_2$ (-)
2a$_2$ (↑)	2a$_2$ (↓)
11a$_1$ (↑)	11a$_1$ (↓)
4b$_1$ (↑)	4b$_1$ (↓)
1a$_2$ (↑)	1a$_2$ (↓)
5b$_2$ (↑)	10a$_1$ (↓)
10a$_1$ (↑)	5b$_2$ (↓)

Table S6. Molecular orbitals of the uB3LYP/6-311++G(d,p) optimized $^2B_1$ (C_{2v}) open-shell electronic state for the CuO_2 doublet.

alpha	beta
$12a_1$ (-)	$12a_1$ (-)
$6b_2$ (↑)	$4b_1$ (-)
$2a_2$ (↑)	$2a_2$ (↓)
$11a_1$ (↑)	$6b_2$ (↓)
$4b_1$ (↑)	$11a_1$ (↓)
$10a_1$ (↑)	$10a_1$ (↓)
$1a_2$ (↑)	$3b_1$ (↓)
$9a_1$ (↑)	$1a_2$(↓)

5b$_2$ (↑)	9a$_1$ (↓)
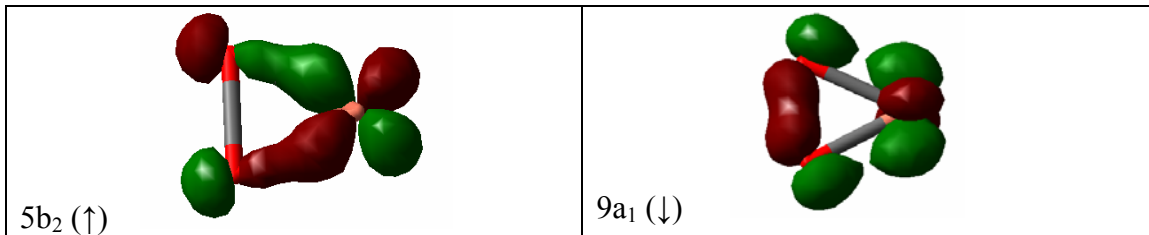
Table S7. Molecular orbitals of the uB3LYP/6-311++G(d,p) optimized ^{2}A"(C_s) open-shell electronic state for the CuO_2 doublet.

alpha	beta
18a' (-)	6a'' (-)
17a' (↑)	18a' (-)
6a'' (↑)	17a' (↓)
16a' (↑)	16a' (↓)
5a'' (↑)	5a'' (↓)
15a' (↑)	4a'' (↓)
14a' (↑)	15a' (↓)
4a'' (↑)	14a' (↓)

Table S8. Molecular orbitals of the uB3LYP/6-311++G(d,p) optimized $^2A^{'}$ (C_s) open-shell electronic state for the CuO_2 doublet.

alpha	beta
18a' (-)	18a' (-)
6a'' (↑)	17a' (-)
17a' (↑)	6a'' (↓)
16a' (↑)	16a' (↓)
5a'' (↑)	5a'' (↓)
15a' (↑)	15a' (↓)
4a'' (↑)	14a' (↓)
14a' (↑)	4a'' (↓)

TABLE S9. Mulliken Charges (a.u.) for the copper atom of the Ground and Low-Lying Electronic States of CuO_2 at Different Levels of Theory with Basis 6-311+G(d).

symmetry	state	HF	BLYP	OLYP	OPBE	B3LYP	B3LYP*	BHandH	VSXC	HCTH	TPSS
C_s	$^2A''$	0.653	0.184	0.178	0.158	0.269	0.244	0.432	0.228	0.181	0.192
	$^2A'$	0.672	0.344	0.361	0.355	0.439	0.414	0.532	0.040	-0.006	-0.001
C_{2v}	$^2A_2$	0.659	0.378	0.386	0.369	0.451	0.430	0.503	0.435	0.403	0.364
	$^2B_2$	0.638	0.410	0.421	0.410	0.468	0.452	0.510	0.473	0.436	0.404
	$^2A_1$	0.444	0.467	0.021	0.004	0.021	0.027	0.181	0.068	0.029	0.011
	$^2B_1$	0.893	$-^a$	0.383	0.363	0.481	0.453	0.621	0.445	0.396	0.351

symmetry	state	Parameter set									
		0	1	2	3	4	5	6	7	8	9
C_s	$^2A''$	0.184	0.228	0.275	0.336	0.418	0.490	0.543	0.584	0.618	0.645
	$^2A'$	0.344	0.315	0.444	0.489	0.529	0.564	0.594	0.621	0.645	0.666
C_{2v}	$^2A_2$	0.378	0.419	0.458	0.493	0.525	0.555	0.582	0.606	0.629	0.649
	$^2B_2$	0.410	0.443	0.472	0.500	0.527	0.552	0.575	0.597	0.612	0.635
	$^2A_1$	0.032	0.031	0.051	0.101	0.176	0.257	0.318	0.361	0.393	0.419
	$^2B_1$	$-^a$	0.435	0.487	0.540	0.601	0.674	0.734	0.785	0.832	0.875

[a] This state can not be converged with the BLYP functional.

TABLE S10. O–O bond distances (Å) in O_2 and O_2^- species at Different Levels of Theory with Basis 6-311+G(d).

System	HF	BLYP	OLYP	OPBE	B3LYP	B3LYP*	BHandH	VSXC	HCTH	TPSS	CCSD(T)	Exp.
O_2	1.158	1.232	1.215	1.205	1.206	1.210	1.171	1.214	1.204	1.221	1.211	1.208[a]
O_2^-	1.289	1.381	1.341	1.335	1.346	1.351	1.341	1.360	1.339	1.367	1.354	1.347[a]

[a] From Huber, K. P.; Herzberg, G., *Molecular spectra and molecular structure*, Vol. 4, Van Nostrand Reinhold, New York, **1979**.

System	Parameter set									
	0	1	2	3	4	5	6	7	8	9
O_2	1.232	1.219	1.208	1.197	1.188	1.179	1.171	1.164	1.157	1.150
O_2^-	1.381	1.364	1.350	1.336	1.324	1.313	1.303	1.294	1.286	1.278

Table S11. Calculated harmonic vibrational frequencies (cm^{-1}) for the ground and low-lying electronic states of CuO, free O$_2$ and free O$_2^-$ at different levels of theory with the 6-311+G(d) basis set.

System	symmetry	state	HF			OLYP			OPBE		
			1(A')	**2(A')**	**3(A')**	**1(A')**	**2(A')**	**3(A')**	**1(A')**	**2(A')**	**3(A')**
CuO$_2$	C$_s$	^{2}A"	148.8	490.1	1268.7	220.4	380.0	1228.0	219.0	375.8	1285.5
		^{2}A'	146.9	484.7	1245.1	165.2	467.0	1068.3	165.0	478.3	1121.5
			1(B$_2$)	**2(A$_1$)**	**3(A$_1$)**	**1(B$_2$)**	**2(A$_1$)**	**3(A$_1$)**	**1(B$_2$)**	**2(A$_1$)**	**3(A$_1$)**
	C$_{2v}$	^{2}A$_2$	-117.5	384.3	1408.8	-229.1	384.5	1041.5	-221.5	390.4	1093.6
		^{2}B$_2$	-209.2	349.9	1361.0	118.8	383.9	945.1	147.4	397.9	994.5
		^{2}A$_1$	-604.8	384.4	1360.6	210.3	222.0	1262.2	246.6	248.3	1303.8
		^{2}B$_1$	624.6	750.0	897.2	295.5	364.2	605.9	341.0	378.0	628.2
			A$_g$			**A$_g$**			**A$_g$**		
free O$_2$		$^3\Sigma_g^-$	1983.5			1573.0			1635.6		
free O$_2^-$		$^2\Pi_g$	1425.7			1359.6			1175.2		

Table S12. Calculated harmonic vibrational frequencies (cm^{-1}) for the ground and low-lying electronic states of CuO, free O$_2$ and free O$_2^-$ at different levels of theory with the 6-311+G(d) basis set.

system	symmetry	state	B3LYP			B3LYP*			BHandH		
			1(A')	**2(A')**	**3(A')**	**1(A')**	**2(A')**	**3(A')**	**1(A')**	**2(A')**	**3(A')**
CuO$_2$	C$_s$	^{2}A"	215.7	416.6	1168.0	221.8	420.9	1177.6	193.3	513.1	1249.3
		^{2}A'	152.3	514.5	1085.5	153.2	517.9	1067.2	138.2	563.1	1291.8
			1(B$_2$)	**2(A$_1$)**	**3(A$_1$)**	**1(B$_2$)**	**2(A$_1$)**	**3(A$_1$)**	**1(B$_2$)**	**2(A$_1$)**	**3(A$_1$)**
	C$_{2v}$	^{2}A$_2$	-191.9	412.8	1107.3	-589.4	412.3	1081.3	143.1	447.1	1312.1
		^{2}B$_2$	113.0	375.6	1020.1	136.6	385.3	989.5	139.4	405.5	1245.4
		^{2}A$_1$	240.2	285.2	1311.2	250.4	269.3	1254.4	535.8	584.1	812.9
		^{2}B$_1$	195.4	292.2	1334.3	387.0	406.6	657.7	593.2	603.5	851.4
			A$_g$			**A$_g$**			**A$_g$**		
free O$_2$		$^3\Sigma_g^-$	1633.4			1607.2			1861.3		
free O$_2^-$		$^2\Pi_g$	1165.5			1146.2			1358.9		

Table S13. Calculated harmonic vibrational frequencies (cm^{-1}) for the ground and low-lying electronic states of CuO, free O_2 and free O_2^- at different levels of theory with the 6-311+G(d) basis set.

System	symmetry	state	VSXC			HCTH			TPSS		
			1(A')	2(A')	3(A')	1(A')	2(A')	3(A')	1(A')	2(A')	3(A')
CuO_2	C_s	$^2A''$	189.0	395.1	1185.4	226.6	391.4	1256.5	232.8	444.7	1135.6
		$^2A'$	127.2	269.6	1317.3	164.0	251.8	1403.4	187.8	304.4	1276.9
			1(B_2)	2(A_1)	3(A_1)	1(B_2)	2(A_1)	3(A_1)	1(B_2)	2(A_1)	3(A_1)
	C_{2v}	$^2A_2$	284.9	403.4	1013.2	-85.8	372.7	1052.9	-191.8	412.7	1006.4
		$^2B_2$	256.5	392.2	920.7	138.7	390.6	958.9	214.9	418.9	904.1
		$^2A_1$	237.3	268.6	1236.7	154.8	172.6	1315.0	313.8	322.9	1179.5
		$^2B_1$	284.5	399.0	612.0	316.8	378.3	612.3	231.5	397.8	644.7
			A_g			A_g			A_g		
free O_2		$^3\Sigma_g^-$	1575.4			1613.0			1544.1		
free O_2^-		$^2\Pi_g$	1098.1			1133.9			1091.3		

Table S14. Calculated harmonic vibrational frequencies (cm^{-1}) for the ground and low-lying electronic states of CuO, free O_2 and free O_2^- at different levels of theory with the 6-311+G(d) basis set.

System	Symmetry	state	CCSD(T)			B3LYP					
						Set 0			Set 1		
			1(A')	2(A')	3(A')	1(A')	2(A')	3(A')	1(A')	2(A')	3(A')
CuO_2	C_s	$^2A''$	151.4	483.0	1055.9	234.1	422.6	1134.7	223.3	413.6	1156.2
		$^2A'$				155.2	503.1	981.2	154.2	503.0	1023.4
			1(B_2)	2(A_1)	3(A_1)	1(B_2)	2(A_1)	3(A_1)	1(B_2)	2(A_1)	3(A_1)
	C_{2v}	$^2A_2$	172.1	407.7	1045.9	-238.6	397.3	963.5	-182.7	404.1	1035.0
		$^2B_2$	225.4	366.2	996.3	137.2	398.8	868.6	121.6	380.8	940.0
		$^2A_1$	–	–	–	257.1	270.8	1161.7	242.7	267.6	1229.8
		$^2B_1$	–	–	–				362.9	372.3	634.8
			A_g			A_g			A_g		
free O_2		$^3\Sigma_g^-$	1592.4			1483.4			1554.9		
free O_2^-		$^2\Pi_g$	1113.9			1048.7			1102.3		

Table S15. Calculated harmonic vibrational frequencies (cm^{-1}) for the ground and low-lying electronic states of CuO, free O_2 and free O_2^- at different levels of theory with the 6-311+G(d) basis set.

System	Symmetry	state	B3LYP								
			Set 2			Set 3			Set 4		
			1(A')	2(A')	3(A')	1(A')	2(A')	3(A')	1(A')	2(A')	3(A')
CuO$_2$	C$_s$	^{2}A"	213.4	410.1	1155.0	204.6	415.7	1135.0	199.8	448.0	1146.4
		^{2}A'	152.7	505.2	1073.0	149.9	505.7	1124.4	146.3	505.0	1171.3
			1(B$_2$)	2(A$_1$)	3(A$_1$)	1(B$_2$)	2(A$_1$)	3(A$_1$)	1(B$_2$)	2(A$_1$)	3(A$_1$)
	C$_{2v}$	^{2}A$_2$	-196.8	408.2	1098.5	-138.6	409.1	1155.7	-94.3	408.8	1209.6
		^{2}B$_2$	91.1	369.0	1013.6	44.3	365.7	1083.8	-64.1	365.9	1149.3
		^{2}A$_1$	226.4	271.0	1225.7	260.6	266.8	1216.4	259.2	337.7	1184.8
		^{2}B$_1$	386.5	424.6	657.6	414.1	461.3	680.9	473.1	509.6	716.3
			A$_g$			A$_g$			A$_g$		
free O$_2$		$^3\Sigma_g^-$	1623.0			1687.6			1748.8		
free O$_2^-$		$^2\Pi_g$	1154.4			1204.6			1251.9		

Table S16. Calculated harmonic vibrational frequencies (cm^{-1}) for the ground and low-lying electronic states of CuO, free O_2 and free O_2^- at different levels of theory with the 6-311+G(d) basis set.

System	symmetry	state	B3LYP								
			Set 5			Set 6			Set 7		
			1(A')	2(A')	3(A')	1(A')	2(A')	3(A')	1(A')	2(A')	3(A')
CuO$_2$	C$_s$	^{2}A"	189.7	477.1	1221.8	176.0	491.4	1277.3	162.5	499.1	1316.8
		^{2}A'	143.2	504.0	1213.0	140.7	502.9	1248.7	138.6	502.5	1279.6
			1(B$_2$)	2(A$_1$)	3(A$_1$)	1(B$_2$)	2(A$_1$)	3(A$_1$)	1(B$_2$)	2(A$_1$)	3(A$_1$)
	C$_{2v}$	^{2}A$_2$	-44.8	407.4	1258.6	49.9	406.7	1307.6	68.3	404.8	1353.2
		^{2}B$_2$	-80.7	368.0	1204.2	-98.6	368.3	1255.9	-111.9	369.1	1305.4
		^{2}A$_1$	246.0	396.0	1206.0	293.9	408.2	1260.3	407.4	522.1	1310.3
		^{2}B$_1$	561.4	569.6	797.8	593.0	632.3	838.1	611.8	678.4	867.3
			A$_g$			A$_g$			A$_g$		
free O$_2$		$^3\Sigma_g^-$	1807.1			1862.6			1916.2		
free O$_2^-$		$^2\Pi_g$	1297.6			1343.0			1383.2		

Table S17. Calculated harmonic vibrational frequencies (cm^{-1}) for the ground and low-lying electronic states of CuO, free O_2 and free O_2^- at different levels of theory with the 6-311+G(d) basis set.

system	symmetry	state	B3LYP					
			Set 8			Set 9		
			1(A')	**2(A')**	**3(A')**	**1(A')**	**2(A')**	**3(A')**
CuO_2	C_s	$^2A''$	150.3	502.9	1347.0	141.0	506.2	1367.8
		$^2A'$	137.5	502.1	1306.0	137.0	502.0	1328.4
			1(B$_2$)	**2(A$_1$)**	**3(A$_1$)**	**1(B$_2$)**	**2(A$_1$)**	**3(A$_1$)**
	C_{2v}	$^2A_2$	75.8	403.5	1397.0	141.0	506.2	1367.8
		$^2B_2$	-6.8	374.0	1305.8	-140.3	367.9	1395.0
		$^2A_1$	-1505.7	405.8	1353.7	-690.4	404.9	1395.2
		$^2B_1$	628.5	659.2	895.6	643.7	750.8	924.3
			A$_g$			**A$_g$**		
free O_2		$^3\Sigma_g^-$	1966.6			2015.0		
free O_2^-		$^2\Pi_g$	1423.9			1462.8		

Table S18. First ionization potential (eV) of Cu at Different Levels of Theory.

	HF	BLYP	OLYP	OPBE	B3LYP	B3LYP*	BHandH	VSXC	HCTH	TPSS	CCSD(T)
PI (eV)	6.43	8.20	7.76	8.36	8.04	8.10	7.44	7.77	7.98	7.92	7.26

	aug-cc-pVTZ	aug-cc-pVQZ	extr. Infinite Basis
PI (eV)	7.47	7.51	7.54

Parameter Set	0	1	2	3	4	5	6	7	8	9
PI (eV)	8.20	8.13	8.05	7.99	7.92	7.86	7.80	7.75	7.70	7.66

Table S19. Binding dissociation energies (kcal·mol^{-1}) of CuO_2 in its the electronic ground state with the 6-311+G(d) basis set for different parameter sets used in B3LYP-like functionals.

Parameter Set	0	1	2	3	4	5	6	7	8	9
BDE (kcal/mol)	19.94	15.35	11.68	8.75	6.64	5.47	5.07	5.24	5.85	6.80

3.5. Importance of the basis set for the spin-state energetics of iron complexes

Güell, M.; Luis, J.M.; Solà, M.; Swart, M.

Institut de Química Computacional and Departament de Química, Campus Montilivi, Universitat de Girona, 17071 Girona, Spain, and Institució Catalana de Recerca i Estudis Avançats (ICREA), 08010 Barcelona, Spain

Abstract

We have performed a systematic investigation of the influence of the basis set on relative spin-state energies for a number of iron compounds. In principle, with an infinitely large basis set, both Slater-type orbital (STO) and Gaussian-type orbital (GTO) series should converge to the same final answer, which is indeed what we observe for both *vertical* and *relaxed* spin-state splittings. However, we see throughout the paper that the STO basis sets give consistent and rapidly converging results, while the convergence with respect to the basis set size is much slower for the GTO basis sets. For example, the large GTO basis sets that give good results for the *vertical* spin-state splittings of compounds **1**−**3** (6-311+G**, Ahlrichs VTZ2D2P) fail for the *relaxed* spin-state splittings of compound **4** (where **1** is Fe−(PyPepS)$_2$ (PyPepSH$_2$ = N-(2-mercaptophenyl)-2-pyridinecarboxamide), **2** is Fe(tsalen)Cl (tsalen = N,N'-ethylenebis-(thiosalicylideneiminato)), **3** is Fe(N(CH$_2$−o-C$_6$H$_4$S)$_3$)(1-Me-imidazole), and **4** is FeFHOH). Very demanding GTO basis sets like Dunning's correlation-consistent (cc-pVTZ, cc-pVQZ) basis sets are needed to achieve good results for these *relaxed* spin states. The use of popular (Pople-type) GTO, effective core potentials basis set (ECPB), or mixed ECPB(Fe):GTO(rest) basis sets is shown to lead to substantial deviations (2−10 kcal/mol, 14−24 kcal/mol for 3-21G), in particular for the high spin states that are typically placed at too low energy. Moreover, the use of an effective core potential in the ECPB basis sets results in spin-state splittings that are systematically different from the STO−GTO results.

3.6. The spin-states and spin-transitions of mononuclear iron(II) complexes of tris-pyrazolylborate and tris-pyrazyolylmethane ligands

Güell, M.; Solà, M.; Swart, M.
Polyhedron, Accepted

Mireia Güell, Miquel Solà and Marcel Swart. "Spin-state splittings of iron(II) complexes with trispyrazolyl ligands". *Polyhedron*. Article in Press

Institut de Química Computacional and Departament de Química, Universitat de Girona, Campus Montilivi, 17071 Girona, SpainInstitució Catalana de Recerca i Estudis Avançats (ICREA), 08010 Barcelona, Spain

Abstract

We report a computational study at the OPBE/TZP level on the chemical bonding and spin ground-states of mono-nuclear iron(II) complexes with trispyrazolylborate and trispyrazolylmethane ligands. We are in particular interested in how substitution patterns on the pyrazolyl-rings influence the spin-state splittings, and how they can be rationalized in terms of electronic and steric effects. One of the main observations of this study is the large similarity of the covalent metal–ligand interactions for both the borate and methane ligands. Furthermore, we find that the spin-state preference of an individual transition-metal (TM) complex does not always concur with that of an ensemble of TM-complexes in the solid-state. Finally, although the presence of methyl groups at the 3-position of the pyrazolyl groups leads to ligand–ligand repulsion, it is actually the loss of metal–ligand bonding interactions that is mainly responsible for shifts in spin-state preferences.

Graphical abstract

What determines the spin-state splittings of iron(II) complexes with trispyrazolyl ligands ? Is it steric interaction between substituents on the pyrazolyl-rings, direct covalent metal–ligand bonding, or the presence of counter-ion and solvent molecules? Here, we have studied these intriguing systems with density functional methods at the OPBE/TZP level.

Keywords: Iron complexes; Pyrazolylborate ligands; Pyrazolylmethane ligands; Density Functional Theory

Spin-state splittings of iron(II) complexes with trispyrazolyl ligands

Mireia Güell[a]   Miquel Solà[a] and Marcel Swart[a,b],**

a) Institut de Química Computacional and Departament de Química, Universitat de Girona, Campus Montilivi, 17071 Girona, Spain

b) Institució Catalana de Recerca i Estudis Avançats (ICREA), 08010 Barcelona, Spain
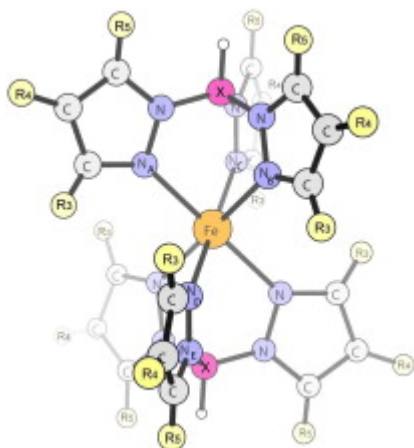
E-mail: marcel.swart@icrea.es

Detailed description of Energy Decomposition Analysis

Table S1. Geometric parameters (Å, deg) of complexes studied

Figure S1. MO Diagram of borate and methane ligands

References

Energy decomposition analysis. The total energy ΔE_{total} for the heterolytic association[1,2] reaction between the iron(II) cation and n ligands L with charge q ($Fe^{2+} + n \cdot L^q \rightarrow FeL_n^{nq+2}$) results directly from the Kohn-Sham molecular orbital (KS-MO) model[3] and is made up of two major components (Eq. 1):

$$\Delta E_{total} = \Delta E_{prep} + \Delta E_{int} \tag{1}$$

In this formula, the preparation energy ΔE_{prep} is the energy needed to prepare the (ionic/neutral) fragments and consists of three terms (eq. 2):

$$\Delta E_{prep} = \Delta E_{deform} + \Delta E_{lig\text{-}lig} + \Delta E_{valexc} \tag{2}$$

The first is the energy needed to deform the separate molecular fragments (in this case only for the ligands) from their equilibrium structure to the geometry that they attain in the overall molecular system (ΔE_{deform}). The second ($\Delta E_{lig\text{-}lig}$) is the interaction energy between the ligands when they are placed at the geometry of the molecule (but without the iron present) to make one fragment file that contains all ligands. This interaction results mainly from electrostatic repulsion in case of negatively charged ligands. The third term (ΔE_{valexc}) is the valence-excitation energy needed to prepare the metal from its atomic spin-unrestricted (polarized) ionic ground-state to the spin-restricted (polarized) ionized form. The valence-excitation energy consists of two terms: the first (positive, e.g. destabilizing) term is the energy difference between the spin-polarized metal cation in its ground state (e.g. the quintet ^5D state for Fe^{2+}) and the spin-restricted, non-polarized (singlet) cationic form used for the metal cation fragment (the fragments need to be spin-restricted). For the ground state of the cation, we use the "average of configuration" approach,[4] which gives an approximate single-determinant description of the true atomic spin ground-state. Note also that the metal cation fragment is prepared with the occupation of the orbitals it attains in the molecule, i.e. it does not necessarily, and usually does not, correspond to the isolated metal cation. As a result, the ΔE_{valexc} values can not be compared directly with experimental excitation energies for the metal cation (see also refs. [4] and [5]). The second term results from preparing (polarizing) the cation fragment with the multiplet state it attains in the metal compound; this term is negative (stabilizing) for triplet and quintet, and zero for singlet states. It is achieved by changing the occupations of the fragment orbitals. For instance for iron(II), the spin-restricted cationic fragment would be prepared with 3 α and 3 β d-electrons; within the molecule calculation, the

occupations of the iron-fragment are changed to make 4 α and 2 β d-electrons for a triplet state, or to 5 α and 1 β d-electrons for a quintet state. There is a discrepancy (of ca. 2 kcal mol^{-1}) between the interaction energy thus obtained from these fragments (*vide infra*) and the change in energy when going from the isolated ligands and (spin-unrestricted, polarized) metal cation to the metal compound. This difference results from the fact the α and β orbitals are kept the same in the former (fragment) approach, while they are allowed to relax in the latter. There are two possibilities to deal with this discrepancy, either to make this energy difference part of the preparation energy (as done here), or to scale the interaction energy components accordingly. However, this energy difference is generally negligible (1-2 kcal·mol^{-1}) compared to the interaction energy components, and is therefore of no consequence for the importance of the components of the interaction energy.

The interaction energy ΔE_{int} is the energy released when the prepared fragments (i.e. Fe^{2+} + n·L^q) are brought together into the position they have in the overall molecule. It is analyzed for our model systems in the framework of the KS-MO model[3] using a Morokuma-type[6] decomposition into electrostatic interaction, Pauli repulsion (or exchange repulsion), and (attractive) orbital interactions (Eq. 3).

$$\Delta E_{int} = \Delta V_{elstat} + \Delta E_{Pauli} + \Delta E_{orbint} \tag{3}$$

The term ΔV_{elstat} corresponds to the classical electrostatic interaction between the unperturbed charge distributions of the prepared (i.e. deformed) fragments and is usually attractive. The Pauli-repulsion, ΔE_{Pauli}, comprises the destabilizing interactions between occupied orbitals and is responsible for the steric repulsion. The orbital interaction ΔE_{orbint} in any MO model, and therefore also in Kohn-Sham theory, accounts for electron-pair bonding, charge transfer (i.e., donor-acceptor interactions between occupied orbitals on one fragment with unoccupied orbitals of the other, including the HOMO-LUMO interactions), and polarization (empty-occupied orbital mixing on one fragment due to the presence of another fragment). In the case of metal compounds with symmetry, the orbital interaction energy can be further decomposed into the contributions from each irreducible representation of the interacting system (Eq. 4) using the extended transition state (ETS) scheme developed by Ziegler and Rauk.[7,8]

$$\Delta E_{orbint} = \sum_{\Gamma} \Delta E_{\Gamma} \tag{4}$$

Table S1. Geometric parameters (Å, deg) of complexes studied[a]

Complex	spin-state	d(Fe-N_A)	d(Fe-X)	a(N_A-Fe-N_B)	D(N_A-Fe-N_B-N_C)	D(N_A-Fe-N_D-N_E)
[Fe(T$_b$)$_2$]	singlet	1.960	3.057	88.7	-88.7	135.6
	triplet	2.081	3.136	86.6	-86.8	136.6
	quintet	2.210	3.208	85.1	-85.5	137.3
[Fe(T$_c$)$_2$]$^{2+}$	singlet	1.955	2.971	87.7	-87.8	136.1
	triplet	2.076	3.059	85.3	-85.7	137.2
	quintet	2.205	3.146	83.2	-83.9	138.0
[Fe(T$_b$^{3Me})$_2$]	singlet	2.013	3.018	90.3	-90.3	134.8
	triplet	2.139	3.100	88.2	-88.2	135.9
	quintet	2.263	3.171	86.5	-86.7	136.6
[Fe(T$_c$^{3Me})$_2$]$^{2+}$	singlet	2.012	2.955	88.7	-88.7	135.7
	triplet	2.135	3.048	86.1	-86.4	136.8
	quintet	2.257	3.137	83.9	-84.5	137.8
[Fe(T$_b$^{3FMe})$_2$]	singlet	2.084	2.982	91.6	-91.6	134.2
	triplet	2.193	3.023	90.6	-90.6	134.7
	quintet	2.298	3.057	90.0	-90.0	135.0
[Fe(T$_c$^{3FMe})$_2$]$^{2+}$	singlet	2.045	2.898	90.5	-90.5	134.7
	triplet	2.148	2.945	89.4	-89.4	135.3
	quintet	2.270	3.004	88.0	-88.0	136.0
[Fe(T$_b$^{4Me})$_2$]	singlet	1.960	3.055	88.6	-88.7	135.7
	triplet	2.082	3.134	86.6	-86.8	136.6
	quintet	2.209	3.205	85.1	-85.5	137.3
[Fe(T$_c$^{4Me})$_2$]$^{2+}$	singlet	1.957	2.968	87.7	-87.8	136.1
	triplet	2.079	3.055	85.4	-85.7	137.1
	quintet	2.207	3.142	83.3	-84.0	138.0
[Fe(T$_b$^{4Br})$_2$]	singlet	1.964	3.057	88.8	-88.8	135.6
	triplet	2.083	3.133	86.8	-87.0	136.5
	quintet	2.211	3.203	85.3	-85.7	137.2
[Fe(T$_c$^{4Br})$_2$]$^{2+}$	singlet	1.963	2.974	87.6	-87.7	136.1
	triplet	2.085	3.062	85.3	-85.7	137.2
	quintet	2.210	3.149	83.2	-83.9	138.0
[Fe(T$_b$^{5Me})$_2$]	singlet	1.954	3.056	88.6	-88.6	135.7
	triplet	2.070	3.135	86.5	-86.7	136.7
	quintet	2.194	3.205	84.9	-85.4	137.3
[Fe(T$_c$^{5Me})$_2$]$^{2+}$	singlet	1.950	2.974	87.5	-87.6	136.2
	triplet	2.065	3.063	85.0	-85.4	137.3
	quintet	2.190	3.157	82.7	-83.5	138.2
[Fe(T$_b$^{5FMe})$_2$]	singlet	1.932	3.042	89.3	-89.3	135.4
	triplet	2.035	3.111	87.4	-87.5	136.2
	quintet	2.152	3.181	85.8	-86.1	136.9
[Fe(T$_c$^{5FMe})$_2$]$^{2+}$	singlet	1.925	2.970	87.9	-87.9	136.0
	triplet	2.030	3.058	85.4	-85.7	137.1
	quintet	2.148	3.157	82.9	-83.7	138.2
[Fe(T$_b$$^{3,5-Me2}$)$_2$]	singlet	2.006	3.014	90.3	-90.4	134.8
	triplet	2.124	3.094	88.2	-88.2	135.9
	quintet	2.247	3.168	86.4	-86.6	136.7
[Fe(T$_c$$^{3,5-Me2}$)$_2$]$^{2+}$	singlet	2.002	2.959	88.5	-88.5	135.8
	triplet	2.121	3.057	85.7	-86.0	137.0
	quintet	2.238	3.156	83.2	-83.9	138.0
[Fe(T$_b$$^{3,4,5-Me3}$)$_2$]	singlet	2.016	3.014	90.3	-90.3	134.9
	triplet	2.133	3.096	88.0	-88.1	135.9
	quintet	2.244	3.164	86.4	-86.6	136.7
[Fe(T$_c$$^{3,4,5-Me3}$)$_2$]$^{2+}$	singlet	2.004	2.941	88.8	-88.9	135.6

	triplet	2.116	3.032	86.3	-86.5	136.7
	quintet	2.236	3.125	84.0	-84.6	137.7
$[Fe(T_b^{3,5-Me2-4Cl})_2]$	*singlet*	2.008	3.011	90.4	-90.4	134.8
	triplet	2.119	3.087	88.4	-88.4	135.8
	quintet	2.237	3.159	86.7	-86.9	136.6
$[Fe(T_c^{3,5-Me2-4Cl})_2]^{2+}$	*singlet*	2.000	2.945	88.8	-88.8	135.6
	triplet	2.113	3.036	86.3	-86.5	136.7
	quintet	2.232	3.131	83.9	-84.5	137.7
$[Fe(T_b^{N4})_2]$	*singlet*	1.954	3.076	88.5	-88.6	135.7
	triplet	2.078	3.156	86.5	-86.7	136.6
	quintet	2.206	3.226	85.0	-85.4	137.3
$[Fe(T_c^{N4})_2]^{2+}$	*singlet*	1.955	2.991	87.5	-87.6	136.2
	triplet	2.078	3.079	85.2	-85.6	137.2
	quintet	2.203	3.162	83.2	-83.9	138.0
$[Fe(T_b^{4,5-Ph})_2]$	*singlet*	1.958	3.047	89.0	-89.0	135.5
	triplet	2.078	3.127	86.9	-87.0	136.5
	quintet	2.213	3.208	85.0	-85.4	137.3
$[Fe(T_c^{4,5-Ph})_2]^{2+}$	*singlet*	1.958	2.969	87.8	-87.9	136.1
	triplet	2.080	3.060	85.3	-85.6	137.2
	quintet	2.211	3.155	82.9	-83.7	138.1
$[Fe(T_b^{4,5-Ph-N3})_2]$	*singlet*	1.937	3.029	89.6	-89.6	135.2
	triplet	2.059	3.110	87.5	-87.6	136.2
	quintet	2.201	3.202	85.3	-85.7	137.2
$[Fe(T_c^{4,5-Ph-N3})_2]^{2+}$	*singlet*	1.931	2.958	88.5	-88.5	135.7
	triplet	2.048	3.047	86.1	-86.3	136.8
	quintet	2.192	3.161	83.2	-84.0	138.0

a) see Scheme 3 for labels of atoms

Figure S1. MO Diagram of borate and methane ligands

borate-ligand   methane-ligand
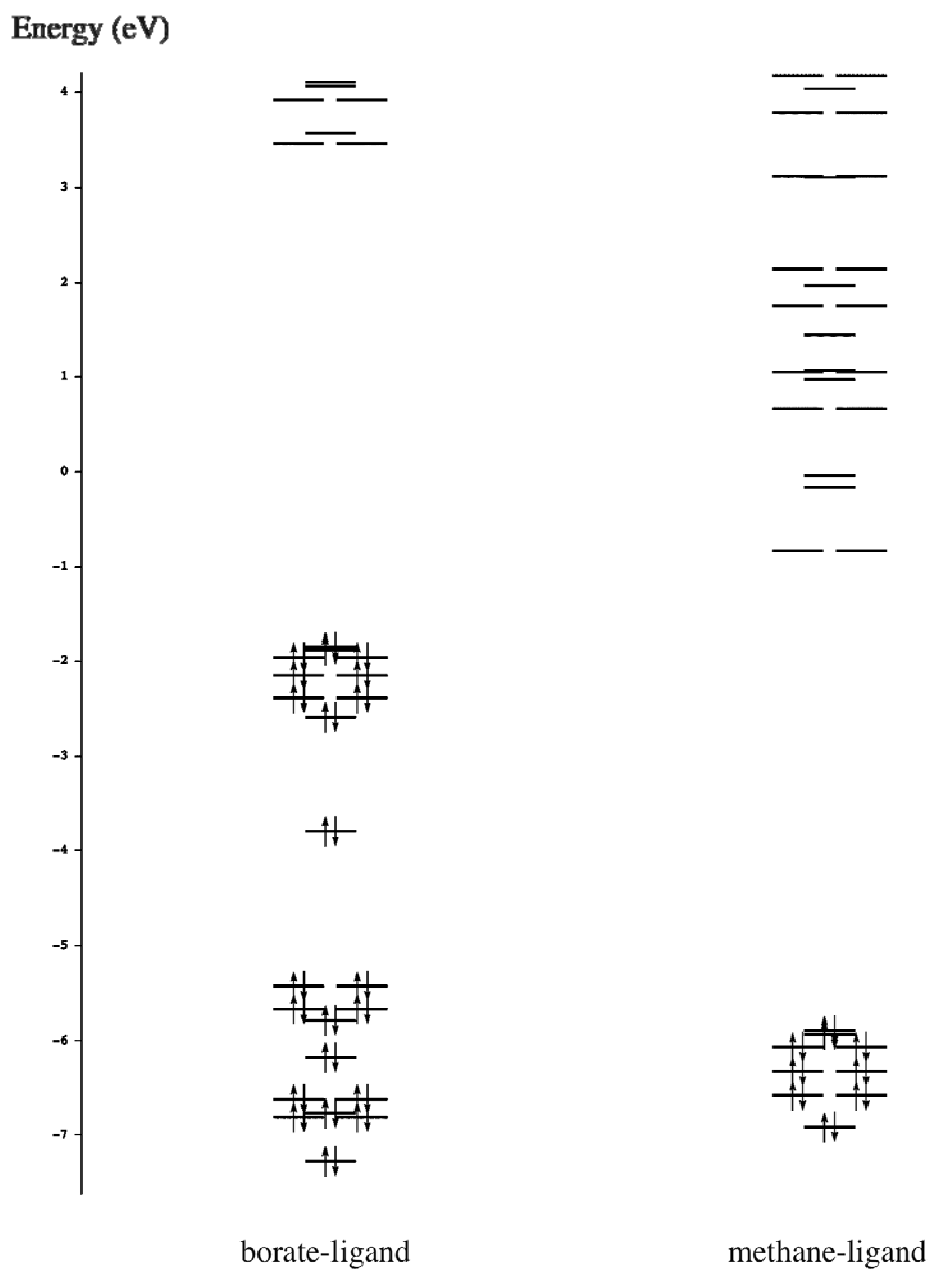
References

(1) Swart, M. J. Chem. Theor. Comp. **2008**, online: DOI 10.1021/ct800277a.

(2) Swart, M. Inorg. Chim. Acta **2007**, 360, 179.

(3) Bickelhaupt, F. M.; Baerends, E. J. Kohn-Sham density functional theory: Predicting and understanding chemistry. In Reviews in Computational Chemistry, Vol 15; Wiley-VCH: New York, 2000; Vol. 15; pp 1.

(4) Baerends, E. J.; Branchadell, V.; Sodupe, M. Chem. Phys. Lett. **1997**, 265, 481.

(5) Fouqueau, A.; Mer, S.; Casida, M. E.; Daku, L. M. L.; Hauser, A.; Mineva, T.; Neese, F. J. Chem. Phys. **2004**, 120, 9473.

(6) Morokuma, K. Acc. Chem. Res. **1977**, 10, 294.

(7) Ziegler, T.; Rauk, A. Inorg. Chem. **1979**, 18, 1558.

(8) Ziegler, T.; Rauk, A. Inorg. Chem. **1979**, 18, 1755.

3.7. Accurate spin state energies for 1st row transition metal compounds

Swart, M.; Güell, M.; Luis, J.M.; Solà, M
Proceedings of the 9th European Biological Inorganic Chemistry Conference,
Wroclaw, Poland, 2-6 September 2008.

Accurate Spin State Energies for 1st Row Transition Metal Compounds

M. Swart[1,2,*], M. Güell[1], J.M. Luis[1] and M. Solà[1,*]

[1]*Institut de Química Computacional and Departament de Química, Universitat de Girona, Campus Montilivi, 17071 Girona, Spain*
[2]*Institució Catalana de Recerca i Estudis Avançats (ICREA), Pg. Lluís Companys 23, 08010 Barcelona, Spain*
E-mail: marcel.swart@icrea.es, Fax +34-972-183241

Summary

An overview is given of spin-state splittings for a number of compounds containing iron and other first-row transition metals, which were obtained by DFT calculations using the OPBE functional with Slater-Type Orbitals. This functional was recently shown to give accurate spin-state splittings for iron compounds, and is here reported to work excellently also for other transition metals.

Introduction

Determining spin ground-states of transition metal compounds remains a challenging task for both theory and experiment.[1-2] On the experimental side, the situation may be complicated by ligand-exchange reactions, dimerization processes, oxidation/reduction, impurities, or temperature-dependences of the spin ground-states. The latter is for instance observed in spin-crossover compounds, where low-spin compounds upon heating change to high-spin, or high-spin compounds upon cooling change to low-spin.

In principle, theory should be able to help with the interpretation of the experimental data, predict the spin ground-state and help to determine reaction mechanisms. However, theory is not without its own problems. The most accurate ab initio theoretical methods (CCSD(T), MR-CI) are too demanding for everyday use, and in some cases (such as CASPT2) need expert knowledge of the methodology. More efficient are calculations based on density functional theory (DFT), but the results are shown to depend largely on the choice of DFT functional that is being used.

This is in particular true for the calculation of relative spin-state energies, where the choice of the DFT functional[1] and the basis set[3] used both play a major role. Standard pure functionals (like LDA or BLYP) systematically over-stabilize low-spin states,[1-2] while hybrid functionals (e.g. B3LYP) over-stabilize high-spin states due to the inclusion of a portion of Hartree-Fock (HF) exchange.[2,4] Reiher and co-workers therefore reduced the amount HF exchange to 15% (instead of 20% in B3LYP), dubbed B3LYP*,[5] which in-deed improves the B3LYP results for many systems. However, it was not successful for all iron compounds, as for instance is the case for the $Fe(phen)_2(NCS)_2$ spin-crossover compound,[6] for which a further reduction to 12% of HF exchange seems necessary. Therefore, with B3LYP and B3LYP*, it is *a priori* unknown if the amount of HF exchange is appropriate for the transition metal compound under study, which is an undesirable situation.

The influence of the basis set was found to be substantial.[3] In principle, with an infinitely large basis set, both Slater-type orbital (STO) and Gaussian-type orbital (GTO) series should converge to the same final answer, which is indeed what we observed for both *vertical* and *relaxed* spin-state splittings. However, we found that the STO basis sets give consistent and rapidly con-verging results, while the convergence with respect to the basis set size is much slower for the GTO basis sets (see Figure 1). The use of basis sets containing effective core potentials (ECPBs) resulted in spin-state splittings that are systematically different from the converged STO-GTO results.
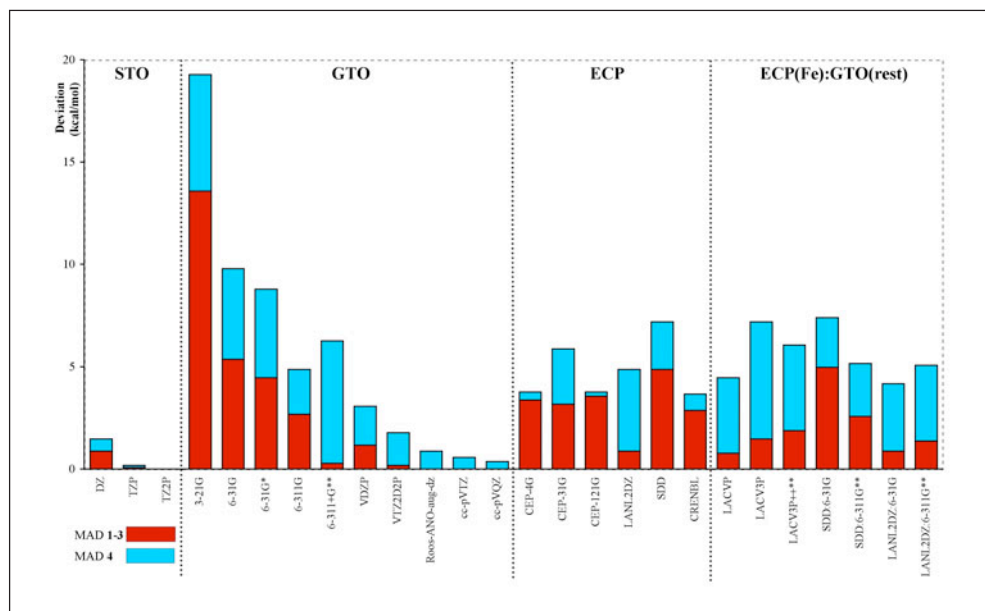

Figure 1. Mean absolute deviations (MAD) for different basis sets (from ref. 3).

From these and related studies, it became clear that recent and improved functionals provide more accurate results. This is in particular true for the OPBE functional, that combines Handy and Cohen's optimized exchange (OPTX)[7] functional with the PBE[8] correlation functional, which provided the correct spin ground-state for a number of Fe(II)/Fe(III) compounds.[1] This good performance of OPBE concurs with recent benchmark studies on the energy profiles of nucleophilic substitution reactions,[9] and on the NMR chemical shifts of organic molecules.[10] Han and Noodleman recently obtained the Mössbauer isomer shift parameters for OPBE,[11] and used these to study hydroxylase intermediates of soluble methane monooxygenase (MMOH).[12] It was shown that OPBE does not overestimate Fe-ligand covalency and correctly predicted high-spin anti-ferromagnetically (AF) coupled Fe^{4+} sites.

Here we give an overview of previous OPBE results for iron compounds, and some preliminary results for first-row transition metal compounds. In all cases does OPBE give excellent results.

Methods

All DFT calculations were performed with the Amsterdam Density Functional (ADF) suite of program.[13] MOs were expanded in an uncontracted set of Slater type orbitals (STOs) of triple-ζ quality containing diffuse functions and one (TZP) or two (TZ2P) sets of polarization functions. Energies and gradients were calculated using the local density approximation (LDA; Slater exchange and VWN correlation) with gradient-corrections (GGA) for exchange (OPTX)[7] and correlation (PBE)[8] included self-consistently, i.e. the OPBE functional.[14] Geometries were optimized with the QUILD program[15] using adapted delocalized coordinates[16] until the maximum gradient component was less than 1.0e-4 atomic units. The solvent environment was in some cases included through a dielectric continuum (COSMO) model.[17]

Results

The OPBE functional has recently[1-2] been used to obtain the spin-state splittings for a number of iron compounds, which consist of three benchmark systems (Figure 2) and difficult compounds (Figure 3), among others.

The benchmark systems had previously[18] been studied with high-level CASPT2 calculations and, for comparison, with Hartree-Fock and some DFT functionals. Hartree-Fock always predicted a high-spin ground-state, wrongly also for the low-spin bipyridyl compound, and showed spin-state splittings with large deviations from the reference CASPT2 data. Somewhat better results were obtained in the CASPT2 paper[18] with DFT functionals, which showed deviations between 9-15 kcal·mol^{-1}; however, the hybrid functionals (B3LYP, PBE0) also failed to predict the low-spin ground-state for the bipyridyl compound. These results are improved upon[2] by OPBE, whose deviation from the reference CASPT2 data is an order of magnitude smaller (1-2 kcal·mol^{-1}). In fact, the difference between CASPT2 and OPBE falls well within the estimated accuracy of the reference CASPT2 data.
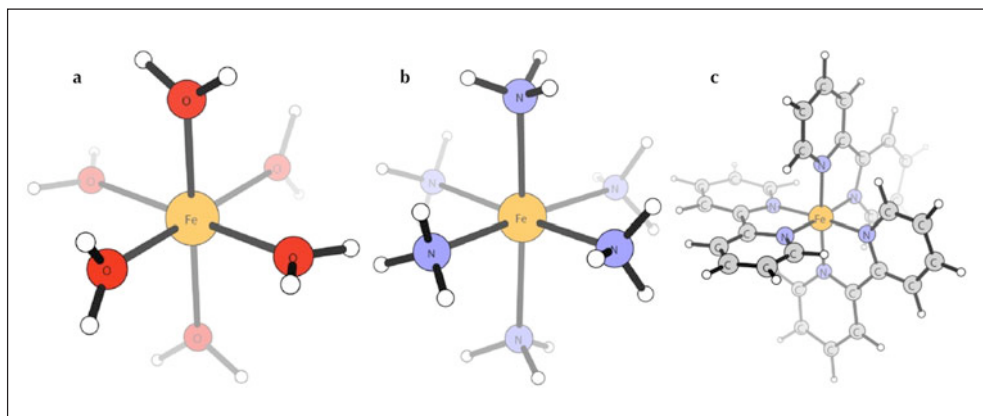
Figure 2. Benchmark iron compounds: Fe(II)(H₂O)₆²⁺ (a), Fe(II)(NH₃)₆²⁺ (b), Fe(II)(bpy)₃²⁺ (c).

The pyridylmethylamine (pma) compounds (Figure 3b-c) had been studied because they are structurally similar with approximately an octahedral arrangement of ligands around the iron, yet they show a different spin ground-state. The combination of these two molecules therefore is a very stringent check on the performance of computational methods. The mono-pma compound is high-spin and the di-pma compound low-spin, both in experiment and by OPBE.[2] In contrast, standard pure DFT functionals fail to predict the high-spin ground-state of mono-pma, while hybrid functionals fail to predict the low-spin ground-state of di-pma.[2]

The spin-crossover compound Fe(phen)₂(NCS)₂ (Figure 3a) was previously studied by Reiher, who showed that both B3LYP and B3LYP* were unable
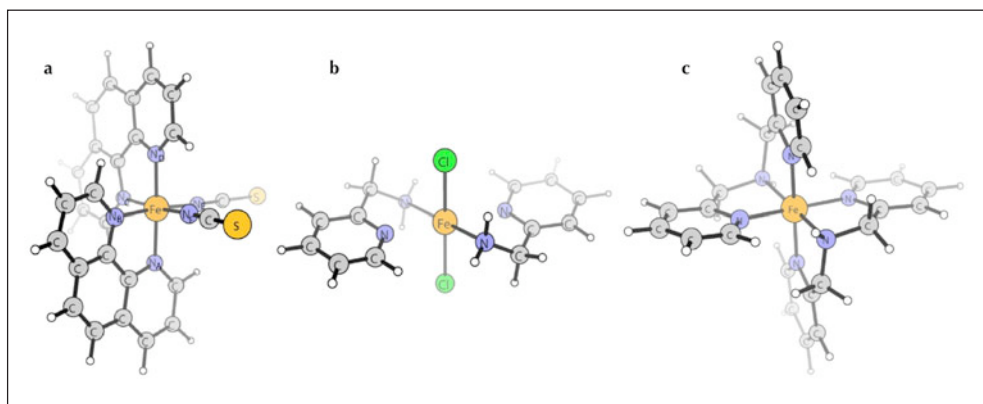

Figure 3. Difficult iron compounds: spin-crossover compound Fe(II)(phen)₂(NCS)₂ (a), mono-pyridylmethylamine Fe(II)(amp)₂Cl₂ (b), di-pyridylmethylamine Fe(II)(dpa)₂²⁺ (c)
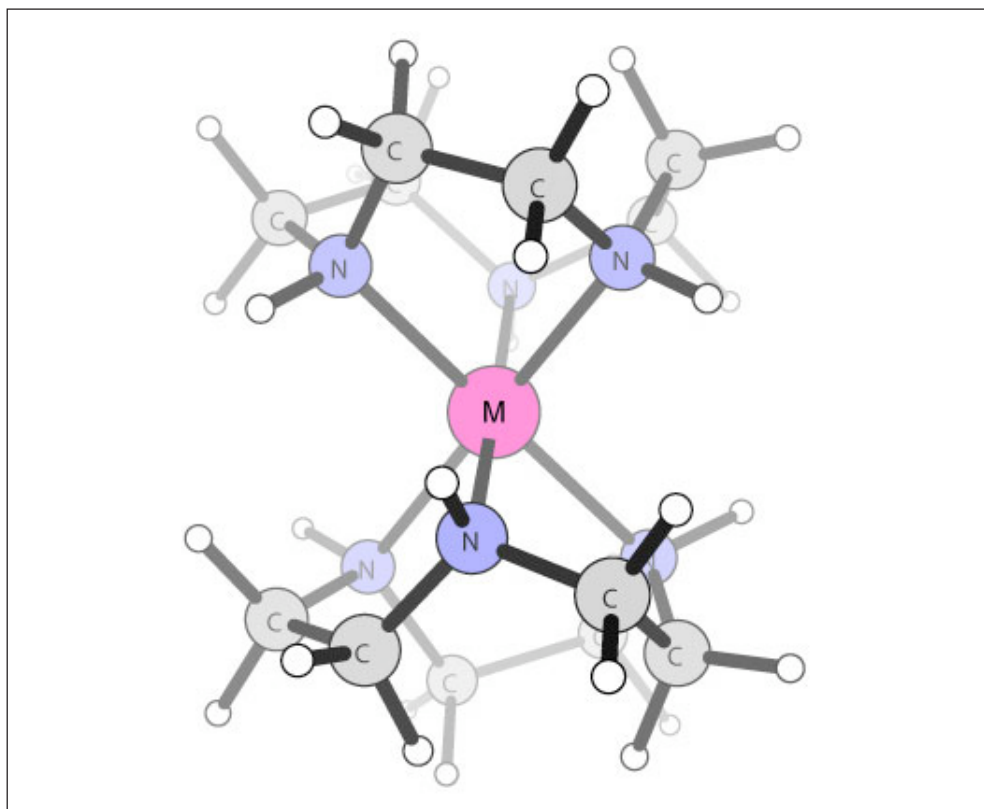
Figure 4. Bis complex of transition-metal (TM) with 1,4,7-triazacyclononane ligands TM([9]aneN_3)_2^{n+}.

to classify this molecule as a spin-crossover compound.[6] Instead, both these methods predicted it to have a high-spin ground-state at all temperatures. Only by lowering the amount of Hartree-Fock exchange to 12% did Reiher obtain a reasonable energy splitting of ca. 3 kT, and a low-spin ground-state. In contrast, OPBE directly predicts a low-spin ground state and an (ΔE_{HL}) energy splitting of 2.1 kcal·mol^{-1} (3.5 kT), in excellent agreement with experiment. Similar to the pma-compounds, other DFT functionals are unable to classify this molecule as spin-crossover, e.g. they either predict a too large energy splitting, or one with the wrong sign.

   With this good performance[1-2] of OPBE for these iron compounds in mind, we were interested if it would also work as well for other transition metals.[19] Therefore, we took a complex for which experimental data are available for a series of transition metals (Cr, Mn, Fe, Co, Ni, Cu, Zn; some of which in different oxidation states), which are based on the triazacyclononane ligand (Figure 4). It was already shown that OPBE correctly predicts the spin ground-

state for the Fe(III) compound, and also for the other transition metals, for those which more than one spin-state is available, does OPBE predict the correct ground-state.

Similar good performance is observed for a set of spin-crossover compounds, for which B3LYP was shown to fail. In contrast, our studies with OPBE[19] show that it correctly predicts a low-spin ground-state with a small ΔE_{HL} energy splitting between high and low-spin.

Conclusions

We have presented an overview of recent studies on spin ground-states of first-row transition-metal compounds, as obtained with the OPBE functional. The mean absolute deviation from benchmark high-level CASPT2 data is ca. 1 kcal·mol⁻¹, i.e. an order of magnitude smaller than other DFT functionals. Moreover, it correctly predicts the splittings for spin-crossover compounds, pyridylmethylamine compounds, and for a series of cyc[9]ane compounds.

References

1   M. Swart, A.R. Groenhof, A.W. Ehlers, K. Lammertsma, *J. Phys. Chem. A* 108, 5479-5483, 2004.

2   M. Swart, *submitted for publication.*

3   M. Güell, J.M. Luis, M. Solà, M. Swart, *J. Phys. Chem. A* 112, 6384-6391, 2008.

4   M. Swart, *Inorg. Chim. Acta* 360, 179-189, 2007.

5   M. Reiher, O. Salomon, B.A. Hess, *Theor. Chem. Acc.* 107, 48-55, 2001.

6   M. Reiher, *Inorg. Chem.* 41, 6928-6935, 2002.

7   N.C. Handy, A.J. Cohen, *Mol. Phys.* 99, 403-412, 2001.

8   J.P. Perdew, K. Burke, M. Ernzerhof, *Phys. Rev. Lett.* 77, 3865-3868, 1996.

9   M. Swart, M. Solà, F.M. Bickelhaupt, *J. Comput. Chem.* 28, 1551-1560, 2007.

10 A. Wu, Y. Zhang, X. Xu, Y. Yan, *J. Comput. Chem.* 28, 2431-2442, 2007.

11 W.G. Han, L. Noodleman, *Inorg. Chim. Acta* 361, 973-986, 2008.

12 W.G. Han, L. Noodleman, *Inorg. Chem.* 47, 2975-2986, 2008.

13 E.J. Baerends et al., ADF2007.01, SCM, Amsterdam.

14 M. Swart, A.W. Ehlers, K. Lammertsma, *Mol. Phys.* 102, 2467-2474, 2004.

15 M. Swart, F.M. Bickelhaupt, *J. Comput. Chem.* 29, 724-734, 2008.

16 M. Swart, F.M. Bickelhaupt, *Int. J. Quant. Chem.* 106, 2536-2544, 2006.

17 M. Swart, E. Rösler, F.M. Bickelhaupt, *Eur. J. Inor. Chem.*, 3646-3654, 2007.

18 K. Pierloot, S. Vancoillie, *J. Chem. Phys.* 125, 124303, 2006.

19 M. Güell, J.M. Luis, M. Solà, M. Swart, *in preparation.*

4. Results and discussion

4. Results and discussion

This section has been written with the aim of giving to the reader a general idea of all the results obtained in this Thesis. An accurate reading of each article of the previous section is necessary to know more details about them, especially for the computational methodology used in each case. In this summary of the results, we highlight the most interesting aspects of each study and emphasise the importance of theoretical studies to understand the experimental results.

The studies carried out during this Thesis can be divided into two different sections. In the first one, the reaction mechanism of systems containing copper at their active site has been studied using the B3LYP DFT functional. In the second one, the reliability of different theoretical methods to study systems containing copper, iron or other transition metals have been evaluated.

4.1. Theoretical studies of the reaction mechanism of systems containing copper

As it has been previously mentioned in the introduction, proteins that contain copper at their active site have a very important role in biologic systems. We decided to study the reaction mechanism of different systems containing copper: the catechol oxidase enzyme and two biomimetic complexes of copper proteins. These systems have at least one copper ion, which is coordinated to nitrogen and oxygen atoms. One important feature of this type of copper systems is that they are able to carry out the oxidation of specific aromatic substrates.

It should be said that in order to be able to carry out our theoretical studies, we had to simplify the systems and use models of the different active sites. We chose the B3LYP functional to perform the theoretical study of oxidation reaction mechanisms for the abovementioned copper systems. However, in two of these studies we carried out additional calculations with two other functionals, BLYP and OPBE, in order to check the reliability of the B3LYP method for the studied systems. In the following sections, the characteristics of each one of the systems and the reaction mechanisms proposed are described.

4.1.1. Theoretical study of reaction mechanism of catechol oxidase

The catechol oxidase is a type-3 active site copper protein which is able to catalyse the oxidation of catechol to the corresponding *o*-quinones (Scheme 13).[39] It should be mentioned that tyrosinase, another type-3 active site copper protein, is also capable of catalysing this reaction.[38]
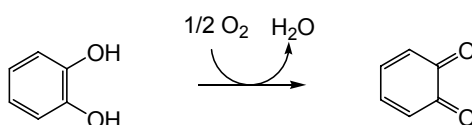
Scheme 13. Oxidation catalysed by catechol oxidase and tyrosinase.

The model of the catechol oxidase active site in our study (**Article I**) is based on the X-ray structure of the oxidized form from sweet potato.[54] It includes the first-shell histidine ligands and a cysteine which is linked covalently to one of the histidines. The structural histidines were modelled by imidazoles and the cysteine was modelled by SCH_3. This type of modelling has been shown to be appropriate on the basis of previous DFT studies of various enzymes.[188] To reproduce the protein strain and a realistic positioning of the different chemical units, specific restrictions on some nuclear coordinates were applied. This is important in modelling fragments not directly bound to the metal.[189,190]
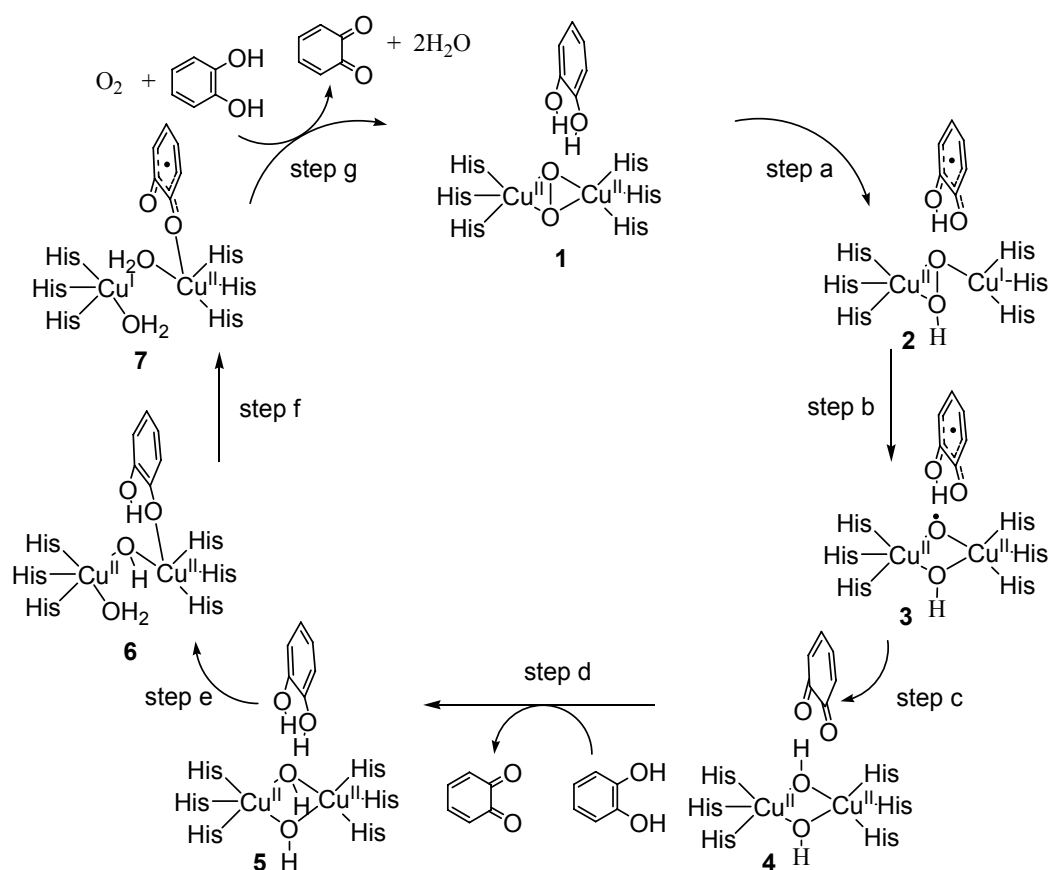
Scheme 14. Suggested catalytic cycle for catechol oxidase.

The mechanism and PESs that we obtained for our model are summarised in Scheme 14 and in Fig. 3, respectively. As can be seen in Scheme 14, in each catalytic cycle one dioxygen molecule and two catechols are consumed and two molecules of water and quinones are obtained. There is no variation of the charge of the active site during the reaction, since no protons or electrons leave or enter into the active site and all the substrates or products of the reaction are neutral. The catalytic cycle starts from the oxidised form of the enzyme and can be divided into two different half-reactions. In each one of them, a molecule of catechol is oxidised to a quinone. The first half-reaction goes from Structure 1 to Structure 4 and the second one goes from Structure 5 to Structure 7 (see Scheme 14). When the two water molecules and the quinone are released by Structure 7, a catechol and a dioxygen molecule enter into the system. At this point the catalytic cycle can start again.

For all the structures that intervene in the catalytic cycle, both the open-shell singlet and the triplet spin state were considered. The triplet state structures were always at least 2.0 kcal/mol higher in energy than the singlet ones. However, there were almost no differences in the geometries obtained for the two spin states and the reaction pathways for the catalytic cycle were the same.

In Fig. 3 the potential energy profile obtained for the open-shell singlet, which is the ground state, is depicted. The rate-determining step for the whole catalytic cycle is step b (see Scheme 14, Fig. 3), which corresponds to the O-O bond cleavage (TS23). Furthermore, the barrier obtained for this step is 12.1 kcal/mol, which is in reasonable agreement with the experimental energy barrier (13 kcal/mol).[191]
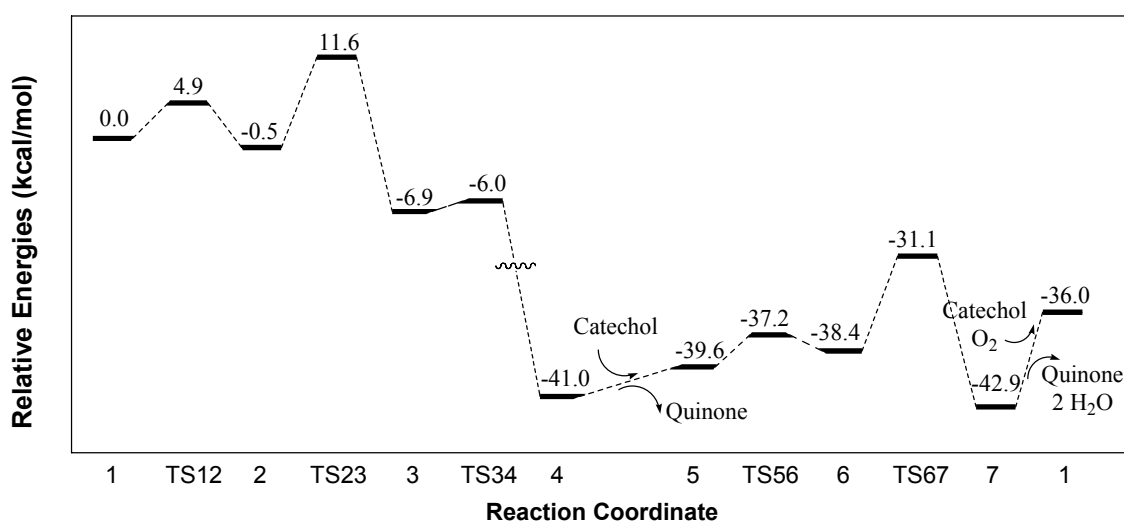

Fig 3. Potential energy profile obtained for ground state for the catalytic cycle of the catechol oxidase.

4.1.2. Theoretical study of reaction mechanism of biomimetic complexes of copper enzymes

Biomimetic complexes are widely used to study the reaction mechanism of enzymes. The high efficiency of tyrosinase catalysing the *ortho*-hydroxylation of monophenols has elicited extensive synthetic efforts to create copper complexes that can oxidize C-H bonds.[61,62] Recently, Stack and coworkers reported a synthetic $\mu\text{-}\eta^2\text{:}\eta^2\text{-}$peroxodicopper(II)(DBED)$_2$ complex (DBED = N,N'-di-*tert*-butylethylendiamine), which rapidly hydroxylates phenolates (Scheme 15).[85] A reactive intermediate consistent with a bis-μ-oxo-dicopper(III)-phenolate complex, with the O-O bond fully cleaved, was observed experimentally (intermediate A in Scheme 15). The evidence for sequential O-O bond cleavage and C-O bond formation in this synthetic complex suggested an alternative mechanism to the concerted or late stage O-O bond scission generally accepted for the phenol hydroxylation reaction performed by tyrosinase.[29,192] Consequently, we decided to model the reaction mechanism for the abovementioned complex (**Article II**). To reduce the computational costs, we replaced the DBED ligand by DMED (DMED = N,N'-dimethylethylendiamine), and the 2,4-di-*tert*-butylphenolate by phenolate as the substrate of the reaction.
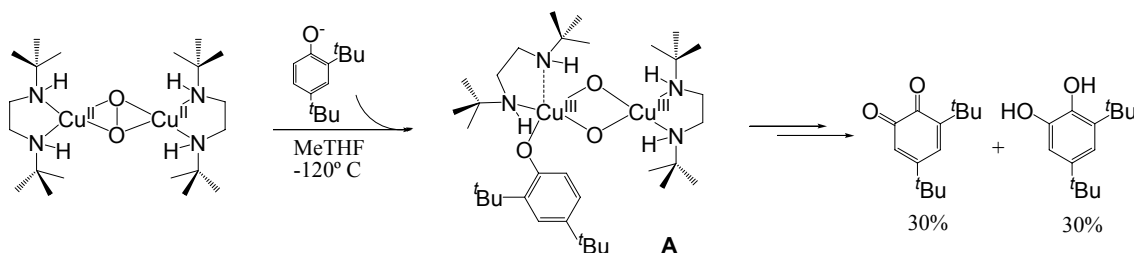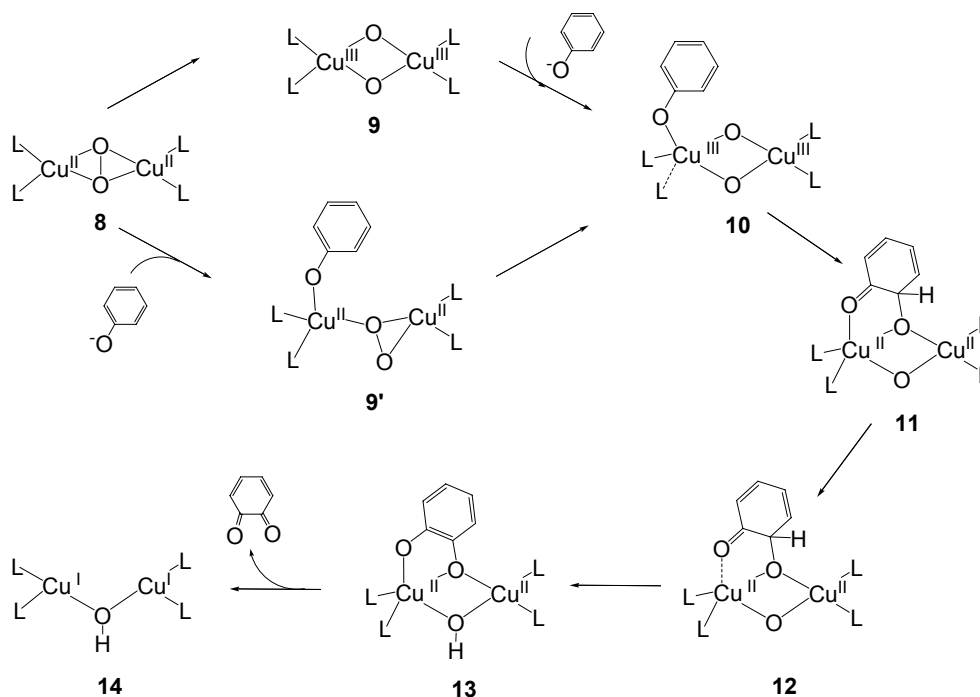
Scheme 15: Experimental results obtained by Stack and coworkers.[85]

At this point it should be said that for most of the biomimetic systems of tyrosinase, including the μ-η^2:η^2-peroxodicopper(II)(DBED)$_2$ complex we modelled, the substrate is an anion, a phenolate, while for the enzyme the substrate is neutral, a phenol.[61,62] Tyrosinase is thought to be capable of abstracting the proton of the phenol that it releases later to give the products. But for the studied complex, protons have to be added in the last step of the reaction in order to obtain the quinone and/or the catechol.[38] Moreover, since tyrosinase biomimetic complexes cannot restart the reaction by themselves, the reaction assisted by these compounds can be more exothermic than the reaction catalyzed by the enzyme.

Both bis-μ-oxo-dicopper(III) and μ-η^2:η^2-peroxodicopper(II) intervene in the reaction mechanism for the hydroxylation of phenolates by μ-η^2:η^2-peroxodicopper(II)(DMED)$_2$ complex. Some authors claim that comparisons of bis-μ-oxo to side-on peroxo energies should be made with pure functionals containing no HF exchange.[193,194] Consequently, we decided to study the dependence of the energy difference between the μ-η^2:η^2-peroxodicopper(II) and the bis-μ-oxo forms of the studied complex on the degree of HF exchange of the B3LYP functional. From the free energies of optimized isomers with the different degree of HF exchange, we can see that, in our Cu$_2$O$_2$(DMED)$_2^{2+}$ complex, when pure functional BLYP is used, the bis-μ-oxo isomer is 17.6 kcal/mol more stable than the peroxo isomer. The more the degree of HF exchange, the more stable the peroxo form of the studied complex is. It should be remarked that from all the functionals we used, the one whose parameters are the most similar to those used in B3LYP, is the best reproducing the experimental results for the Cu$_2$O$_2$(DBED)$_2^{+2}$ species. Furthermore, in a previous study, it was shown that geometry optimizations of the peroxo species computed with the HF method and pure DFT methods either gave unreasonable geometrical parameters or converged to the bis-μ-oxo isomer.[195] On the other hand, hybrid DFT methods reproduced nicely the measured geometrical parameters. For these reasons, we consider that B3LYP is a suitable method to carry out the study of the mechanism with our model.

For the open shell structures that intervene in the reaction mechanism, both the open-shell singlet and triplet spin states were considered. The mechanism and the potential energy profile that we obtained for the hydroxylation of phenolates by the μ-η^2:η^2-peroxodicopper(II)(DMED)$_2$ complex are summarised in Scheme 16 and in Fig. 4, respectively.

The proposed reaction mechanism follows an electrophilic aromatic substitution pattern that involves an intermediate with the O-O bond cleaved and the phenolate coordinated to a copper centre, which would correspond to the intermediate observed experimentally by Stack and coworkers (Structure 10, Scheme 16). The rate determining step for the hydroxylation of this intermediate to the final products is the attack of one oxygen atom of the Cu$_2$O$_2$ unit to the aromatic ring leading to a new C-O bond (Structure 10 $\rightarrow$ Structure 11, Scheme 16). It should also be highlighted that in this step a spin-crossing occurs.

Scheme 16. Suggested reaction mechanism for the μ-η^2:η^2-peroxodicopper(II)(DMED)$_2$ complex.

The barrier and the KIE for this ring hydroxylation step obtained with the B3LYP functional are in good agreement with the experimental results. After this step, in our model complex, the reaction proceeds with smooth energy barriers until the final quinone products are reached (Fig. 4). Our calculations seem to point that the O-O

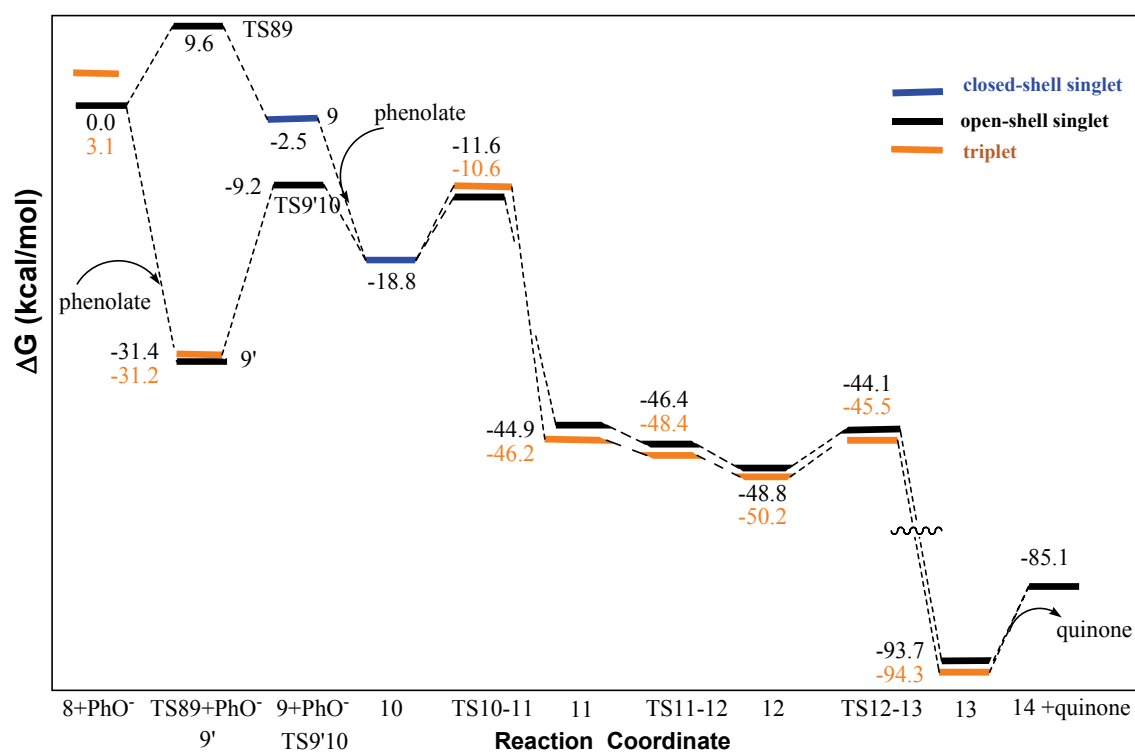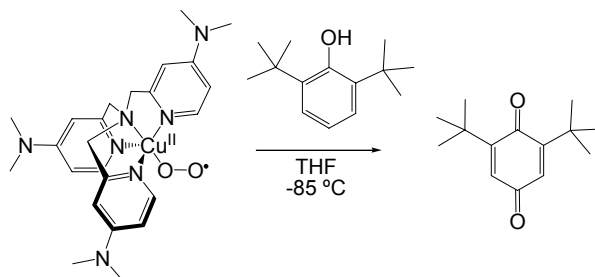**Fig. 4:** Free energy profile obtained for the mechanism of the hydroxylation of phenolates by μ-η^2:η^2-peroxodicopper(II)(DMED)$_2$ complex. Calculated Free Energies (G), relative to structure 8 plus phenolate, are given in kcal/mol.

cleavage could take place after the binding of the substrate. But unfortunately, to get a definitive answer on the first steps of the studied reaction mechanism, it is essential to include explicitly several solvent molecules in the model and to perform a study of the dynamics of the reaction.

Very recently,[196] Stack, Solomon and coworkers proposed an alternative mechanism for the hydroxylation of phenolates by the μ-η^2:η^2-peroxodicopper(II)(DMED)$_2$ complex. Their proposal differs from ours in the last steps of the mechanism and it suggests that the *ortho*-H$^+$ of the substrate of Structure 12 is transferred to nearby exogenous base, which leads to the formation of a new C-O bond. Subsequently the protonation of the oxygen atom not bound to the substrate by an exogenous base takes place. Finally another external proton is added, which leads to dimer dissociation into a Cu(II)-semiquinone monomer and a Cu(I) monomer.

The second biomimetic compound studied in the present Thesis is a copper(II)-superoxo complex, [Cu(II)(NMe$_2$-TMPA)-(O$_2$$^{\cdot-}$)]$^+$ (NMe$_2$-TMPA = tris(4-dimethylamino-2-pyridylmethyl)amine), capable of hydroxylating phenols with incorporated oxygen atoms derived from the Cu(II)–O$_2$$^{\cdot-}$ moiety (Scheme 17) (**Article III**).[94] Model studies addressing Cu(II)-superoxide reactivity patterns and the O-O cleavage reaction of the Cu(II)OOH species are of considerable interest.[197] This is due to the fact that the hydroxylation mechanism of mononuclear copper containing proteins such as peptidylglycine α-amidating monooxygenase (PAM) and dopamine β-monooxygenase (DβM) is not completely known.[23,56] There are several possible mechanisms for the reductive O$_2$-activation at the active site of these enzymes.[197] The aim of our analysis of the reaction mechanism for the [Cu(II)(NMe$_2$-TMPA)-(O$_2$$^{\cdot-}$)]$^+$ was to provide some insight into the nature of the chemical and biological copper-promoted oxidative processes with 1:1 Cu(I)/O$_2$-derived species.

Scheme 17: Experimental results obtained for the [Cu(II)(NMe$_2$-TMPA)-(O$_2$$^{\cdot-}$)]$^+$ complex.

In order to reduce the size of the studied system, we decided to replace the NMe$_2$ substituents of the rings by hydrogen atoms. In the new model, the geometry of the core and the spin density values as well as the relative energies of the different electronic states studied, are almost identical to the ones of the complete system.

Like in the two preceding studies, B3LYP functional has also been used to carry out the study of hydroxylation of phenols by the [Cu(II)(NMe$_2$-TMPA)-(O$_2$$^{\cdot-}$)]$^+$ complex and both the open-shell singlet and triplet spin states were considered. At this point it should be said that previous studies show that B3LYP functional gives good results when studying systems with the Cu(II)–O$_2$$^{\cdot-}$ moiety.[198] Furthermore, since for this reaction the open-shell singlet and the triplet give different reaction pathways (*vide infra*), we have explored the capability of B3LYP to determine the relative energies between different spin states. To do so, we carried out single point calculations for several structures that intervene in the present reaction mechanism using OPBE, which has very good performance for spin state-splitting.[149,151,169] In all the studied cases there

178
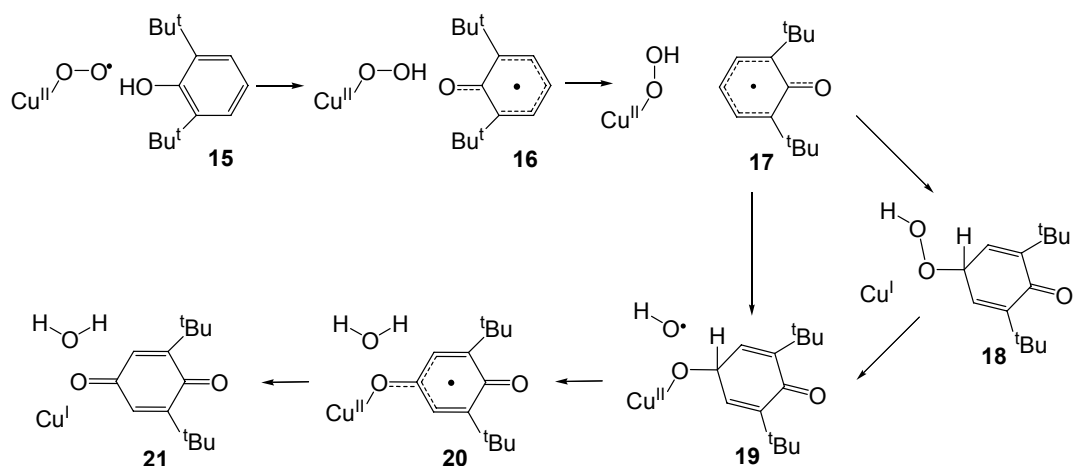
Scheme 18: Suggested reaction mechanism for hydroxylation of phenols by the [Cu(II)(NMe$_2$-TMPA)-(O$_2$$^{\cdot-}$)]$^+$ complex.

is no difference between the ground-state found using B3LYP and the one found using OPBE.

The mechanism and the potential energy profile obtained for the hydroxylation of phenols by our model of the [Cu(II)(NMe$_2$-TMPA)-(O$_2$$^{\cdot-}$)]$^+$ complex are summarised in Scheme 18 and in Fig. 5, respectively. The following other possible pathways have also been studied: i) the direct attack of the copper superoxo species at the *para*-carbon followed by H transfer reactions ii) the isomerisation of the hydroperoxo species after/during the attack on the aromatic system iii) the O-O bond cleavage previous to the attack on the ring. But all these alternative mechanisms have free energy barriers higher than the rate-determining step of the mechanism shown in Scheme 18. For the studied
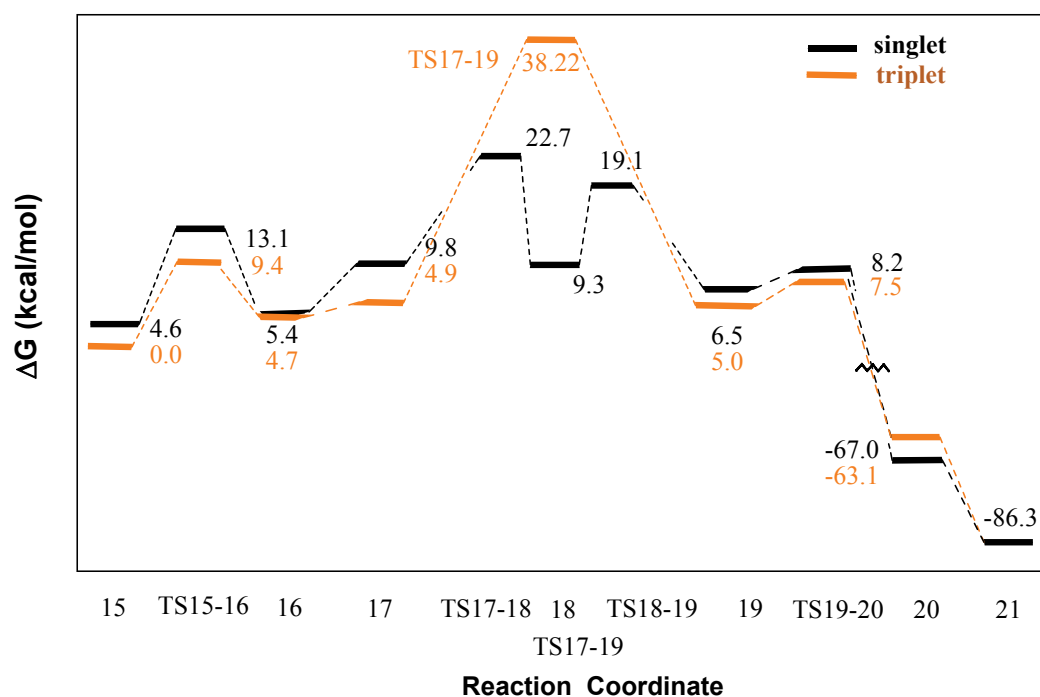

Fig. 5: Free energy profile obtained for the mechanism of the complex at the B3LYP level of theory. Calculated Free Energies (G) are given in kcal/mol.

complex, there are two different pathways depending on the spin state after the hydrogen transfer from the substrate. For the open-shell singlet spin state, first the attack on the ring by the terminal oxygen atom of the complex takes place (Structure 17 → Structure 18, Scheme 18) and then there is the O-O bond cleavage (Structure 18 → Structure 19, Scheme 18). On the other hand, for the triplet spin state, there is a step where the C-O bond formation and the O-O bond cleavage occur in a concerted manner (Structure 17 → Structure 19, Scheme 18). The rate-determining step for the mechanism is the C-O bond formation, which occurs in the open-shell singlet state (see Fig. 6). For the studied system, the O-O bond cleavage cannot take place before the C-O bond formation. Consequently, the corresponding $[Cu=O]^{2-}$ species does not exist as an intermediate. Finally, from the studied pathways, it can be said that the hydroxoperoxo intermediate itself is capable of mediating the hydroxylation of the substrate.

In all the three previous studies, the hybrid DFT functional has been used and, despite the simplifications carried out in the systems, the obtained results are in reasonable agreement with the available experimental data. For all of them, both the singlet and the triplet spin states have been studied. It should be highlighted that for the catechol oxidase enzyme and the $Cu_2O_2(DMED)_2^{2+}$ complex, the singlet and triplet spin states have the same reaction pathway, while for the $[Cu(II)(NMe_2\text{-}TMPA)\text{-}(O_2^{\cdot-})]^+$ complex we obtain two reaction paths that have different rate-determining steps. It is also interesting to note that the reactions carried out by the two biomimetic complexes are much more exothermic than the catalysed by the enzyme. Consequently, the reaction carried out by the formers cannot be restarted.

All the three studied systems have active sites with copper and oxygen atoms but, they mediate oxidation reactions of different aromatic substrates. On one hand, as it is indicated by its name, the catechol oxidase enzyme oxidases catechols. On the other hand, the $Cu_2O_2(DMED)_2^{2+}$ complex and $[Cu(II)(NMe_2\text{-}TMPA)\text{-}(O_2^{\cdot-})]^+$ intervene in the hydroxylation of phenolates and phenols (which only differ in one proton) respectively. However, the reaction mechanisms of the two latter compounds are very different.

Another interesting comparison among the three studied compounds is the rate-determining step. For the catechol oxidase and $Cu_2O_2(DMED)_2^{2+}$ complex, both of them having $Cu_2O_2(DMED)_2^{2+}$ complex structure at the starting point of the mechanism, the rate-determining step is the O-O bond-cleavage. In contrast, for the $[Cu(II)(NMe_2\text{-}TMPA)\text{-}(O_2^{\cdot-})]^+$ complex, the attack on the ring by the hydroperoxide moiety, which leads to the formation of a new C-O bond, is the rate limiting step.

Finally, the localization of the unpaired electrons also presents differences in the three systems. In the reaction pathway for the $Cu_2O_2(DMED)_2^{2+}$ complex the unpaired electrons of the system are always on the copper or oxygen atoms that form the core of the $Cu_2O_2(DMED)_2^{2+}$ complex in the first step of the reaction. On the other hand, for the other two systems, the unpaired electrons can be in the copper atoms, the oxygen atoms that formed the dioxygen molecule or delocalized on the substrate.

To sum up, three copper-containing systems with different $Cu_n\text{-}O_2$ structures have been studied with the same methodology and we obtain results that agree with the experimental data. We have found differences but also common aspects among these three different systems. Finally, we provided some insight into the nature of the chemical and biological copper-promoted oxidative processes with 1:1 and 2:1 $Cu(I)/O_2$-derived species.

4.2. DFT studies of complexes containing Fe and Cu and other transition metals

Choosing the right methodology is essential in the theoretical studies of the reaction mechanisms. Density functional theory (DFT) is the usual method of choice for studies of enzymatic or organometallic catalytic reaction mechanisms.[155,165] This is due to the fact that the current hybrids or meta-GGA functionals provide, in general, similar or even better results on geometries and relative energies than MP2 calculations but using far less computer time. B3LYP, the hybrid DFT functional used in the first part of this Thesis, in general performs well in systems that contain transition metals. Unfortunately, however, this is not always the case and before starting to study a system the methodology used has to be carefully checked. In this second part of the Thesis, systematic studies of systems containing copper, iron and some other transition metals using different methods have been done in order to determine their reliability to study such transition metal compounds.

4.2.1. Theoretical study of the ground and low-lying electronic states of CuO$_2$.

One of the most important enzymes in humans that contains copper in the active site is the superoxide dismutase (SOD).[199] This enzyme provides cellular defense against the oxidative stress by catalyzing O_2^- disproportionation into the less toxic dioxygen and hydrogen peroxide:

$$2\ O_2^- + 2H^+ \rightarrow O_2 + H_2O_2 \tag{12}$$

The copper site is at the heart of the enzymatic active site of the SOD protein. The catalysis is a two-step process: one molecule of superoxide first reduces Cu^{2+} to form dioxygen and then a second molecule of O_2^- reoxidizes Cu^+ to form hydrogen peroxide (See Eq. 12).[200,201] To study theoretically the mechanism for the toxic superoxide radical disproportionation by SOD, it is necessary to employ methods that describe correctly the interaction between copper ions (Cu^+ and Cu^{2+}) and the superoxide radical (O_2^-).

It should be mentioned that recently it was shown that many DFT methods fail to predict the correct ground electronic state of Cu^{2+}-H_2O.[202] It was also found that the relative stability of the different electronic states in Cu^{2+}-H_2O strongly depends on the degree of mixing of exact HF and DFT exchange functional.[202] Consequently, we decided to study the performance of different DFT methods for the description of the geometry and energetics of the ground and low-lying states of CuO$_2$ and CuO$_2^+$ (**Article IV**).

Preliminary calculations of the singlet and triplet CuO$_2^+$ species showed that, qualitatively, the DFT relative energies of the ground and low-lying electronic states follow the same trends as those provided by the CCSD(T) method. For this reason, we focused on the capability of DFT to provide the right energetic order and geometry (end-on C$_s$ or side-on C$_{2v}$, Fig. 6) of the ground and low-lying states of the doublet CuO$_2$.
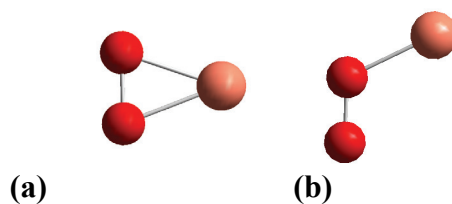
(a)   **(b)**

Fig. 6: (a) Side-on (C$_{2v}$) and (b) end-on (C$_s$) structures of CuO$_2$

The C$_{2v}$ and C$_s$ stationary point geometries and energies of doublet CuO$_2$ were examined in the ground and low-lying states for a series of different type of density functional methods (pure, hybrid and meta-hybrid) and CCSD(T) methods using the 6-311+G(d). The single point energies of the C$_{2v}$ and C$_s$ ground and low-lying states at the optimized CCSD(T)/6-311+G(d) basis set geometries using the aug-cc-pVTZ and aug-cc-pVQZ basis sets and extrapolating to the CBS limit have also been computed. Furthermore, the effect of changing the amount of HF exchange included in the B3LYP functional was accurately analyzed. At this point it should be noted that we had previously analysed the effect of the exact exchange in the B3LYP functional in the energy difference between the μ-η^2:η^2-peroxodicopper(II) and the bis-μ-oxo forms of the Cu$_2$O$_2$(DMED)$_2^{2+}$ complex (**see Article II**).

At the CCSD(T)/6-311+G(d) level, the ground electronic state for the CuO$_2$ doublet presents C$_{2v}$ geometry and it is a $^2A_2$ state. However, the end-on C$_s$ $^2A''$ electronic state lies, less than 1 kcal mol^{-1} above. At the CCSD(T) level of theory the relative order of the electronic states is $^2A_2(C_{2v})$ < $^2A''(C_s)$ < $^2B_2(C_{2v})$ < $^2A'(C_s)$ << $^2A_1(C_{2v})$ < $^2B_1(C_{2v})$. The same relative stability order is obtained with single point energy calculations at the optimized CCSD(T)/6-311+G(d) geometries using the aug-cc-pVTZ and aug-cc-pVQZ basis sets and extrapolating to the CBS limit. However, at the CBS limit, the difference between $^2A_2$ and the $^2A''$ increases from 0.03 kcal mol^{-1} to 1.5 kcal mol^{-1} (Fig. 7).
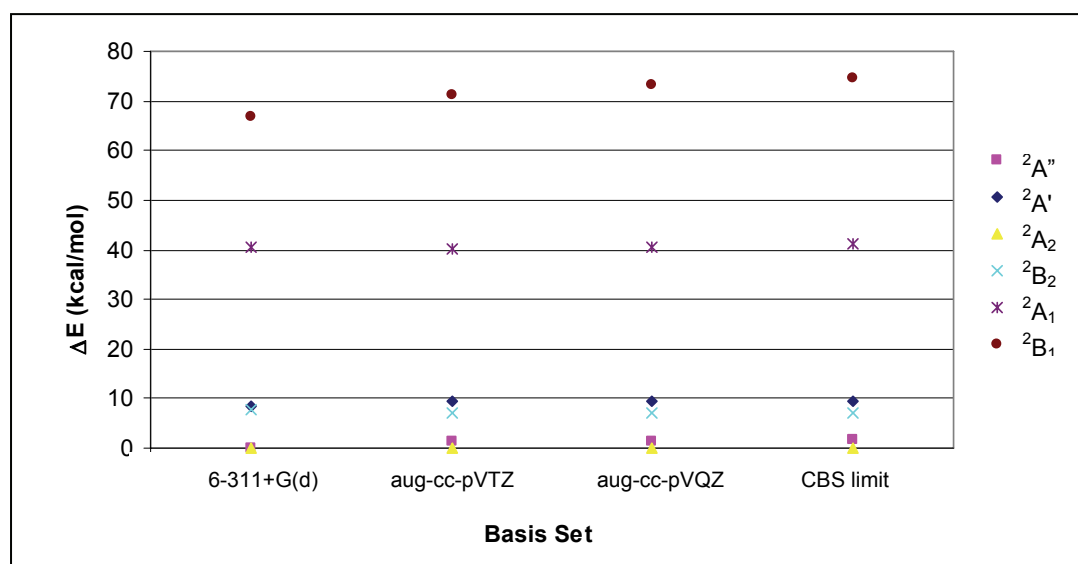

Fig. 7: Relative Energies (in kcal/mol) of the Ground and Low-Lying Electronic States of CuO$_2$ at CCSD(T) level of theory with different basis sets at the optimized CCSD(T)/6-311+G(d) geometry.

The previous results are reproduced by none of the DFT functionals that have been used, since in all cases the computed ground state is the ^{2}A'' with an end-on C_s geometry. The relative energy between the $C_{2v}(^2A_2)$ and $C_s(^2A'')$ structures computed for the different functionals ranges between 2 and 16 kcal mol^{-1}, being the BHandH the functional that better compares with CCSD(T). However, when one compares the best geometries and relative energies with respect to CCSD(T) results for *all* the different electronic states analyzed, it is found that B3LYP gives the smallest standard deviations.

At this point it should be mentioned that one of the DFT functionals used in this study is the OPBE, which has shown an excellent performance for spin-state splittings.[149,151,203] However, for both geometries and energies OPBE functional gives similar results to the ones given by other functionals.

As to the effect of the exact exchange is concerned, it is found that the B3LYP-like functional yielding better geometries contains 20% of exact exchange. On the other hand, for relative energies the B3LYP-like functional with a larger contribution of exact exchange (90%) is the one giving the smaller standard deviation (Fig. 8).
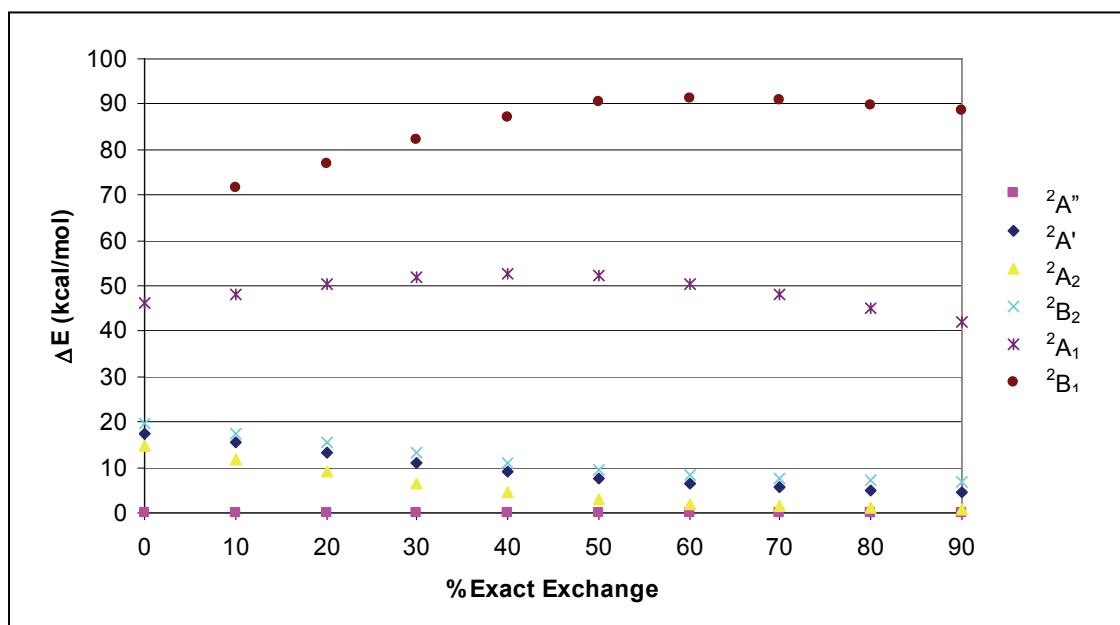
Fig. 8: Relative energies (in kcal mol^{-1}) of the ground and low-lying electronic states of CuO_2 computed with the B3LYP method using different percentage of exact exchange parameter sets with basis 6-311+g(d).

From our calculations it is clear that only high level *ab initio* methods providing a good estimation of correlation energy (such as MCSCF or CCSD) are able to give the correct relative energies of the different states in CuO_2. Since such methods are usually not affordable for large $L_nCu(I)$-O_2^- species, the functional of choice for these cases should be the B3LYP method for geometry optimizations followed by single point calculations with a B3LYP-like functional containing a large percentage of HF exchange.

4.2.2. Theoretical calculation of relative energies of spin states of iron and other first row transition metal compounds

Correctly predicting relative energies of spin states (i.e. spin-state splittings) of transition-metal complexes is a necessary requirement for being able to distinguish between competing pathways for reactions of (bio)inorganic compounds. Recent validation studies of Density Functional Theory (DFT)[139] functionals[169] have shown an excellent performance of the OPBE[149,151,203] functional for iron spin-state splittings. Other recent papers criticized the OPBE functional, and questioned its reliability for the spin-state splittings.[204-207] However, several of these papers used Gaussian-type orbitals (GTOs) or Effective Core Potentials Basis-sets (ECPBs),[138]while the abovementioned successes of OPBE were mainly shown in studies that use Slater-type orbital (STO)[138,208] basis sets. Therefore, the criticism of the OPBE functional might as well be resulting from the choice of basis set used. Consequently, we decided to carry out a systematic investigation of the influence of the basis set on spin-state splittings of iron complexes when using the OPBE functional (**Articles V and VII**).

The relative *vertical* spin-state energies for three Fe(III) compounds (see Scheme 19) that have either a low (22),[209] intermediate (23)[210] or high (24)[211] spin ground state experimentally have been used. The spin-state splittings were computed using the OPBE functional with a variety of basis sets that include STOs, GTOs, ECPBs, and mixed ECPB(Fe):GTO(rest) basis sets. Moreover, we also examined the influence of the basis set on the geometry optimization for the three spin-states of a small iron complex (25, FeFHOH), by looking at both the structure and the resulting *relaxed* spin-state splittings.
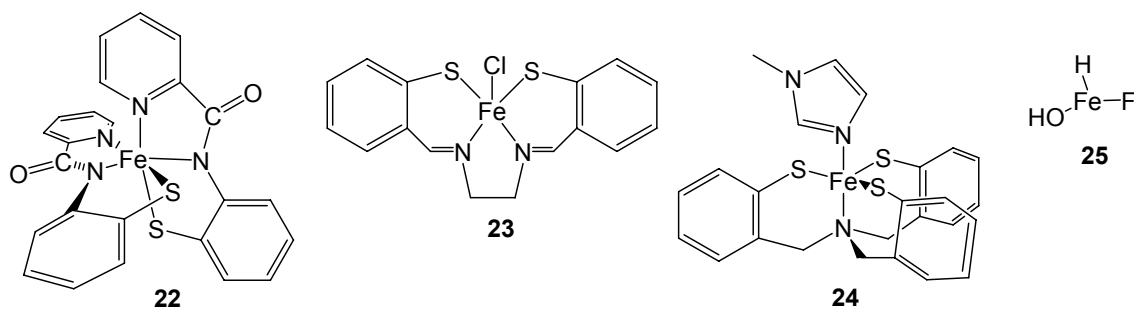
Scheme 19: Iron complexes studied with OPBE using different basis sets: (1) Fe-(PyPepS)$_2$ (PyPepSH$_2$ = *N*-(2-mercaptophenyl)-2-pyridinecarboxamide) (22), Fe(tsalen)Cl (tsalen) = *N*,*N*′-ethylenebis-(thiosalicylideneiminato)) (23), Fe(N(CH$_2$-*o*-C$_6$H$_4$S)$_3$)(1-Me-imidazole) (24), FeFHOH (25).

Reliable and consistent results for spin state energies and geometries have been obtained when using Slater-type orbital (STO) and very large Gaussian-type orbital (GTO) basis sets. An infinitely large GTO basis set should in principle give the same final results as the STO series, which is indeed what we see happening for the *vertical* and *relaxed* spin-state splittings. However, the convergence of the result with basis set size is much slower for GTOs than for STOs. Substantial deviations (2-10 kcal/mol) and inconsistencies are observed when using small GTO, Effective Core Potential (ECPB) or mixed ECPB(Fe):GTO(rest) basis sets (Fig. 9). Using three primitive GTOs for core electrons (3-21G) is shown to be insufficient and results in large deviations (14 kcal/mol on average for compounds 1-3, 19-24 kcal/mol for high spin states).

The ECPB and mixed ECPB(Fe):GTO(rest) basis sets are unable to give an accurate prediction of spin-state splittings. Most ECPBs underestimate the energy for
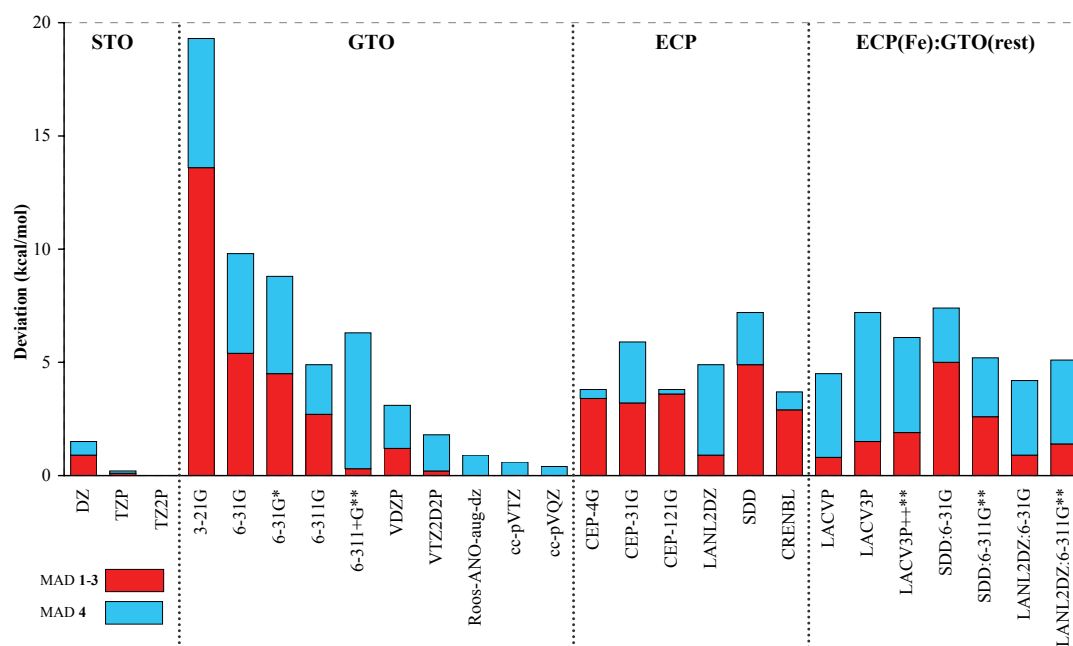
Fig. 9: MAD values (kcal/mol) for different basis sets (MAD **1-3** value not available for large GTO basis sets Roos-ANO-aug-dz, cc-pVTZ, and cc-pVQZ).

the high spin-state, typically by some 5 kcal/mol, while increasing the valence GTO basis set does not always lead to better results. This shows clearly that the replacement of the effect of core electrons by a model (ECP) Hamiltonian differs systematically from the accurate STO-GTO results.

After the success of OPBE functional predicting correctly the ground spin state when using Slater-type orbital (STO) and large Gaussian-type orbital (GTO) basis sets (**Article V**), we decided to carry out another investigation to study the reliability of this functional for a very special type of iron(II) complexes (**Article VI**). We selected a wide range of iron(II) complexes with *tris*-pyrazolylborate and *tris*-pyrazolylmethane ligands (see Scheme 20), whose spin states depend very much on the substituents in the pyrazolyl rings, and in many cases on the counterion.[212,213] The majority of Fe(II)-pyrazolylborate complexes have the advantage of being neutral molecular complexes while Fe(II)-pyrazolylmethane complexes have a positive charge of 2. For this reason, we considered that studying both types of complexes was challenging in order to test the reliability of OPBE with these tricky compounds. Moreover, these calculations would enable the straightforward analysis of the spin-state preferences of these compounds, and how these are influenced by substitution patterns. At the same time, they would provide the structures of all species, including for those complexes that are experimentally either unattainable (e.g. crystallization disorders) or inconclusive due to counterion effects.

For the majority of these compounds there is a wealth of experimental data available, which makes the study even more interesting since the obtained results could be compared directly with the experimental data. Since thermally or pressure induced high-low spin transition has been evidenced by ^{57}Fe Mössbauer spectroscopy for both iron(II) poly(pyrazolyl)borate and poly(pyrazolyl)methane complexes, we have also computed the isomer shift and the quadrupole splitting and compared them with the experimental values.

	X	R_3	R_4	R_5
B1	B	H	H	H
C1	C	H	H	H
B2	B	CH_3	H	H
C2	C	CH_3	H	H
B3	B	CF_3	H	H
C3	C	CF_3	H	H
B4	B	H	CH_3	H
C4	C	H	CH_3	H
B4'	B	H	Br	H
C4'	C	H	Br	H
B5	B	H	H	CH_3
C5	C	H	H	CH_3
B6	B	H	H	CF_3
C6	C	H	H	CF_3
B7	B	CH_3	H	CH_3
C7	C	CH_3	H	CH_3
B8	B	CH_3	CH_3	CH_3
C8	C	CH_3	CH_3	CH_3
B8'	B	CH_3	Cl	CH_3
C8'	C	CH_3	Cl	CH_3

	X
B9	B
C9	C

	X	Y
B10	B	C
C10	C	C
B11	B	N
C11	C	N
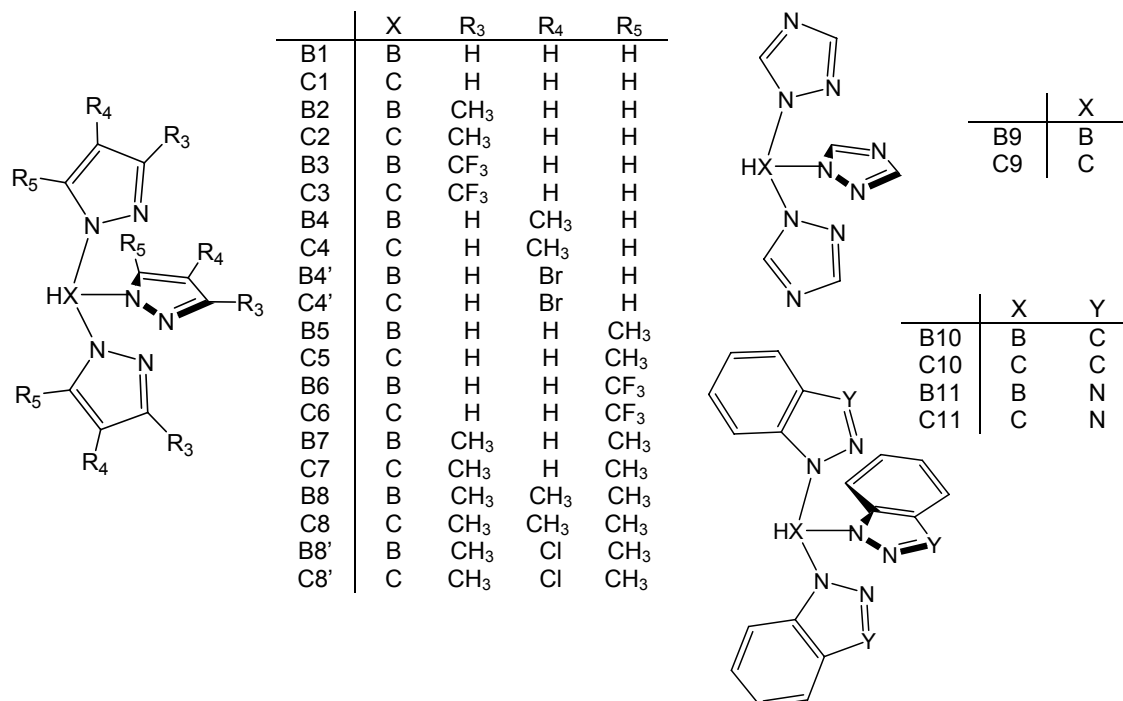
Scheme 20: Tris-pyrazolylborate and tris-pyrazolylmethane ligands for the mononuclear iron(II) complexes studied

Our study suggests that the spin-state of mononuclear iron(II) *tris*-pyrazolylborate and *tris*-pyrazolylmethane can be regarded, in a first approximation, as a balance between electronic (σ-donation and π-donation) and steric interactions of the *tris*-pyrazolylborate and *tris*-pyrazolylmethane ligands with the iron center. A decrease in the steric requirements in the ligands, obtained by a suitable substitution, promotes the low-spin population in SCO complexes, and vice versa.

The pyrazolylborate and corresponding pyrazolylmethane complexes bear a striking resemblance in terms of preference for spin ground-state and structural characteristics. This is governed completely by the covalent bonding interactions between the iron(II) and the ligating nitrogens, which is found to be highly similar between any borate complex and its corresponding methane complex. The only and major difference in metal-ligand bonding between the borates and methanes is observed in the electrostatic interactions, which explains the greater stability of the former. Moreover, it explains the critical dependence of the spin-state splittings on the presence, location and nature of counter-ions

For almost all the studied complexes, the theoretical results at the OPBE/TZ2P level were in agreement with the experimental data. Furthermore, the computed isomer shift and quadrupole splitting were very close to the experimental values. Consequently, we can say that the OPBE functional, when is used with STO basis set, is able to give the correct spin state even for compounds whose ground state is very dependent on the substitution pattern of its ligands and/or the nature and position of the counterions.

With this good performance of OPBE with TZ2P basis set for iron compounds in mind, we were interested if this functional would also work as well for other transition metals. Therefore, we studied several complexes for which experimental data are available for a series of transition metals (Cr, Mn, Fe, Co, Ni, Cu, Zn; some of which in different oxidation states). We chose a complex based on the triazacyclononane ligand,

$(TM([9]ane_3)_2^{n+}$ (Fig. 10, left) and also complexes with some of the *tris*-pyrazolylborate ligands of the iron(II) complexes studied previously, $TM(Tp)_2^{n-2}$ (Fig. 10, right) (**Article VII**). At this point it should be said that it was already shown that OPBE correctly predicts the spin ground-state for the $(Fe([9]ane_3)_2^{3+}$ and in one of our previous studies we were also able to predict the spin-ground state for the $Fe(Tp)_2$, $Fe(Tp^{3,5Me})_2$, $Fe(Tp^{4Me})_2$ and $Fe(Tp^{4Br})_2$ compounds (**Article VI**).
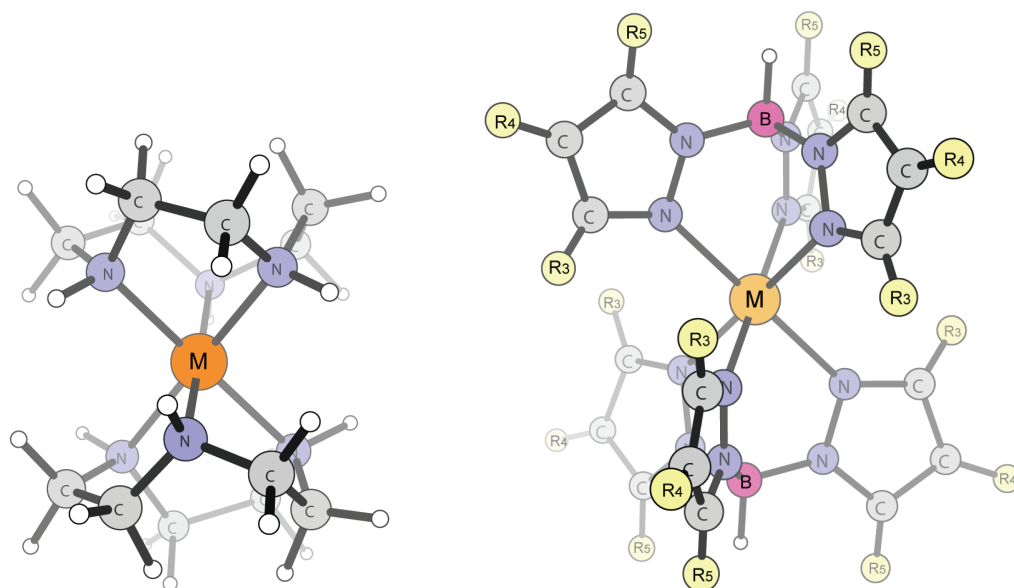
Fig. 10: Bis complexes of transition-metals (TM) with 1,4,7-triazacyclononane and *tris*-pyrazolylborate ligands $(TM([9]ane_3)_2^{n+}$ and $TM(Tp)_2^{n+})$

For the all the studied bis complexes of transition-metals with 1,4,7-triazacyclononane and *tris*-pyrazolylborate ligands and several transition metals, the ground-state predicted using the OPBE/TZ2P level of theory agrees with the experimental data.

At this point it should be highlighted that the success of OPBE depends on the type and size of basis set used in the calculations. In order to obtain the best results, STO basis sets have to be used. Using OPBE functional with STO basis sets, we succeeded in predicting the ground spin state of a wide range of iron(II) complexes with *tris*-pyrazolylborate and *tris*-pyrazolylmethane ligands, whose spin states depend very much on the substituents in the pyrazolyl rings, and in many cases on the counterion. Furthermore, the reliability of OPBE is not only restricted to iron complexes, since we also managed to obtain the correct ground state for several bis complexes of transition-metals (Cr, Mn, Fe, Co, Ni, Cu, Zn) with 1,4,7-triazacyclononane and *tris*-pyrazolylborate ligands.

To sum up, the selection of the functional or/and the basis set to use depends on the problem at hand, i.e., on both the property and type of system under study, and on the availability and computational expense associated and carefully weighting all these aspects is essential before embarking in a new DFT study.

5. Conclusions

5. Conclusions

The most remarkable conclusions that can be taken out from the previous computational studies performed for systems of biochemical interest containing Fe and Cu transition metals can be summarised in the next points:

FIRST:

The catalytic cycle of catechol oxidase has been studied at the B3LYP level of theory with a model where no proton enters or leaves the active site region, thus keeping the charge constant at the active site. The suggested mechanism starts out with an oxidation of $Cu_2(I,I)$ by dioxygen to $Cu_2(II,II)$, forming a $\mu-\eta^2{:}\eta^2$ bridging peroxide. The most critical step of the proposed catalytic cycle is the peroxide O-O bond cleavage, which has a barrier that is in reasonable agreement with the experimental rate. In some steps there is a monodentate coordination of the substrate to the dicopper core, which is in line with the proposal by Krebs and co-workers.

SECOND:

The full reaction mechanism of the hydroxylation of phenols mediated by the $Cu_2O_2(N,N'\text{-dimethylethylendiamine})_2^{2+}$ complex has been studied at the B3LYP level of theory. The proposed reaction mechanism follows an electrophilic aromatic substitution pattern that involves an intermediate with the O-O bond cleaved and the phenolate coordinated to a copper centre. The rate determining step for the hydroxylation of this intermediate to the final products is the attack of one oxygen atom of the Cu_2O_2 unit to the aromatic ring leading to a new C-O bond. The barrier and the KIE for this ring hydroxylation step obtained with the B3LYP functional are in good agreement with the experimental results. Including explicitly several solvent molecules in the model and performing a study of the dynamics of the reaction would be necessary to get a definitive answer on whether O-O cleavage takes place before or after the binding of the substrate.

THIRD:

The mechanism of the hydroxylation of phenols mediated by the end-on bound superoxo copper(II) complex $[Cu(II)(NMe_2\text{-TMPA})\text{-}(O_2{}^{\cdot-})]^+$ has been described at the B3LYP level of theory. The triplet spin state is the ground state. The rate-determining step for the mechanism is the C-O bond formation, which occurs in the open-shell singlet state. For the studied system, the O-O bond cleavage cannot take place before the C-O bond formation. Consequently, the corresponding $[Cu=O]^{2-}$ species does not exist as an intermediate. Finally, the hydroxoperoxo intermediate itself is capable of mediating the hydroxylation of the substrate.

FOURTH:

The C_{2v} and C_s ground and low-lying states stationary point geometries and energies of doublet CuO_2 have been examined for a series of different type density functional (pure, hybrid, and meta-hybrid) and CCSD(T) methods. The effect of changing the B3LYP functional a_o parameter is also explored. All DFT methods analyzed in this work erroneously predict the end-on ^2A" state as the ground state for CuO_2 irrespective of the type of functional and percentage of Hartree-Fock (exact) exchange included in the B3LYP-like functional. Among the different functionals tested, B3LYP gives the best geometries and relative energies for the different electronic states when compared to CCSD(T) results. As to the effect of the a_o parameter is concerned, it is found that the B3LYP-like functional yielding better geometries contains 20% of exact exchange and for relative energies, the B3LYP-like functional with a larger contribution of exact exchange (90%) is the one giving the smaller standard deviation.

FIFTH:

We have analysed the influence of the basis set on the spin-state energies of iron compounds when using the OPBE functional. Reliable and consistent results for spin-state energies and geometries have been obtained when using STO and large GTO basis sets. Substantial inconsistencies and deviations are observed when using (small) GTO, ECPB, or mixed ECPB(Fe):GTO(rest) basis sets. Large GTO basis give the same final results as the STO series, but the convergence of the result with respect to basis set size is much slower for GTOs than for STOs. The ECPB and mixed ECPB(Fe):GTO(rest) basis sets are not capable to give an accurate prediction of spin-state splittings. Most ECPBs underestimate the energy for the high spin state, while increasing the valence GTO basis set does not always lead to better results.

SIXTH:

We have studied a wide range of iron(II) complexes with *tris*-pyrazolylborate and *tris*-pyrazolylmethane ligands whose spin state depend very much on the substituents in the pyrazolyl rings and in many cases on the counterion using OPBE functional and STO basis sets. The pyrazolylborate and corresponding pyrazolylmethane complexes are very similar in terms of preference for spin ground-state and structural characteristics. This is governed by the covalent bonding interactions between the iron(II) and the ligating nitrogens, which are found to be highly similar between any borate complex and its corresponding methane complex. The only difference in metal-ligand bonding between the borates and methanes is observed in the electrostatic interactions, which explains the greater stability of the former. Moreover, it explains the critical dependence of the latter as well as the spin-state splittings on the presence, location and nature of counterions.

SEVENTH:

    We have studied several bis complexes of transition-metals (Cr, Mn, Fe, Co, Ni, Cu, Zn) with 1,4,7-triazacyclononane and *tris*-pyrazolylborate ligands using OPBE functional with Slater-Type Orbitals. For all the studied complexes, the predicted ground-state agrees with the experimental data available in the literature.

6. Complete List of Publications

6. Complete List of Publications

This Thesis is based on the following papers:

I.   Theoretical study of the catalytic mechanism of catechol oxidase, **Güell, M.; Siegbahn, P.E.M.,** J. Biol. Inorg. Chem. 12 (2007) 1251–1264

II.   Theoretical study of the hydroxylation of phenolates by the $Cu_2O_2(N,N'$-dimethylethylendiamine$)_2^{2+}$ complex **Güell, M.; Luis, J.M.; Solà, M.; Siegbahn, P.E.M. ,** J. Biol. Inorg. Chem. 14 (2009) 229-242

III.   Theoretical study of the hydroxylation of phenols mediated by an end-on bound superoxo copper(II) complex **Güell, M.; Luis, J.M.; Siegbahn, P.E.M.; Solà, M.** J. Biol. Inorg. Chem. 14 (2009) 273-285

IV.   The Ground and Low-Lying Electronic States of CuO_2. Yet another problematical species for DFT methods **Güell, M.; Luis, J.M.; Rodríguez-Santiago, L.; Sodupe, M.; Solà, M.** J. Phys. Chem. A. 113 (2009) 1308-1317

V.   Importance of the basis set for the spin-state energetics of iron complexes, **Güell, M.; Luis, J.M.; Solà, M.; Swart, M.,** J. Phys. Chem. A. 112 (2008) 6384-6391

VI.   The spin-states and spin-transitions of mononuclear iron(II) complexes of *tris*-pyrazolylborate and *tris*-pyrazolylmethane ligands **Güell, M.; Solà, M.; Swart, M.,** Polyhedron, accepted.

VII.   Accurate spin state energies for 1st row transition metal compounds, **Swart, M.; Güell, M.; Luis, J.M.; Solà, M.** Proceedings of the 9th European Biological Inorganic Chemistry Conference, Wroclaw, Poland, 2-6 September 2008.

Publications not included in this Thesis:

I.   Olefin-Dependent Discrimination Between Two Nonheme HO-Fe^V=O Tautomeric Species in Catalytic H_2O_2 Epoxidations, **Company, A.; Feng, Y.; Güell, M.; Ribas, X.; Luis, J.M.; Que, L., Jr.; Costas, M.** Chem. Eur. J. 15 (2009) 3359-3362

II.   Nanosized trigonal prismatic and antiprismatic CuII coordination cages based on tricarboxylate linkers, **Company, A.; Roques, N.; Güell, M.; Mugnaini, V.; Gómez, L.; Imaz, I.; Datcu, A.; Solà, M.; Luis, J.M.; Veciana, J.; Ribas, X.; Costas, M.**, Dalton Trans. (2008) 1679-1682

III.   A Theoretical Study of the Reaction Mechanisms Involved in the Thermal Intramolecular Reactions of 1,6-Fullerenynes, **Güell, M.; Martín, N.; Altable, M.; Filippone, S.; Martín-Domenech, A.; Solà, M.**, J. Phys. Chem. A 111 (2007) 5253-5258

IV.   Alkane Hydroxylation by a Nonheme Iron Catalyst that Challenges the Heme Paradigm for Oxygenase Action, **Company, A.; Gómez, L.; Güell, M.; Ribas, X.; Luis, J. M.; Que, L., Jr.; Costas, M.**, J. Am. Chem. Soc. 129 (2007) 15766-15767

V.   Analysis of Electron Delocalization in Aromatic Systems: Individual Molecular Orbital Contributions to Para-Delocalization Indexes (PDI), **Güell, M.; Matito, E.; Luis, J.M.; Poater, J.; Solà, M.**, J. Phys. Chem. A 110 (2006) 11569-11574

VI.   Intramolecular Ene Reaction of 1,6-Fullerenynes: A New Synthesis of Allenes, **Altable, M.; Filippone, S.; Martín-Domenech, A.; Güell, M.; Solà, M.; Martín, N.**, Org. Lett. 8 (2006) 5959-5962

VII.   Redox-Controlled Molecular Flipper Based on a Chiral Cu Complex, **Company, A.; Güell, M.; Popa, D.; Benet-Buchholz, J.; Parella, T.; Fontrodona, X.; Llobet, A.; Solà, M.; Ribas, X.; Luis, J.M.; Costas, M.**, Inorg. Chem. 45 (2006) 9643-9645

VIII.   Unprecedented Thermal [2+2] Intramolecular Cyclization of Fuller-1,6-enynes, **Martín, N.; Altable, M.; Filippone, S.; Martín-Domenech, A.; Güell, M.; Solà, M.**, Angew. Chem. Int. Ed. Eng. 45 (2006) 1439-1442

IX.   Aromaticity Analysis of Lithium-Cation/pi Complexes of Aromatic Systems, **Güell, M.; Poater, J.; Luis, J.M.; Mó, O.; Yáñez, M.; Solà, M.**, ChemPhysChem 6 (2005) 2552-2561

X.   Accurate description of spin states and its implications for catalysis, **Güell, M.; Solà, M.; Swart, M.**, Book chapter in "Quantum Biochemistry: Electronic structure and biological activity"; Matta, C.F. (Ed.); Wiley, 2009, accepted

XI. O_2 binding and activation at an asymmetric dicopper complex that exhibits camaleonic reactivity, **Garcia-Bosch, I.; Company, A; Güell, M.; Cardellach, M.M.; Fisch, J.; Que, L., Jr.; Solà, M.; Ribas, X.; Luis, J.M; Costas, M.** submitted

7. Acknowledgments

7. Acknowledgments

Primer de tot, vull començar pels de casa. Als meus pares pel recolzament que m'han donat ara i sempre. A en Marc pel seu optimisme i alegria sense límits tan encomanadissos. A la iaia Anita, per ser una dona amb tanta empenta i energia i per la seva dedicació durant tots aquest anys i a la iaia Antònia per les bones estones passades a Tortellà, el meu altre poble.

A tots els membres de l'IQC, especialment als meus directors de Tesi, dels quals he après tantes coses durant tot aquest temps. A en Miquel Solà per obrir-me les portes de la Química Teòrica i acompanyar-me en el camí que vaig emprendre fa uns quants anys. A en Josep Maria per ser tan meticulós i perfeccionista i voler anar sempre més enllà. A en Marcel, totes les estones que m'ha dedicat des que va arribar a l'IQC.

No em puc oblidar dels companys de despatx que he tingut al llarg d'aquests anys tant la Universitat com al Parc (David, Juanma, Quim, Albert, Edu, Pata, Sílvia, Óscar, Samat, Cristina), per les bones estones compartides, per fer que tot sembli més fàcil quan ho veig tan negre, per la paciència que han tingut de vegades i per l'ajuda que sempre estan diposats a donar. Ni dels de Can Experimental, els que encara hi són i els que ja han marxat. Per les estones compartides, els sopars de benvinguda, de comiat, de fires, de tesi, de tesina i de qualsevol cosa que es pugui celebrar.

Als companys dels cursos de doctorat per un mes tan intens i inoblidable a l'Espanya profunda. Per les experiències que vam compartir i també pel que hem compartit des de llavors.

No em puc pas oblidar tampoc de tota la gent que he conegut durant les estades que he fet a Estocolm. I would like to thank Per and Margareta for having the opportunity to work with them. I learned a lot in your group as a researcher and also as person. Working in the Theoretical Biochemistry group of the Stockhom University have been an incredible experience and all the present and former group members have contributed to creating a friendly and stimulating atmosphere! Muchas gracias Itxaso por tu hospitalidad des del primer día. Por los cafés compartidos, por los consejos, las conversaciones… Y no olvides que tienes un viajecito pendiente!!! Gràcies Àlex pel portátil! No sé que hauria sigut de mi si no t'hagués conegut!!! Gracias a la colonia española de Estocolmo (Agustí, Claudia, Jesús, Pablo…). Me sentí como en casa!! Thank you very much to my corridor mates (Nicole, Stephanie, Bin, Abdi, Jesús, Sara, Karolina, Pontus and Davide)! I had a wonderful time with you!!! Y gracias Pamela por los dos meses geniales que compartimos!

Finalment només em quedes tu, Adrià. Què podria dir-te aquí que no t'hagi dit ja? No existeixen paraules per donar-te les gràcies per tots aquests anys que has estat al meu costat. El teu món i el meu són tan diferents com la nit i el dia, però tot i això, sempre has sabut entendre'm. Hem compartit moltes coses i estic segura que en compartirem moltes més.

8. References

8. References

(1)   Bairoch, A. *Nucl. Acids Res.* 2000, *28*, 304.

(2)   Jencks, W. P. *Catalysis in Chemisty and Enzymology*; Dover: Mineola, New York, 1987.

(3)   Nelson, D. L. *Lehninger principles of biochemistry* Worth: New York, 2000.

(4)   Wolfenden, R.; Snider, M. J. *Acc. Chem. Res.* 2001, *34*, 938.

(5)   Warshel, A.; Sharma, P. K.; Kato, M.; Xiang, Y.; Liu, H. B.; Olsson, M. H. M. *Chem. Rev.* 2006, *106*, 3210.

(6)   Jaeger, K. E.; Eggert, T. *Curr. Opin. Biotechnol.* 2004, *15*, 305.

(7)   Fischer, E. *Ber. Dt. Chem. Ges.* 1894, *27*, 2985.

(8)   Pauling, L. *Chem. Eng. News* 1946, *24*, 1375.

(9)   Koshland, D. E. *Proc. Natl. Acad. Sci.* 1958, *44*, 98.

(10)   Vasella, A.; Davies, G. J.; Bohm, M. *Curr. Opin. Chem. Biol.* 2002, *6*, 619.

(11)   Kraatz, H.; Metzler-Nolte, N. E. *Concepts and Models in Bioinorganic Chemistry*; Wiley-VCH: Bochum, 2006.

(12)   Renugopalakrishnan, V.; Garduno-Juarez, R.; Narasimhan, G.; Verma, C. S.; Wei, X.; Li, P. Z. *J. Nanosci. Nanotechnol.* 2005, *5*, 1759.

(13)   Hult, K.; Berglund, P. *Curr. Opin. Biotechnol.* 2003, *14*, 395.

(14)   Goodwin, J. A.; Stanbury, D. M.; Wilson, L. J.; Eigenbrot, C. W.; Scheidt, W. R. *J. Am. Chem. Soc.* 1987, *109*, 2979.

(15)   Tyeklar, Z.; Jacobson, R. R.; Wei, N.; Murthy, N. N.; Zubieta, J.; Karlin, K. D. *J. Am. Chem. Soc.* 1993, *115*, 2677.

(16)   Borzel, H.; Comba, P.; Hagen, K. S.; Katsichtis, C.; Pritzkow, H. *Chem.-Eur. J.* 2000, *6*, 914.

(17)   McGregor, K. T.; Watkins, N. T.; Lewis, D. L.; Drake, R. F.; Hodgson, D. J.; Hatfield, W. E. *Inorg. Nucl. Chem. Lett.* 1973, *9*, 423.

(18)   Diaddario, L. L.; Robinson, W. R.; Margerum, D. W. *Inorg. Chem.* 1983, *22*, 1021.

(19)   Hanss, J.; Kruger, H. J. *Angew. Chem.-Int. Edit. Engl.* 1996, *35*, 2827.

(20)   Company, A.; Palavicini, S.; Garcia-Bosch, I.; Mas-Balleste, R.; Que, L.; Rybak-Akimova, E. V.; Casella, L.; Ribas, X.; Costas, M. *Chem.-Eur. J.* 2008, *14*, 3535.

(21)   Krebs, C.; Glaser, T.; Bill, E.; Weyhermuller, T.; Meyer-Klaucke, W.; Wieghardt, K. *Angew. Chem.-Int. Edit.* 1999, *38*, 359.

(22)   Holm, R. H.; Kennepohl, P.; Solomon, E. I. *Chem. Rev.* 1996, *96*, 2239.

(23)   Klinman, J. P. *Chem. Rev.* 1996, *96*, 2541.

(24)   Ito, N.; Phillips, S. E. V.; Stevens, C.; Ogel, Z. B.; McPherson, M. J.; Keen, J. N.; Yadav, K. D. S.; Knowles, P. F. *Nature* 1991, *350*, 87.

(25)   Lu, Y. Bio-coordination Chemistry; Que Jr., L., Tolman, W. B., Eds.; Elsevier Ltd.: Oxford, 2004; Vol. 8; pp 91.

(26)   Lieberman, R. L.; Arciero, D. M.; Hooper, A. B.; Rosenzweig, A. C. *Biochemistry* 2001, *40*, 5674.

(27)   Steiner, R. A.; Kalk, K. H.; Dijkstra, B. W. *Proc. Natl. Acad. Sci.* 2002, *99*, 16625.

(28)   Lieberman, R. L.; Rosenzweig, A. C. *Nature* 2005, *434*, 177.

(29) Solomon, E. I.; Sundaram, U. M.; Machonkin, T. E. *Chem. Rev.* 1996, *96*, 2563.

(30) Solomon, E. I.; Baldwin, M. J.; Lowery, M. D. *Chem. Rev.* 1992, *92*, 521.

(31) Koval, I. A.; Gamez, P.; Belle, C.; Selmeczi, K.; Reedijk, J. *Chem. Soc. Rev.* 2006, *35*, 814.

(32) Guckert, J. A.; Lowery, M. D.; Solomon, E. I. *J. Am. Chem. Soc.* 1995, *117*, 2817.

(33) Gray, H. B.; Malmstrom, B. G.; Williams, R. J. P. *J. Biol. Inorg. Chem.* 2000, *5*, 551.

(34) Tainer, J. A.; Getzoff, E. D.; Richardson, J. S.; Richardson, D. C. *Nature* 1983, *306*, 284.

(35) Eisensmith, R. C.; Woo, S. L. C. *Molec. Biol. Med.* 1991, *8*, 3.

(36) Duff, A. P.; Cohen, A. E.; Ellis, P. J.; Kuchar, J. A.; Langley, D. B.; Shepard, E. M.; Dooley, D. M.; Freeman, H. C.; Guss, J. M. *Biochemistry* 2003, *42*, 15148.

(37) Volbeda, A.; Hol, W. G. J. *J. Mol. Biol.* 1989, *209*, 249.

(38) Matoba, Y.; Kumagai, T.; Yamamoto, A.; Yoshitsu, H.; Sugiyama, M. *J. Biol. Chem.* 2006, *281*, 8981.

(39) Gerdemann, C.; Eicken, C.; Krebs, B. *Acc. Chem. Res.* 2002, *35*, 183.

(40) Piontek, K.; Antorini, M.; Choinowski, T. *J. Biol. Chem.* 2002, *277*, 37663.

(41) Messerschmidt, A.; Rossi, A.; Ladenstein, R.; Huber, R.; Bolognesi, M.; Gatti, G.; Marchesini, A.; Petruzzelli, R.; Finazziagro, A. *J. Mol. Biol.* 1989, *206*, 513.

(42) Musci, G. *Protein Pept. Lett.* 2001, *8*, 159.

(43) Tsukihara, T.; Aoyama, H.; Yamashita, E.; Tomizaki, T.; Yamaguchi, H.; Shinzawaitoh, K.; Nakashima, R.; Yaono, R.; Yoshikawa, S. *Science* 1995, *269*, 1069.

(44) Prudencio, M.; Pereira, A. S.; Tavares, P.; Besson, S.; Cabrito, I.; Brown, K.; Samyn, B.; Devreese, B.; Van Beeumen, J.; Rusnak, F.; Fauque, G.; Moura, J. J. G.; Tegoni, M.; Cambillau, C.; Moura, I. *Biochemistry* 2000, *39*, 3899.

(45) Kadenbach, B. *Angew. Chem.-Int. Edit. Engl.* 1996, *34*, 2635.

(46) Brown, K.; Djinovic-Carugo, K.; Haltia, T.; Cabrito, I.; Saraste, M.; Moura, J. J. G.; Moura, I.; Tegoni, M.; Cambillau, C. *J. Biol. Chem.* 2000, *275*, 41133.

(47) Brown, K.; Tegoni, M.; Prudencio, M.; Pereira, A. S.; Besson, S.; Moura, J. J.; Moura, I.; Cambillau, C. *Nat. Struct. Biol.* 2000, *7*, 191.

(48) Mason, H. S.; Fowlks, W. L.; Peterson, E. *J. Am. Chem. Soc.* 1955, *77*, 2914.

(49) Rompel, A.; Fischer, H.; Meiwes, D.; Buldt-Karentzopoulos, K.; Dillinger, R.; Tuczek, F.; Witzel, H.; Krebs, B. *J. Biol. Inorg. Chem.* 1999, *4*, 56.

(50) Wilcox, D. E.; Porras, A. G.; Hwang, Y. T.; Lerch, K.; Winkler, M. E.; Solomon, E. I. *J. Am. Chem. Soc.* 1985, *107*, 4015.

(51) Siegbahn, P. E. M. *J. Biol. Inorg. Chem.* 2003, *8*, 567.

(52) Deverall, B. J. *Nature* 1961, *189*, 311.

(53) Mayer, A. M.; Harel, E. *Phytochemistry* 1979, *18*, 193.

(54) Klabunde, T.; Eicken, C.; Sacchettini, J. C.; Krebs, B. *Nat. Struct. Biol.* 1998, *5*, 1084.

(55) Eicken, C.; Zippel, F.; Buldt-Karentzopoulos, K.; Krebs, B. *FEBS Lett.* 1998, *436*, 293.

(56) Klinman, J. P. *J. Biol. Chem.* 2006, *281*, 3013.

(57) Rolff, M.; Tuczek, F. *Angew. Chem.-Int. Edit.* 2008, *47*, 2344.

(58)   Evans, J. P.; Ahn, K.; Klinman, J. P. *J. Biol. Chem.* 2003, *278*, 49691.

(59)   Prigge, S. T.; Eipper, B. A.; Mains, R. E.; Amzel, L. M. *Science* 2004, *304*, 864.

(60)   Chen, P.; Solomon, E. I. *Proc. Natl. Acad. Sci.* 2004, *101*, 13105.

(61)   Lewis, E. A.; Tolman, W. B. *Chem. Rev.* 2004, *104*, 1047.

(62)   Mirica, L. M.; Ottenwaelder, X.; Stack, T. D. P. *Chem. Rev.* 2004, *104*, 1013.

(63)   Karlin, K. D.; Zuberbühler, A. D. In *Bioinorganic catalysis*; Reedijk, J., Bouwman, E., Eds.; Marcel Dekker: New York, 1999; pp 469.

(64)   Zhang, C. X.; Liang, H.-C.; Humphreys, K. J.; Karlin, K. D. In *Catalytic activation of dioxygen by metal complexes*; L, S., Ed.; Kluwer: Dordrecht, 2003; pp 79.

(65)   Karlin, K. D.; Kaderli, S.; Zuberbuhler, A. D. *Acc. Chem. Res.* 1997, *30*, 139.

(66)   Karlin, K. D.; Gultneh, Y. *Prog. Inorg. Chem.* 1987, *35*, 219.

(67)   Hatcher, L. Q.; Karlin, K. D. *J. Biol. Inorg. Chem.* 2004, *9*, 669.

(68)   Hatcher, L. Q.; Karlin, K. D. *Adv. Inorg. Chem.* 2006, *58*, 131.

(69)   Hatcher, L. Q.; Vance, M. A.; Sarjeant, A. A. N.; Solomon, E. I.; Karlin, K. D. *Inorg. Chem.* 2006, *45*, 3004.

(70)   Magnus, K. A.; Tonthat, H.; Carpenter, J. E. *Chem. Rev.* 1994, *94*, 727.

(71)   Brackman, W.; Havinga, E. *Recl. Trav. Chim. Pays-Bas* 1955, *74*, 937.

(72)   Brackman, W.; Havinga, E. *Recl. Trav. Chim. Pays-Bas* 1955, *74*, 1021.

(73)   Brackman, W.; Havinga, E. *Recl. Trav. Chim. Pays-Bas* 1955, *74*, 1070.

(74)   Brackman, W.; Havinga, E. *Recl. Trav. Chim. Pays-Bas* 1955, *74*, 1100.

(75)   Brackman, W.; Havinga, E. *Recl. Trav. Chim. Pays-Bas* 1955, *74*, 1107.

(76)   Karlin, K. D.; Hayes, J. C.; Gultneh, Y.; Cruse, R. W.; McKown, J. W.; Hutchinson, J. P.; Zubieta, J. *J. Am. Chem. Soc.* 1984, *106*, 2121.

(77)   Nasir, M. S.; Cohen, B. I.; Karlin, K. D. *J. Am. Chem. Soc.* 1992, *114*, 2482.

(78)   Karlin, K. D.; Nasir, M. S.; Cohen, B. I.; Cruse, R. W.; Kaderli, S.; Zuberbuhler, A. D. *J. Am. Chem. Soc.* 1994, *116*, 1324.

(79)   Pidcock, E.; Obias, H. V.; Zhang, C. X.; Karlin, K. D.; Solomon, E. I. *J. Am. Chem. Soc.* 1998, *120*, 7841.

(80)   Holland, P. L.; Rodgers, K. R.; Tolman, W. B. *Angew. Chem.-Int. Edit.* 1999, *38*, 1139.

(81)   Mahapatra, S.; Kaderli, S.; Llobet, A.; Neuhold, Y. M.; Palanche, T.; Halfen, J. A.; Young, V. G.; Kaden, T. A.; Que, L.; Zuberbuhler, A. D.; Tolman, W. B. *Inorg. Chem.* 1997, *36*, 6343.

(82)   VanOrman, C. A.; Reddy, K. V.; Sayre, L. M.; Urbach, F. L. *Polyhedron* 2001, *20*, 541.

(83)   Palavicini, S.; Granata, A.; Monzani, E.; Casella, L. *J. Am. Chem. Soc.* 2005, *127*, 18031.

(84)   Mirica, L. M.; Rudd, D. J.; Vance, M. A.; Solomon, E. I.; Hodgson, K. O.; Hedman, B.; Stack, T. D. P. *J. Am. Chem. Soc.* 2006, *128*, 2654.

(85)   Mirica, L. M.; Vance, M.; Rudd, D. J.; Hedman, B.; Hodgson, K. O.; Solomon, E. I.; Stack, T. D. P. *Science* 2005, *308*, 1890.

(86)   Que, L.; Tolman, W. B. *Angew. Chem.-Int. Edit.* 2002, *41*, 1114.

(87)   Fujisawa, K.; Tanaka, M.; Morooka, Y.; Kitajima, N. *J. Am. Chem. Soc.* 1994, *116*, 12079.

(88)   Cramer, C. J.; Tolman, W. B. *Acc. Chem. Res.* 2007, *40*, 601.

(89)   Aboelella, N. W.; Kryatov, S. V.; Gherman, B. F.; Brennessel, W. W.; Young, V. G.; Sarangi, R.; Rybak-Akimova, E. V.; Hodgson, K. O.; Hedman, B.; Solomon, E. I.; Cramer, C. J.; Tolman, W. B. *J. Am. Chem. Soc.* 2004, *126*, 16896.

(90)   Hong, S.; Huber, S. M.; Gagliardi, L.; Cramer, C. C.; Tolman, W. B. *J. Am. Chem. Soc.* 2007, *129*, 14190.

(91)   Kunishita, A.; Teraoka, J.; Scanlon, J. D.; Matsumoto, T.; Suzuki, M.; Cramer, C. J.; Itoh, S. *J. Am. Chem. Soc.* 2007, *129*, 7248.

(92)   Osako, T.; Nagatomo, S.; Kitagawa, T.; Cramer, C. J.; Itoh, S. *J. Biol. Inorg. Chem.* 2005, *10*, 581.

(93)   Maiti, D.; Lucas, H. R.; Sarjeant, A. A. N.; Karlin, K. D. *J. Am. Chem. Soc.* 2007, *129*, 6998.

(94)   Maiti, D.; Fry, H. C.; Woertink, J. S.; Vance, M. A.; Solomon, E. I.; Karlin, K. D. *J. Am. Chem. Soc.* 2007, *129*, 264.

(95)   Maiti, D.; Sarjeant, A. A. N.; Karlin, K. D. *J. Am. Chem. Soc.* 2007, *129*, 6720.

(96)   Maiti, D.; Lee, D. H.; Gaoutchenova, K.; Wurtele, C.; Holthausen, M. C.; Sarjeant, A. A. N.; Sundermeyer, J.; Schindler, S.; Karlin, K. D. *Angew. Chem.-Int. Edit.* 2008, *47*, 82.

(97)   Wallar, B. J.; Lipscomb, J. D. *Chem. Rev.* 1996, *96*, 2625.

(98)   Costas, M.; Mehn, M. P.; Jensen, M. P.; Que, L. *Chem. Rev.* 2004, *104*, 939.

(99)   Tshuva, E. Y.; Lippard, S. J. *Chem. Rev.* 2004, *104*, 987.

(100)   Solomon, E. I.; Szilagyi, R. K.; George, S. D.; Basumallick, L. *Chem. Rev.* 2004, *104*, 419.

(101)   Ortiz de Montellano, P. R. *Cytochrome P450: structure, mechanism and biochemistry*; Kluwer Academic/Plenum Publishers: New York, 2004.

(102)   Sligar, S. G. *Biochemistry* 1976, *15*, 5399.

(103)   Dawson, J. H.; Holm, R. H.; Trudell, J. R.; Barth, G.; Linder, R. E.; Bunnenberg, E.; Djerassi, C.; Tang, S. C. *J. Am. Chem. Soc.* 1976, *98*, 3707.

(104)   Denisov, I. G.; Makris, T. M.; Sligar, S. G.; Schlichting, I. *Chem. Rev.* 2005, *105*, 2253.

(105)   Shaik, S.; de Visser, S. P. Computational Approaches To Cytochrome P450 Function. In *Cytochrome P450: structure, mechanism and biochemistry*; Ortiz de Montellano, P. R., Ed.; Kluwer Academic/Plenum Publishers: New York, 2004.

(106)   Gütlich, P.; Goodwin, H. A. *Top. Curr. Chem.* 2004, *233*, 1.

(107)   Gütlich, P.; García, Y.; Goodwin, H. A. *Chem. Soc. Rev.* 2000, *29*, 419.

(108)   Cambi, L.; Szego, L. *Ber. Dtsch. Chem. Ges.* 1931, *64*, 2591.

(109)   Ewald, A. H.; Ross, I. G.; White, A. H.; Martin, R. L. *Proc. Roy. Soc. London Ser. A* 1964, *280*, 235.

(110)   Krober, J.; Codjovi, E.; Kahn, O.; Groliere, F.; Jay, C. *J. Am. Chem. Soc.* 1993, *115*, 9810.

(111)   Hauser, A. *Top. Curr. Chem.* 2004, *234*, 155.

(112)   Moussa, N. O.; Trzop, E.; Mouri, S.; Zein, S.; Molnar, G.; Gaspar, A. B.; Collet, E.; Cointe, M. B. L.; Real, J. A.; Borshch, S.; Tanaka, K.; Cailleau, H.; Bousseksou, A. *Phys. Rev. B* 2007, *75*.

(113)   Hollingsworth, M. D. *Science* 2002, *295*, 2410.

(114)   Maspoch, D.; Ruiz-Molina, D.; Veciana, J. *Chem. Soc. Rev.* 2007, *36*, 770.

(115)   Galet, A.; Gaspar, A. B.; Munoz, M. C.; Bukin, G. V.; Levchenko, G.; Real, J. A. *Adv. Mater.* 2005, *17*, 2949.

(116)   Kahn, O.; Martinez, C. J. *Science* 1998, *279*, 44.

(117)   Real, J. A.; Gaspar, A. B.; Niel, V.; Muñoz, M. C. *Coord. Chem. Rev.* 2003, *236*, 121.

(118)   Ksenofontov, V.; Gaspar, A. B.; Gütlich, P. *Top. Curr. Chem.* 2004, *235*, 23.

(119)   Gütlich, P.; Hauser, A.; Spiering, H. *Angew. Chem. Int. Ed. Engl.* 1994, *33*, 2024.

(120)   Bousseksou, A.; Varret, F.; Goiran, M.; Boukheddaden, K.; Tuchagues, J. P. *Top. Curr. Chem.* 2004, *235*, 65.

(121)   Decurtins, S.; Gütlich, P.; Kohler, C. P.; Spiering, H.; Hauser, A. *Chem. Phys. Lett.* 1984, *105*, 1.

(122)   Gütlich, P.; García, Y.; Woike, T. *Coord. Chem. Rev.* 2001, *219*, 839.

(123)   García, Y.; Gütlich, P. *Top. Curr. Chem.* 2004, *234*, 49.

(124)   Reinen, D.; Friebel, C.; Propach, V. *Z. Anorg. Allg. Chem.* 1974, *408*, 187.

(125)   van Koningsbruggen, P. J.; Maeda, Y.; Oshio, H. *Top. Curr. Chem.* 2004, *233*, 259.

(126)   Goodwin, H. A. *Top. Curr. Chem.* 2004, *234*, 23.

(127)   Konig, E. *Prog. Inorg. Chem.* 1987, *35*, 527.

(128)   Halcrow, M. A. *Polyhedron* 2007, *26*, 3523.

(129)   Konig, E.; Kremer, S. *Theor. Chim. Acta.* 1971, *23*, 12.

(130)   Millet, J. M. M. Mossbauer Spectroscopy in Heterogeneous Catalysis. In *Advances in Catalysis, Vol 51*, 2007; Vol. 51; pp 309.

(131)   Han, W. G.; Liu, T. Q.; Lovell, T.; Noodleman, L. *J. Comput. Chem.* 2006, *27*, 1292.

(132)   Bandyopadhyay, D. *Int. Mat. Rev.* 2006, *51*, 171.

(133)   Paulsen, H.; Schunernann, V.; Trautwein, A. X.; Winkler, H. *Coord. Chem. Rev.* 2005, *249*, 255.

(134)   Greenwood, N. N.; Gibb, T. C. *Mössbauer spectroscopy*; Chapman and Hall Ltd: London, 1971.

(135)   Gütlich, P.; Link, R.; Trautwein, A. X. *Mössbauer spectroscopy and transition metal chemistry. Inorganic Chemistry Concepts No. 3*; Springer: Berlin, Heidlberg, New York, 1978.

(136)   Szabo, A.; Ostlund, N. S. *Modern quantum chemistry*; McGraw-Hill, 1989.

(137)   Hehre, W. J.; Radom, L.; Schleyer, P. V.; Pople, J. *Ab Initio Molecular Orbital Theory*; John Wiley & Sons, 1986.

(138)   Jensen, F. *Introduction to computational chemistry*; Wiley & Sons: Chicester, UK, 1999.

(139)   Koch, W.; Holthausen, M. C. *A Chemist's Guide to Density Functional Theory*; Wiley-VCH: Weinheim, Germany, 2000.

(140)   Hohenberg, P.; Kohn, W. *Phys. Rev. B* 1964, *136*, 864.

(141)   Kohn, W.; Sham, L. J. *Phys. Rev. A* 1965, *140*, 1133.

(142)   Slater, J. C. *Phys. Rev.* 1951, *81*, 385.

(143)   Vosko, S. H.; Wilk, L.; Nusair, M. *Can. J. Phys.* 1980, *58*, 1200.

(144)   Ceperley, D. *Phys. Rev. B* 1978, *18*, 3126.

(145)   Ceperley, D. M.; Alder, B. J. *Phys. Rev. Lett.* 1980, *45*, 566.

(146)   Perdew, J. P.; Zunger, A. *Phys. Rev. B* 1981, *23*, 5048.

(147)   Solà, M.; Mestres, J.; Carbó, R.; Duran, M. *J. Chem. Phys.* 1996, *104*, 636.

(148) Becke, A. D. *Phys. Rev. A* 1988, *38*, 3098.

(149) Handy, N. C.; Cohen, A. J. *Mol. Phys.* 2001, *99*, 403.

(150) Becke, A. D. *J. Chem. Phys.* 1986, *84*, 4524.

(151) Perdew, J. P.; Burke, K.; Ernzerhof, M. *Phys. Rev. Lett.* 1996, *77*, 3865.

(152) Perdew, J. P. *Phys. Rev. B* 1986, *33*, 8822.

(153) Perdew, J. P. PW91. In *Electronic structure of Solids 1991*; Ziesche, P., Eschrig, H., Eds.; Akademie: Berlin, 1991; pp 11.

(154) Lee, C.; Yang, W.; Parr, R. G. *Phys. Rev. B* 1988, *37*, 785.

(155) Sousa, S. F.; Fernandes, P. A.; Ramos, M. J. *J. Phys. Chem. A* 2007, *111*, 10439.

(156) Becke, A. D. *J. Chem. Phys.* 1996, *104*, 1040.

(157) Tao, J. M.; Perdew, J. P.; Staroverov, V. N.; Scuseria, G. E. *Phys. Rev. Lett.* 2003, *91*, 146401.

(158) Van Voorhis, T.; Scuseria, G. E. *J. Chem. Phys.* 1998, *109*, 400.

(159) Adamo, C.; Barone, V. *J. Chem. Phys.* 1998, *108*, 664.

(160) Lynch, B. J.; Zhao, Y.; Truhlar, D. G. *J. Phys. Chem. A* 2003, *107*, 1384.

(161) Lynch, B. J.; Fast, P. L.; Harris, M.; Truhlar, D. G. *J. Phys. Chem. A* 2000, *104*, 4811.

(162) Torrent, M.; Solà, M.; Frenking, G. *Chem. Rev.* 2000, *100*, 439.

(163) Paulsen, H.; Trautwein, A. X. *Top. Curr. Chem.* 2004, *235*, 197.

(164) Siegbahn, P. E. M. *J. Biol. Inorg. Chem.* 2006, *11*, 695.

(165) Harvey, J. N. *Struct. Bond.* 2004, *112*, 151.

(166) Harvey, J. N. *Annu. Rep. Prog. Chem., Sect. C: Phys. Chem.* 2006, *102*, 203.

(167) Reiher, M.; Salomon, O.; Hess, B. A. *Theor. Chem. Acc.* 2001, *107*, 48.

(168) Salomon, O.; Reiher, M.; Hess, B. A. *J. Chem. Phys.* 2002, *117*, 4729.

(169) Swart, M.; Groenhof, A. R.; Ehlers, A. W.; Lammertsma, K. *J. Phys. Chem. A* 2004, *108*, 5479.

(170) Hehre, W. J.; Stewart, R. F.; Pople, J. A. *J. Chem. Phys.* 1969, *51*, 2657.

(171) Hehre, W. J.; Ditchfie.R; Pople, J. A. *J. Chem. Phys.* 1972, *56*, 2257.

(172) Krishnan, R.; Binkley, J. S.; Seeger, R.; Pople, J. A. *J. Chem. Phys.* 1980, *72*, 650.

(173) Frisch, M. J.; Pople, J. A.; Binkley, J. S. *J. Chem. Phys.* 1984, *80*, 3265.

(174) Dunning, T. H. *J. Chem. Phys.* 1971, *55*, 716.

(175) Almlof, J.; Taylor, P. R. *J. Chem. Phys.* 1990, *92*, 551.

(176) Dunning Jr., T. H. *J. Chem. Phys.* 1989, *90*, 1007.

(177) Laidler, K. J. *Chemical kinetics* Harper Collins Publishers: New York, 1987.

(178) Steinfeld, J. I.; Francisco, J. S.; Hase, W. L. *Chemical kinetics and dynamics*; Prentice Hall: Upper Saddle River, 1999.

(179) Laidler, K. J.; King, M. C. *J. Phys. Chem.* 1983, *87*, 2657.

(180) Truhlar, D. G.; Hase, W. L.; Hynes, J. T. *J. Phys. Chem.* 1983, *87*, 2664.

(181) Siegbahn, P. E. M.; Borowski, T. *Acc. Chem. Res.* 2006, *39*, 729.

(182) Warshel, A.; Levitt, M. *J. Mol. Biol.* 1976, *103*, 227.

(183) Singh, U. C.; Kollman, P. A. *J. Comput. Chem.* 1986, *7*, 718.

(184) Ryde, U. *Curr. Opin. Chem. Biol.* 2003, *7*, 136.

(185) Deeth, R. J. *Struct. Bond.* 2004, *113*, 37.

(186) Pelmenschikov, V.; Siegbahn, P. E. M.; Blomberg, M. R. A. *J. Biol. Inorg. Chem.* 2002, *7*, 284.

(187) Siegbahn, P. E. M.; Blomberg, M. R. A. *Chem. Rev.* 2000, *100*, 421.

(188)   Siegbahn, E. M. *Quart. Rev. Biophys.* 2003, *36*, 91.

(189)   Pelmenschikov, V.; Cho, K. B.; Siegbahn, P. E. M. *J. Comput. Chem.* 2004, *25*, 311.

(190)   Pelmenschikov, V.; Siegbahn, P. E. M. *J. Biol. Inorg. Chem.* 2003, *8*, 653.

(191)   Baruah, P.; Swain, T. *J. Sci. Food Agric.* 1959, *10*, 125.

(192)   Solomon, E. I.; Baldwin, M. J.; Lowery, M. D. *Chem. Rev.* 1992, *92*, 521.

(193)   Lewin, J. L.; Heppner, D. E.; Cramer, C. J. *J. Biol. Inorg. Chem.* 2007, *12*, 1221.

(194)   Gherman, B. F.; Tolman, W. B.; Cramer, C. J. *J. Comput. Chem.* 2006, *27*, 1950.

(195)   Mirica, L., PhD Thesis. Standford University. Available via the ProQuest database, UMI # 3162369, 2006.

(196)   Holt, B. T. O.; Vance, M. A.; Mirica, L. M.; Heppner, D. E.; Stack, T. D. P.; Solomon, E. I. *J. Am. Chem. Soc.* 2009, *131*, 6421.

(197)   Itoh, S. *Curr. Opin. Chem. Biol.* 2006, *10*, 115.

(198)   Cramer, C. J.; Gour, J. R.; Kinal, A.; Wtoch, M.; Piecuch, P.; Shahi, A. R. M.; Gagliardi, L. *J. Phys. Chem. A* 2008, *112*, 3754.

(199)   Miller, A. F. *Curr. Opin. Chem. Biol.* 2004, *8*, 162.

(200)   Fridovich, I. *J. Biol. Chem.* 1997, *272*, 18515.

(201)   Hart, P. J.; Balbirnie, M. M.; Ogihara, N. L.; Nersissian, A. M.; Weiss, M. S.; Valentine, J. S.; Eisenberg, D. *Biochemistry* 1999, *38*, 2167.

(202)   Poater, J.; Solà, M.; Rimola, A.; Rodríguez-Santiago, L.; Sodupe, M. *J. Phys. Chem. A* 2004, *108*, 6072.

(203)   Swart, M.; Ehlers, A. W.; Lammertsma, K. *Mol. Phys.* 2004, *102*, 2467.

(204)   Liao, M.-S.; Watts, J. D.; Huang, M.-J. *J. Comput. Chem.* 2006, *27*, 1577.

(205)   Zein, S.; Borshch, S. A.; Fleurat-Lessard, P.; Casida, M. E.; Chermette, H. *J. Chem. Phys.* 2007, *126*, 014105.

(206)   Hirao, H.; Kumar, D.; Que Jr., L.; Shaik, S. *J. Am. Chem. Soc.* 2006, *128*, 8590.

(207)   Lepetit, C.; Chermette, H.; Gicquel, M.; Heully, J.-L.; Chauvin, R. *J. Phys. Chem. A* 2007, *111*, 136.

(208)   van Lenthe, E.; Baerends, E. J. *J. Comput. Chem.* 2003, *24*, 1142.

(209)   Noveron, J. C.; Olmstead, M. M.; Mascharak, P. K. *Inorg. Chem.* 1998, *37*, 1138.

(210)   Fallon, G. D.; Gatehouse, B. M.; Minari, P. J.; Murray, K. S.; West, B. O. *J. Chem. Soc.-Dalton Trans.* 1984, 2733.

(211)   Govindaswamy, N.; Quarless, D. A.; Koch, S. A. *J. Am. Chem. Soc.* 1995, *117*, 8468.

(212)   Trofimenko, S. *Chem. Rev.* 1993, *93*, 943.

(213)   Pettinari, C.; Pettinari, R. *Coord. Chem. Rev.* 2005, *249*, 525.